



National Library
of Canada

Acquisitions and
Bibliographic Services Branch

395 Wellington Street
Ottawa, Ontario
K1A 0N4

Bibliothèque nationale
du Canada

Direction des acquisitions et
des services bibliographiques

395, rue Wellington
Ottawa (Ontario)
K1A 0N4

Your file - Votre référence

Our file - Notre référence

NOTICE

The quality of this microform is heavily dependent upon the quality of the original thesis submitted for microfilming. Every effort has been made to ensure the highest quality of reproduction possible.

If pages are missing, contact the university which granted the degree.

Some pages may have indistinct print especially if the original pages were typed with a poor typewriter ribbon or if the university sent us an inferior photocopy.

Reproduction in full or in part of this microform is governed by the Canadian Copyright Act, R.S.C. 1970, c. C-30, and subsequent amendments.

AVIS

La qualité de cette microforme dépend grandement de la qualité de la thèse soumise au microfilmage. Nous avons tout fait pour assurer une qualité supérieure de reproduction.

S'il manque des pages, veuillez communiquer avec l'université qui a conféré le grade.

La qualité d'impression de certaines pages peut laisser à désirer, surtout si les pages originales ont été dactylographiées à l'aide d'un ruban usé ou si l'université nous a fait parvenir une photocopie de qualité inférieure.

La reproduction, même partielle, de cette microforme est soumise à la Loi canadienne sur le droit d'auteur, SRC 1970, c. C-30, et ses amendements subséquents.

Canada



UNIVERSITY OF ALBERTA

MICROPHONE POSITIONING SYSTEM FOR M.E.A.N.U.

BY

VINCENT JEFFREY PISIO



A thesis submitted to the Faculty of Graduate Studies and Research in partial fulfillment of the requirements for the degree of Master of Science.

Department of Mechanical Engineering

Fall 1994



National Library
of Canada

Acquisitions and
Bibliographic Services Branch

395 Wellington Street
Ottawa, Ontario
K1A 0N4

Bibliothèque nationale
du Canada

Direction des acquisitions et
des services bibliographiques

395, rue Wellington
Ottawa (Ontario)
K1A 0N4

Your file / Votre référence

Our file / Notre référence

The author has granted an irrevocable non-exclusive licence allowing the National Library of Canada to reproduce, loan, distribute or sell copies of his/her thesis by any means and in any form or format, making this thesis available to interested persons.

L'auteur a accordé une licence irrévocable et non exclusive permettant à la Bibliothèque nationale du Canada de reproduire, prêter, distribuer ou vendre des copies de sa thèse de quelque manière et sous quelque forme que ce soit pour mettre des exemplaires de cette thèse à la disposition des personnes intéressées.

The author retains ownership of the copyright in his/her thesis. Neither the thesis nor substantial extracts from it may be printed or otherwise reproduced without his/her permission.

L'auteur conserve la propriété du droit d'auteur qui protège sa thèse. Ni la thèse ni des extraits substantiels de celle-ci ne doivent être imprimés ou autrement reproduits sans son autorisation.

ISBN 0-315-95095-1

Canada

Name Vincent Jeffrey Pizio

Dissertation Abstracts International is arranged by broad, general subject categories. Please select the one subject which most nearly describes the content of your dissertation. Enter the corresponding four-digit code in the spaces provided.

Mechanical Engineering
SUBJECT TERM

0548
SUBJECT CODE

U·M·I

Subject Categories

THE HUMANITIES AND SOCIAL SCIENCES

COMMUNICATIONS AND THE ARTS

| | |
|----------------------|------|
| Architecture | 0729 |
| Art History | 0377 |
| Cinema | 0900 |
| Dance | 0378 |
| Fine Arts | 0357 |
| Information Science | 0723 |
| Journalism | 0391 |
| Library Science | 0399 |
| Mass Communications | 0708 |
| Music | 0413 |
| Speech Communication | 0459 |
| Theater | 0465 |

EDUCATION

| | |
|-----------------------------|------|
| General | 0515 |
| Administration | 0514 |
| Adult and Continuing | 0516 |
| Agricultural | 0517 |
| Art | 0273 |
| Bilingual and Multicultural | 0282 |
| Business | 0688 |
| Community College | 0275 |
| Curriculum and Instruction | 0727 |
| Early Childhood | 0518 |
| Elementary | 0524 |
| Finance | 0777 |
| Guidance and Counseling | 0519 |
| Health | 0680 |
| Higher | 0745 |
| History of | 0520 |
| Home Economics | 0278 |
| Industrial | 0521 |
| Language and Literature | 0279 |
| Mathematics | 0280 |
| Music | 0522 |
| Philosophy of | 0998 |
| Physical | 0523 |

| | |
|------------------------|------|
| Psychology | 0525 |
| Reading | 0535 |
| Religious | 0527 |
| Sciences | 0714 |
| Secondary | 0533 |
| Social Sciences | 0534 |
| Sociology of | 0340 |
| Special | 0529 |
| Teacher Training | 0530 |
| Technology | 0710 |
| Tests and Measurements | 0288 |
| Vocational | 0747 |

LANGUAGE, LITERATURE AND LINGUISTICS

| | |
|--------------------------|------|
| Language | |
| General | 0679 |
| Ancient | 0289 |
| Linguistics | 0290 |
| Modern | 0291 |
| Literature | |
| General | 0401 |
| Classical | 0294 |
| Comparative | 0295 |
| Medieval | 0297 |
| Modern | 0298 |
| African | 0316 |
| American | 0591 |
| Asian | 0305 |
| Canadian (English) | 0352 |
| Canadian (French) | 0355 |
| English | 0593 |
| Germanic | 0311 |
| Latin American | 0312 |
| Middle Eastern | 0315 |
| Romance | 0313 |
| Slavic and East European | 0314 |

PHILOSOPHY, RELIGION AND THEOLOGY

| | |
|------------------|------|
| Philosophy | 0422 |
| Religion | |
| General | 0318 |
| Biblical Studies | 0321 |
| Clergy | 0319 |
| History of | 0320 |
| Philosophy of | 0322 |
| Theology | 0469 |

SOCIAL SCIENCES

| | |
|-------------------------|------|
| American Studies | 0323 |
| Anthropology | |
| Archaeology | 0324 |
| Cultural | 0326 |
| Physical | 0327 |
| Business Administration | |
| General | 0310 |
| Accounting | 0272 |
| Bar/Juris | 0770 |
| Management | 0454 |
| Marketing | 0338 |
| Canadian Studies | 0385 |
| Economics | |
| General | 0501 |
| Agricultural | 0503 |
| Commerce-Business | 0505 |
| Finance | 0508 |
| History | 0509 |
| Labor | 0510 |
| Theory | 0511 |
| Folklore | 0358 |
| Geography | 0366 |
| Gerontology | 0351 |
| History | |
| General | 0578 |

| | |
|----------------------------------|------|
| Ancient | 0579 |
| Medieval | 0581 |
| Modern | 0582 |
| Black | 0328 |
| African | 0331 |
| Asia, Australia and Oceania | 0332 |
| Canadian | 0334 |
| European | 0335 |
| Latin American | 0336 |
| Middle Eastern | 0333 |
| United States | 0337 |
| History of Science | 0585 |
| Law | 0398 |
| Political Science | |
| General | 0615 |
| International Law and Relations | 0616 |
| Public Administration | 0617 |
| Recreation | 0814 |
| Social Work | 0452 |
| Sociology | |
| General | 0626 |
| Criminology and Penology | 0627 |
| Demography | 0938 |
| Ethnic and Racial Studies | 0631 |
| Individual and Family Studies | 0628 |
| Industrial and Labor Relations | 0629 |
| Public and Social Welfare | 0630 |
| Social Structure and Development | 0700 |
| Theory and Methods | 0344 |
| Transportation | 0709 |
| Urban and Regional Planning | 0999 |
| Women's Studies | 0453 |

THE SCIENCES AND ENGINEERING

BIOLOGICAL SCIENCES

| | |
|------------------------------|------|
| Agriculture | |
| General | 0473 |
| Agronomy | 0285 |
| Animal Culture and Nutrition | 0475 |
| Animal Pathology | 0476 |
| Food Science and Technology | 0359 |
| Forestry and Wildlife | 0478 |
| Plant Culture | 0479 |
| Plant Pathology | 0480 |
| Plant Physiology | 0817 |
| Range Management | 0777 |
| Wood Technology | 0746 |
| Biology | |
| General | 0306 |
| Anatomy | 0287 |
| Biostatistics | 0308 |
| Botany | 0309 |
| Cell | 0379 |
| Ecology | 0329 |
| Entomology | 0353 |
| Genetics | 0369 |
| Limnology | 0793 |
| Microbiology | 0410 |
| Molecular | 0307 |
| Neuroscience | 0317 |
| Oceanography | 0416 |
| Physiology | 0433 |
| Radiation | 0821 |
| Veterinary Science | 0778 |
| Zoology | 0472 |
| Biophysics | |
| General | 0786 |
| Medical | 0760 |
| EARTH SCIENCES | |
| Biogeochemistry | 0425 |
| Geochemistry | 0996 |

| | |
|-----------------------|------|
| Geodesy | 0370 |
| Geology | 0372 |
| Geophysics | 0373 |
| Hydrology | 0388 |
| Mineralogy | 0411 |
| Paleobotany | 0345 |
| Paleoecology | 0426 |
| Paleontology | 0418 |
| Paleozoology | 0985 |
| Palynology | 0427 |
| Physical Geography | 0368 |
| Physical Oceanography | 0415 |

HEALTH AND ENVIRONMENTAL SCIENCES

| | |
|---------------------------------|------|
| Environmental Sciences | 0768 |
| Health Sciences | |
| General | 0566 |
| Audiology | 0300 |
| Chemotherapy | 0992 |
| Dentistry | 0567 |
| Education | 0350 |
| Hospital Management | 0769 |
| Human Development | 0758 |
| Immunology | 0982 |
| Medicine and Surgery | 0564 |
| Mental Health | 0347 |
| Nursing | 0569 |
| Nutrition | 0570 |
| Obstetrics and Gynecology | 0380 |
| Occupational Health and Therapy | 0354 |
| Ophthalmology | 0381 |
| Pathology | 0571 |
| Pharmacology | 0419 |
| Pharmacy | 0572 |
| Physical Therapy | 0382 |
| Public Health | 0573 |
| Radiology | 0574 |
| Recreation | 0575 |

| | |
|------------------|------|
| Speech Pathology | 0460 |
| Toxicology | 0383 |
| Home Economics | 0386 |

PHYSICAL SCIENCES

| | |
|--------------------------------------|------|
| Pure Sciences | |
| Chemistry | |
| General | 0485 |
| Agricultural | 0749 |
| Analytical | 0486 |
| Biochemistry | 0487 |
| Inorganic | 0488 |
| Nuclear | 0738 |
| Organic | 0490 |
| Pharmaceutical | 0491 |
| Physical | 0494 |
| Polymer | 0495 |
| Radiation | 0754 |
| Mathematics | 0405 |
| Physics | |
| General | 0605 |
| Acoustics | 0986 |
| Astronomy and Astrophysics | 0606 |
| Atmospheric Science | 0608 |
| Atomic | 0748 |
| Electronics and Electricity | 0607 |
| Elementary Particles and High Energy | 0798 |
| Fluid and Plasma | 0759 |
| Molecular | 0609 |
| Nuclear | 0610 |
| Optics | 0752 |
| Radiation | 0756 |
| Solid State | 0611 |
| Statistics | 0463 |
| Applied Sciences | |
| Applied Mechanics | 0346 |
| Computer Science | 0984 |

| | |
|----------------------------|------|
| Engineering | |
| General | 0537 |
| Aerospace | 0538 |
| Agricultural | 0539 |
| Automotive | 0540 |
| Biomedical | 0541 |
| Chemical | 0542 |
| Civil | 0543 |
| Electronics and Electrical | 0544 |
| Heat and Thermodynamics | 0348 |
| Hydraulic | 0545 |
| Industrial | 0546 |
| Marine | 0547 |
| Materials Science | 0794 |
| Mechanical | 0548 |
| Metallurgy | 0743 |
| Mining | 0551 |
| Nuclear | 0552 |
| Packaging | 0549 |
| Petroleum | 0765 |
| Sanitary and Municipal | 0554 |
| System Science | 0790 |
| Geotechnology | 0428 |
| Operations Research | 0796 |
| Plastics Technology | 0795 |
| Textile Technology | 0994 |

PSYCHOLOGY

| | |
|---------------|------|
| General | 0621 |
| Behavioral | 0384 |
| Clinical | 0622 |
| Developmental | 0620 |
| Experimental | 0623 |
| Industrial | 0624 |
| Personality | 0625 |
| Physiological | 0989 |
| Psychobiology | 0349 |
| Psychometrics | 0632 |
| Social | 0451 |



UNIVERSITY OF ALBERTA

RELEASE FORM

NAME OF AUTHOR: Vincent Jeffrey Pizio
TITLE OF THESIS: Microphone Positioning System for M.E.A.N.U.
DEGREE: Master of Science
YEAR THIS DEGREE GRANTED: Fall 1994

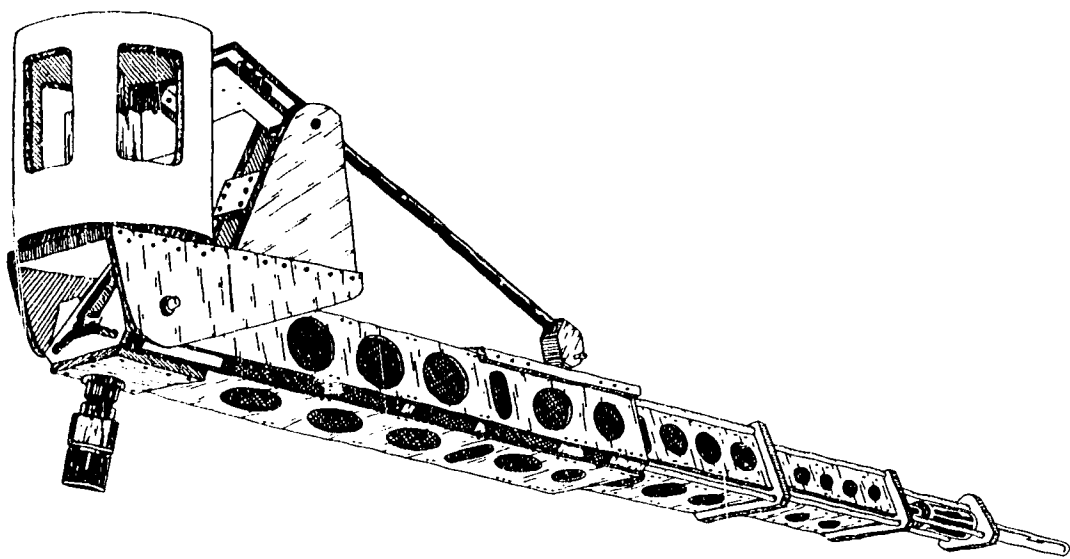
Permission is hereby granted to the University of Alberta Library to reproduce single copies of this thesis and to lend or sell such copies for private, scholarly or scientific research purposes only.

The author reserves all other publication and other rights in association with the copyright in the thesis, and except as hereinbefore provided neither the thesis nor any substantial portion thereof may be printed or otherwise reproduced in any material form whatsoever without the author's prior written permission.


Vincent J. Pizio

3223 15 St. N.W.
Calgary, Alberta
T2L 0J9

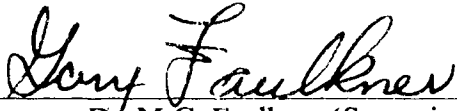
Date: 29/09/15




UNIVERSITY OF ALBERTA

FACULTY OF GRADUATE STUDIES AND RESEARCH

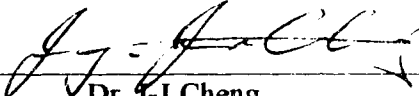
The undersigned certify that they have read, and recommend to the Faculty of Graduate Studies and Research for acceptance, a thesis entitled **Microphone Positioning System for M.E.A.N.U.** submitted by **Vincent Jeffrey Pizio** in partial fulfillment for the degree of **Master of Science.**



Dr. M.G. Faulkner (Supervisor)



Dr. A.W. Lipsett



Dr. J-J Cheng

Date: 1994/09/15

For Kim, and my parents ...

ABSTRACT

Testing performed in the reverberation chambers at the University of Alberta's Mechanical Engineering Acoustics and Noise Unit (M.E.A.N.U.) is sensitive to variations in the air temperature and relative humidity. The errors that these variations induce in the test results are compounded by the practise of entering the chambers periodically to reposition the microphone.

As a result, the implementation of an automated microphone positioning system was undertaken. The objective of this thesis project was to evaluate previous design work, complete the design to the implementation stage, and evaluate the performance of the manipulator.

The configuration selected was a spherical geometry manipulator, consisting of a telescopic boom capable of rotation through two orthogonal axes. Suspended from the ceiling, the manipulator's range of motion is such that the microphone can be positioned to 90% of the legal testing positions based on A.S.T.M., I.S.O., and A.N.S.I. standards, with an accuracy of ± 15 mm.

The main performance objective was that the manipulator be capable of moving to any position in the chamber in under thirty seconds. As installed, the positioning time is limited by the performance of the telescopic boom, which requires just under a minute to move through its full range of motion. Also, depending on the position selected, the azimuth rotation of the manipulator may require a full minute for its range of motion. Although alterations could be made to these axes, the performance of the manipulator is acceptable for its intended purpose.

ACKNOWLEDGEMENTS

I would like to acknowledge the efforts of Blaine Sawchuk, who started this project and provided valuable ideas and suggestions throughout, as well as the Machine Shop technicians, Don Fuhr, Al Muir, Max Schubert, Tony Van Straten, and Albert Yuen for their advice and knowledge during the design stage, and in the accomplishment of fabricating the manipulator. I would also like to sincerely thank Dr. M.Gary Faulkner and Gerald Kiss for their efforts and guidance throughout my involvement with this project.

In addition, I would like to thank the many people, especially Victor del Valle and Don Raboud, for their help and personal sacrifices during the myriad dismantling and reassembly processes, and during the moves to different locations.

CONTENTS

LIST OF TABLES

LIST OF FIGURES

LIST OF NOMENCLATURE

| | | |
|----------|------------------------------------|-----------|
| 1 | INTRODUCTION | 1 |
| 1.1 | BACKGROUND INFORMATION | 1 |
| 1.2 | DESIGN CONSIDERATIONS | 4 |
| 1.3 | EXISTING METHODS | 5 |
| 1.3.1 | NATIONAL RESEARCH COUNCIL | 5 |
| 1.3.2 | BRUEL & KJAER, DENMARK | 7 |
| 1.3.3 | CONTINUOUS PATH AVERAGING | 8 |
| 1.4 | ALTERNATIVE DESIGN CONSIDERATIONS | 10 |
| 1.4.1 | SUSPENSION CABLE NETWORK | 10 |
| 1.4.2 | ARTICULATED LINKAGE | 12 |
| 1.4.3 | TELESCOPIC BOOM | 13 |
| 1.5 | DESIGN OBJECTIVES | 16 |
| 1.6 | THESIS OUTLINE | 16 |
| 2 | MECHANICAL COMPONENT DESIGN | 18 |
| 2.1 | TELESCOPIC BOOM | 19 |
| 2.1.1 | RETRACTED BOOM LENGTH | 19 |
| 2.1.2 | DEPLOYED BOOM LENGTH | 20 |
| 2.1.3 | MEMBER LENGTH | 21 |
| 2.1.4 | BOOM CROSS-SECTION | 23 |

| | | |
|------------|--------------------------------------|-----------|
| 2.1.5 | DYNAMIC MODELLING | 26 |
| 2.1.6 | MEMBER LOADING | 32 |
| 2.1.7 | SUPPORT BEARING SELECTION | 39 |
| 2.1.8 | SUPPORT BEARING DETAILS | 43 |
| 2.1.9 | DYNAMIC MEMBER STRESSES | 45 |
| 2.1.10 | STATIC DEFLECTIONS | 49 |
| 2.1.11 | CABLE ACTIVATION SYSTEM | 54 |
| 2.1.12 | CABLE TENSION | 59 |
| 2.1.13 | ACTIVATION TORQUE | 64 |
| 2.1.14 | EFFECTIVE INERTIA | 66 |
| 2.2 | BOOM ELEVATION | 68 |
| 2.2.1 | SUPPORT REACTIONS | 68 |
| 2.2.2 | LINEAR ACTUATOR LOADING | 70 |
| 2.2.3 | BALL BEARING SCREW | 74 |
| 2.2.4 | ACTIVATION TORQUE | 76 |
| 2.2.5 | EFFECTIVE INERTIA | 76 |
| 2.2.6 | ELEVATION TRUNNION SUPPORT FLANGES | 79 |
| 2.3 | AZIMUTH ROTATION | 84 |
| 2.3.1 | SUPPORT REACTIONS | 84 |
| 2.3.2 | BOOM TRUNNION SUPPORT FLANGES | 86 |
| 2.3.3 | AZIMUTH SLEWING RING | 88 |
| 2.3.4 | MANIPULATOR MOUNTING STRUCTURE | 91 |
| 2.4 | AXIS ACTUATION | 93 |
| 2.4.1 | SELECTION CRITERIA | 94 |
| 2.4.2 | ACTUATOR DRIVE REDUCTIONS | 95 |
| 2.4.3 | HARMONIC DRIVE REDUCERS | 97 |
| 2.4.4 | REDUCTION RATIOS AND MOTOR SELECTION | 100 |
| 2.4.4.1 | Elevation Axis | 100 |

| | | |
|------------|---|------------|
| 2.4.4.2 | Azimuth Axis | 103 |
| 2.4.4.3 | Boom Deployment Axis | 104 |
| 2.4.5 | POSITIONING RESOLUTION | 105 |
| 3 | CONTROL SYSTEM & PERFORMANCE | 106 |
| 3.1 | CONTROL SYSTEM ELEMENTS | 106 |
| 3.1.1 | CONTROLLER | 107 |
| 3.1.2 | INDEXER | 108 |
| 3.1.3 | MOTOR AND MOTOR DRIVE | 109 |
| 3.1.4 | END - OF - TRAVEL SWITCHES | 110 |
| 3.2 | SYSTEM OPERATION | 111 |
| 3.3 | SYSTEM PERFORMANCE | 112 |
| 3.3.1 | POSITIONING TIME | 112 |
| 3.3.2 | POSITIONING ACCURACY | 114 |
| 3.3.3 | MANIPULATOR STATIC DEFLECTION | 122 |
| 3.3.4 | OVERALL PERFORMANCE | 123 |
| 3.3.4.1 | Azimuth Performance | 123 |
| 3.3.4.2 | Elevation Axis | 124 |
| 3.3.4.3 | Deployment Axis | 125 |
| 3.4 | OVERALL EXPENSE | 127 |
| 4 | CONCLUDING REMARKS | 128 |
| 4.1 | SUMMARY | 128 |
| 4.2 | RECOMMENDATIONS | 129 |
| | REFERENCES | 131 |
| A | ACCELERATION & REACTION COMPONENTS | 133 |
| | DYNAMIC LOADING | 133 |
| | STATIC LOADING | 135 |

| | | |
|----------|---|-----|
| B | MEMBER CROSS - SECTION PROPERTIES | 137 |
| C | SHEAR FORCES & BENDING MOMENTS | 145 |
| | DYNAMIC LOADING | 145 |
| | STATIC LOADING | 146 |
| D | PC-23 DRIVER ROUTINE | 152 |
| E | SAMPLE COMMAND FILE | 169 |
| F | POSITIONING ACCURACY DATA | 173 |

TABLES

| | | |
|--------------------------|--|------------|
| <u>Table 2.1:</u> | Axis Accelerations | 28 |
| <u>Table 2.2:</u> | Summary of Member Support Reactions and Directions | 39 |
| <u>Table 2.3:</u> | Bearing Loads and Load Correction Factors for Boom Support Bushings | 42 |
| <u>Table 2.4:</u> | Summary of Dynamic Loading Safety Factors | 48 |
| <u>Table 2.5:</u> | Summary of Axis Actuation Characteristics | 96 |
| <u>Table 2.6:</u> | Full Step Axis Resolutions | 105 |
| | | |
| <u>Table 3.1:</u> | Required Motor Speeds | 112 |
| <u>Table 3.2:</u> | Microstepping Axis Resolutions | 116 |
| <u>Table 3.3:</u> | Axis and Overall Manipulator Positioning Accuracy After Eight Positions | 121 |
| <u>Table 3.4:</u> | List of Expenses | 127 |
| | | |
| <u>Table A.1:</u> | Radial Position of Member Mass Centers | 133 |
| <u>Table A.2:</u> | Individual Member Acceleration Components | 134 |
| <u>Table A.3:</u> | Individual Member Masses and Inertias as Constructed | 134 |
| <u>Table A.4:</u> | Dynamic Support Reactions | 135 |
| <u>Table A.5:</u> | Static Support Reaction Components | 136 |
| | | |
| <u>Table C.1:</u> | Summary of Dynamic Loading on Individual Members | 145 |
| <u>Table C.2:</u> | Member Section Properties | 146 |
| | | |
| <u>Table F.1:</u> | Apparent Homing Error in Microsteps for the First Trial | 173 |
| <u>Table F.2:</u> | Apparent Homing Error in Microsteps for the Second Trial | 174 |

FIGURES

| | | |
|----------------------------|--|-----------|
| <u>Figure 1.1:</u> | M.E.A.N.U. Facility Schematic | 2 |
| <u>Figure 1.2:</u> | Available Testing Volume for Small Chamber | 5 |
| <u>Figure 1.3:</u> | Cylindrical Geometry Manipulator | 6 |
| <u>Figure 1.4:</u> | Suspended Track | 7 |
| <u>Figure 1.5:</u> | Continuous Path Averaging | 9 |
| <u>Figure 1.6:</u> | Suspension Cable Network | 10 |
| <u>Figure 1.7:</u> | Alternative Cable Origin Limitations | 11 |
| <u>Figure 1.8:</u> | Articulated Linkage Manipulator | 12 |
| <u>Figure 1.9:</u> | Spherical Geometry Manipulator | 14 |
| <u>Figure 1.10:</u> | Boom Extension/Retraction Scheme | 14 |
| <u>Figure 2.1:</u> | Major Manipulator Components | 18 |
| <u>Figure 2.2:</u> | Available Test Volume Based on Region Shape | 20 |
| <u>Figure 2.3:</u> | Required Boom Extension | 21 |
| <u>Figure 2.4:</u> | Linear Guidance Shafts and Bushing Arrangement on Second Member | 24 |
| <u>Figure 2.5:</u> | Alternative Member Cross-Sections | 25 |
| <u>Figure 2.6:</u> | Acceleration Profile | 26 |
| <u>Figure 2.7:</u> | Velocity Profile | 27 |
| <u>Figure 2.8:</u> | Global Spherical Coordinate System | 28 |
| <u>Figure 2.9:</u> | Free Body Diagram of Most Extended Member | 32 |
| <u>Figure 2.10:</u> | Alternate Free Body Diagram of First Member | 34 |
| <u>Figure 2.11:</u> | Free Body Diagram of Subsequent Member | 38 |

| | | |
|----------------------------|--|-----------|
| <u>Figure 2.12:</u> | Load Correction Factor for Linear Guidance Rails | 40 |
| <u>Figure 2.13:</u> | Load Correction Factor Based on Service Travel Life | 41 |
| <u>Figure 2.14:</u> | Thomson Super Ball Bushing Pillow Block Assemblies as Supplied | 43 |
| <u>Figure 2.15:</u> | Schematic of Bearing Pillow Block and Support Shafts and Rails | 44 |
| <u>Figure 2.16:</u> | Cross-Section of First Member | 45 |
| <u>Figure 2.17:</u> | Shear Force and Bending Moment Diagrams for Transverse Dynamic Loading on First Member | 47 |
| <u>Figure 2.18:</u> | Static Deflection Model | 49 |
| <u>Figure 2.19:</u> | Deformed Boom Slope with Boundary Conditions Applied for Loading Due to Member Weight | 52 |
| <u>Figure 2.20:</u> | Boom Deflection with Boundary Conditions Applied for Loading Due to Member Weight | 52 |
| <u>Figure 2.21:</u> | Deformed Boom Slope with Boundary Conditions Applied for Loading Due to Member Weight and Payload | 53 |
| <u>Figure 2.22:</u> | Boom Deflection with Boundary Conditions Applied for Loading Due to Member Weight and Payload | 53 |
| <u>Figure 2.23:</u> | Cable Activation System Between First and Second Members | 54 |
| <u>Figure 2.24:</u> | Cable Activation System Between First, Second and Third Members | 55 |
| <u>Figure 2.25:</u> | Cross-Section of 7 x 7 Cable | 56 |
| <u>Figure 2.26:</u> | Schematic of Cable Tensioning Element | 59 |
| <u>Figure 2.27:</u> | Free Body Diagram of First Member | 60 |
| <u>Figure 2.28:</u> | Free Body Diagram of Second Member | 60 |
| <u>Figure 2.29:</u> | Free Body Diagram of Third Member | 61 |

| | |
|--|-----|
| <u>Figure 2.30:</u> Schematic of Cable Arrangement With and Without the Fourth Deployment Cable | 62 |
| <u>Figure 2.31:</u> Free body Diagram of Drum Assembly | 65 |
| <u>Figure 2.32:</u> Free Body Diagram of Last (Fixed) Member | 69 |
| <u>Figure 2.33:</u> Elevation Assembly | 70 |
| <u>Figure 2.34:</u> Elevation Assembly Geometry | 71 |
| <u>Figure 2.35:</u> Simplified Boom Geometry | 73 |
| <u>Figure 2.36:</u> Axial Screw Loading | 74 |
| <u>Figure 2.37:</u> Effective Boom Inertia for Elevation Axis | 79 |
| <u>Figure 2.38:</u> Trunnion Support Flange Loading | 79 |
| <u>Figure 2.39:</u> Azimuth Support Couple | 85 |
| <u>Figure 2.40:</u> Boom Trunnion Flange Loading | 86 |
| <u>Figure 2.41:</u> Azimuth Slewing Ring Loading | 89 |
| <u>Figure 2.42:</u> Dodecahedral Mounting Structure Details | 91 |
| <u>Figure 2.43:</u> Mounting Structure As Installed | 92 |
| <u>Figure 2.44:</u> Axis Actuator Locations | 94 |
| <u>Figure 2.45:</u> Stepper Motor Torque vs. Speed Characteristics | 95 |
| <u>Figure 2.46:</u> Harmonic Drive Components | 98 |
| <u>Figure 2.47:</u> Principle of Harmonic Drive Operation | 99 |
| <u>Figure 2.48:</u> Performance Curve for Compumotor S83 - 135 Stepper Motor | 101 |
| <u>Figure 2.49:</u> Performance Curve for Compumotor S83 - 93 Stepper Motor | 102 |
| <u>Figure 2.50:</u> Performance Curve for Compumotor S106 - 178 Stepper Motor | 103 |

| | | |
|---------------------------|--|------------|
| <u>Figure 3.1:</u> | Motion Control System Elements | 106 |
| <u>Figure 3.2:</u> | Indexer System Diagram | 109 |
| <u>Figure 3.3:</u> | Apparent Home Position for Azimuth Axis - First Trial | 117 |
| <u>Figure 3.4:</u> | Apparent Home Position for Azimuth Axis - Second Trial | 118 |
| <u>Figure 3.5:</u> | Apparent Home Position for Elevation Axis - Both Trials | 119 |
| <u>Figure 3.6:</u> | Apparent Home Position for Deployment Axis - Both Trials | 120 |
| <u>Figure B.1:</u> | Second Member Cross-Sections | 137 |
| <u>Figure B.2:</u> | Bearing Shaft and Support Rail Assembly Geometry and Approximation | 138 |
| <u>Figure B.3:</u> | Schematic of Fifth Member Minimum Cross-Section | 143 |
| <u>Figure C.1:</u> | Shear Force and Bending Moment Diagrams for Transverse Dynamic Loading on First Member | 147 |
| <u>Figure C.2:</u> | Shear Force and Bending Moment Diagrams for Transverse Dynamic Loading on Second Member | 148 |
| <u>Figure C.3:</u> | Shear Force and Bending Moment Diagrams for Transverse Dynamic Loading on Third Member | 149 |
| <u>Figure C.4:</u> | Shear Force and Bending Moment Diagrams for Transverse Dynamic Loading on Fourth Member | 150 |
| <u>Figure C.5:</u> | Shear Force and Bending Moment Diagrams for Transverse Dynamic Loading on Fifth Member | 151 |

NOMENCLATURE

| | |
|--------------------|--|
| $\alpha(r)$ | slope of the elastic curve |
| A | area |
| $a(t)$ | acceleration function |
| a_ϕ | transverse acceleration in elevational plane |
| a_{\max} | absolute magnitude of acceleration function |
| a_θ | transverse acceleration in azimuthal plane |
| a_r | radial acceleration component |
| β | an angle defining the boom member cross-sectional geometry |
| C | constants of integration, in general |
| Δr | incremental boom member extension |
| δ | axis step resolution |
| $\delta(r)$ | deflection of the elastic curve |
| d_{cable} | cable diameter |
| ϵ | mechanical efficiency |
| E | Young's Modulus |
| Φ | diameter |
| ϕ | boom elevation; rotation in a vertical plane |
| F | axial screw force |
| g | acceleration due to gravity |
| h | drum height |
| I | mass moment of inertia, in general |

| | |
|--------------|---|
| I_{ϕ} | mass moment inertia about elevation axis |
| I_{θ} | mass moment of inertia about azimuth axis |
| K | constant of proportionality based on cable type and diameter |
| K_H | load correction factor based on shaft hardness |
| K_L | load correction factor based on service travel life |
| k | constant related to diameter of cable component wire; joint stiffness |
| λ | wavelength of the center frequency of the lowest octave band analyzed |
| L | length, in general |
| L_{max} | length of the telescopic boom when fully deployed |
| L_{mem} | nominal length of the boom element members |
| L_{retr} | retracted length of the telescopic boom |
| M | bending moment, general |
| M_{θ} | boom support couple |
| N | factor of safety |
| n | number of actuator rotations for full range motions, in general |
| n_{mem} | number of boom element members |
| ol | overlap fraction between subsequent members |
| θ | boom azimuth; rotation in a horizontal plane |
| Q | area correction factor based on cable type |
| ρ | density; radius |
| R | support reaction, in general; drive reduction ratio |
| R_{ϕ} | support reaction in elevation plane |
| R_i | inboard reaction; inside radius |

| | |
|------------|---|
| R_o | outboard reaction; outside radius |
| R_θ | support reaction in azimuthal plane |
| R_r | support reaction in radial direction |
| r | radius; boom deployment length |
| σ | normal stress |
| τ | length of acceleration interval |
| T | cable tension; torque |
| t | time, joint thickness |
| V | shear force |
| $v(t)$ | velocity function |
| v_{max} | absolute magnitude of velocity function |
| ω | rotational frequency; distributed loading |
| W | distributed loading |
| y | distance to neutral bending axis |

INTRODUCTION

1

1.1 BACKGROUND INFORMATION

The University of Alberta's Mechanical Engineering Acoustics and Noise Unit (M.E.A.N.U) is capable of determining acoustical properties of building materials, wall assemblies, and machinery. Such measurements as sound absorption, sound transmission loss, and sound power are made using either one, or a pair of reverberation chambers along with the related electronic equipment. A facility schematic is shown in Figure 1.1. The M.E.A.N.U. reverberation chamber suite consists of two rooms, which have been constructed as essentially separate buildings on separate foundations, and are juxtaposed to accommodate a test window that can connect the two chambers.

Each chamber also contains a number of diffuser panels constructed of standard 4' x 8' x 1/2" plywood. The purpose of these panels is to provide a constantly changing room geometry, thereby tending to inhibit the formation of standing waves in the sound field. The panels are hung at random angles about the chamber and are kept moving by a network of ropes connected to a rotating bell crank. The bell crank is located at the ceiling, at approximately the center of the chamber.

For most of the testing performed using the reverberation chamber pair, the sound pressure level (S.P.L.) is measured using a microphone at several positions in one or both of the chambers. Although the precise microphone positions are not parameters of these

measurements, International Organization for Standardization (I.S.O.)[1], American Society for Testing and Materials (A.S.T.M.)[2] and American National Standards Institute (A.N.S.I.)[3] standards suggest the use of multiple microphone positions as well as specifying minimum distances from major surfaces in the chamber, minimum distance from test specimens, and minimum distances between subsequent microphone positions. Typically, for testing performed at M.E.A.N.U., between six and eight microphone positions are sampled.

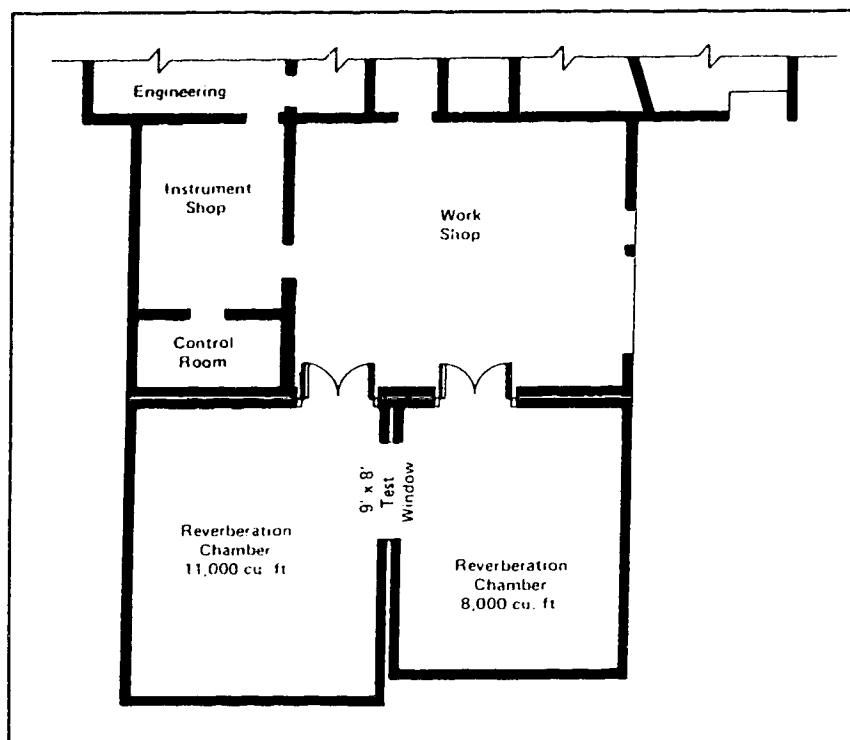


Figure 1.1: M.E.A.N.U. Facility Schematic

In the past, after a position had been tested, the microphone was repositioned manually. Depending on test conditions, it may take up to 45 minutes for the measured S.P.L.'s to converge to a specified confidence interval. Since there are no facilities to control the environmental conditions within the chambers, the temperature and humidity in the

environment outside the reverberation chambers, in either the connecting workshop or the chamber wall exposed to the outside elements, may change considerably over this measurement period. Also, entering the chambers allows interchange of air from the workshop area into the test volume. These changes can only be accounted for in some circumstances and generally result in an increase in the uncertainty of the test results. Although this practice is acceptable within limits by current I.S.O., A.S.T.M., and A.N.S.I. standards, advances in the quality and precision of the testing equipment have increased the significance that these fluctuations have on the uncertainty of the test results. Anticipated modifications to the testing standards may increase the required number of microphone sampling positions, thereby compounding the effect of these environmental variations.

An obvious solution would entail the installation of several microphones and preamps in each chamber. The different positions could be sampled through the use of a multiplexer. For full flexibility this system would require a minimum of 16 microphones and preamps and a 16-channel multiplexer to accommodate eight test positions in each chamber.

For sound power measurements, microphone positions are chosen around the test specimen. As these positions may vary due to specimen size and ancillary connections such as plumbing, ducts, electrical connections, or supports, installation of microphones in fixed positions would not be feasible. Microphones would have to be mounted on microphone stands located on the floor and positioned manually.

Another consideration is the cost of purchasing and maintaining several microphones and preamps. The cost of a microphone and preamp of the type used at M.E.A.N.U. are approximately \$3000 each and \$150 to maintain for a year. For the number of microphones

required to implement this scheme, this would amount to a fixed cost of \$48,000 and an annual cost of \$2400. The fact that these microphones may need to be replaced from time to time would increase the cost of upkeep for such a system.

A system similar to this was set up for a time at the National Research Council[4] but was discontinued. The time required to calibrate each microphone and preamp was sometimes as high as eight hours. This would greatly reduce productivity and would increase the cost of performing tests.

It is for this reason that the design and implementation of an automated microphone positioning system were undertaken. The system would be integrated with present software to move the microphone to a new position once the readings had converged at the current position.

1.2 DESIGN CONSIDERATIONS

A.N.S.I. and A.S.T.M. standards require that the test positions are no closer to any major room surface than either half the wavelength of the center frequency of the lowest octave band (λ) or 1 m, whichever is less. For testing done at M.E.A.N.U., λ is approximately 3.4 m for 100 Hz, so the limiting constraint is that the testing positions are no closer than 1 m from major room surfaces. The volume that conforms to these restrictions is shown for the small chamber in Figure 1.2. It would be desirable that the manipulator be capable of placing the microphone anywhere within this acceptable volume to maximize the number of valid microphone test positions. Also, the range of the manipulator device should not be severely hindered by the presence of the panels and their associated activation ropes.

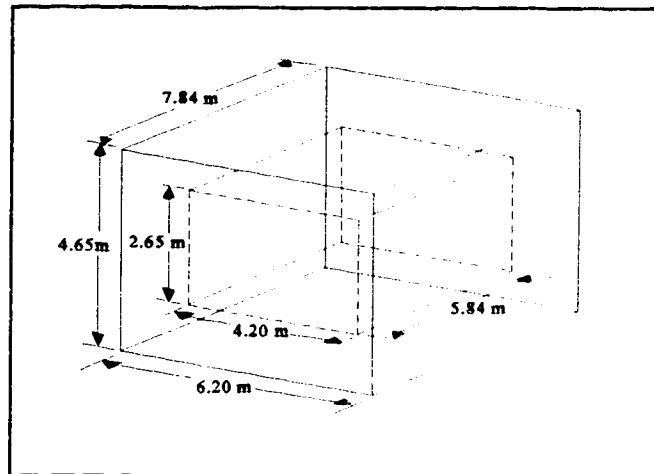


Figure 1.2: Available Testing Volume for Small Chamber

During sound power and sound absorption measurements, it is normally necessary to install test specimens or machinery components in the chamber. These components are typically located on the floor, in the center of the chamber. Therefore, it is important that no permanent component of the manipulator system occupies this volume. This consideration reasonably imposes a constraint that the appropriate manipulator be wall or ceiling mounted.

1.3 EXISTING METHODS

Several automated microphone manipulation systems are currently in use at other facilities equipped with reverberation chambers. It is of interest to consider the advantages and disadvantages of these systems before discussing the current system developed for M.E.A.N.U.

1.3.1 NATIONAL RESEARCH COUNCIL (CANADA)

At the Institute for Research in Construction at the National Research Council[4], in Ottawa, the system used, as illustrated in Figure 1.3, is a cylindrically based robotic

manipulator. The azimuth position (position in the horizontal plane) is achieved by an I-beam with one end that pivots about the center of the chamber. The radial position is reached by a motorized carriage that runs on the lower flange of the I-beam. The depth of the microphone position could be attained by suspending the microphone from a cable with a motorized reel, or an extensible member such as a ball-screw or hydraulic cylinder.

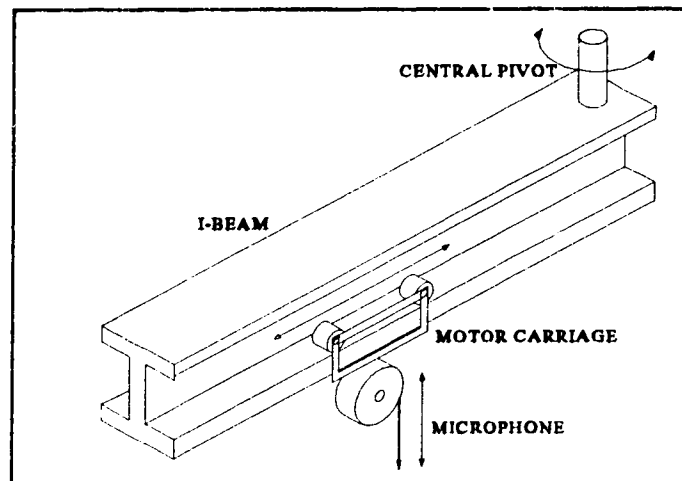


Figure 1.3: Cylindrical Geometry Manipulator

This method is attractive in its simplicity. There are very few moving components, and those that do are quasi-static in nature. The gantry crane is driven by a motor at its ceiling pivot. The motor carriage must overcome its own inertia and that of the microphone and vertical positioning device, but only moves in a horizontal plane (neglecting deflections in the gantry I-beam). Therefore, the carriage actuator has low torque demands and a low performance stepper or servo motor would suffice. The microphone positioning device works in a vertical plane and must therefore overcome its own frictional losses and the acceleration due to gravity.

One of the limiting factors is the allowable length of the gantry beam. At N.R.C. the

diffuser vane configuration is a rotating column at the center of the chamber, and the beam length is limited only by the smallest horizontal dimension of the chamber. This could give the N.R.C. positioning flexibility over the range suggested in A.N.S.I, A.S.T.M., and I.S.O. standards. If a similar system was applied at M.E.A.N.U. the beam length would be further limited by the wall mounted diffuser panels and further restrict the volume in which the system could be used.

1.3.2 BRUEL & KJAER, DENMARK

A method that may have been used in the past by Bruel & Kjaer[5], as shown in Figure 1.4, involves the use of a cart that moves around a suspended track that spirals out from the center of the chamber. When the radius and azimuth position are acceptable, the microphone is lowered on a cable from the cart to the desired height.

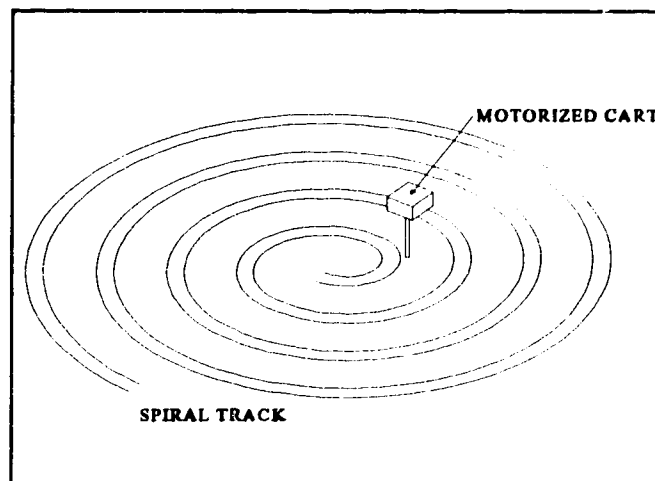


Figure 1.4: Suspended Track

This method is very simple and easy to control, as the only actuators required are one to move the cart on the track, and another to lower and raise the microphone. The motion of the cart would be best suited for control with a stepper motor, where the system could simply

output the number of steps to the new position and manipulate both the azimuth and radial positions.

A limiting factor to the resolution of radial positioning is the track width. For a given azimuth the radial resolution would be the track width and the distance between consecutive track loops. Although with a narrow, closely looped track the radial resolution may be acceptable, microphone positions within the available testing volume are limited.

Once again, a drawback to the application of a positioning system of this type at M.E.A.N.U. is the position of the diffuser panels. The effect would be to limit accessibility to the available testing volume. This is compounded by the radial resolution of the track.

A further problem with this type of system would be the management of the control and microphone signal cables. One method would be to have the cables follow the cart along the track and then reel back up as the cart reverses direction back to the center of the chamber. This would result in lengthy cable runs, which could greatly affect cart performance and also the actual test results. Another method would be to have the cable run out to the cart radially from the center of the spiral. However, to prevent twisting, this would require slip rings in the cable connections that could result in electrical noise in the system, thus decreasing its performance. A compromise would be to supply the microphone cables to the cart in one of the above methods, install a battery on the cart and control its motion by remote control through FM radio signals.

1.3.3 CONTINUOUS PATH AVERAGING

As an alternative to numerous fixed positions for sampling, another acceptable method is the use of a constantly rotating boom to which the microphone is attached. Rather than

sampling at discrete positions, this method samples on a continuous path and averages the measurement in both time and space. A commercially available system from Bruel & Kjaer[5] is shown in Figure 1.5. M.E.A.N.U. was originally equipped with rotating booms mounted on the ceilings of each of the chambers, which swept a circle of up to 10' in diameter, in a plane inclined at 5 degrees to the horizontal. These systems, were removed as the circular path violated distance and clearance criteria during some tests.

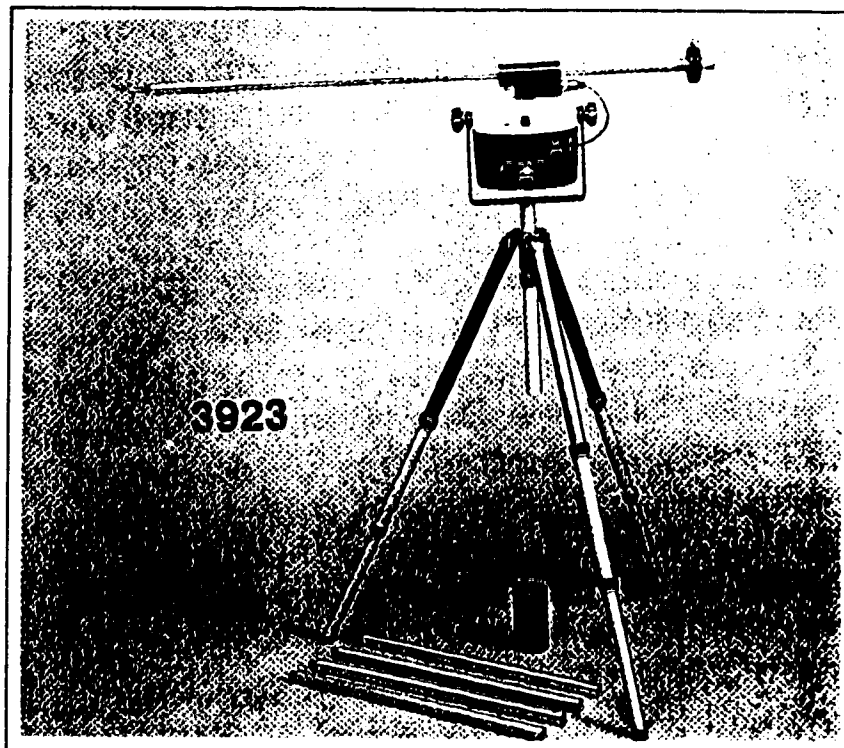


Figure 1.5: Continuous Path Averaging

The measurements from a rotating boom are acceptable only by performing a complete fixed microphone survey of a chamber and comparing averaged results to that of the boom. The confidence intervals obtained by fixed position tests along the boom path are applied to the boom average data. The chamber must be requalified annually or after any

major changes. This qualification procedure is performed with the chamber empty and does not account for statistical changes when a specimen is introduced into the chamber.

1.4 ALTERNATIVE DESIGN CONSIDERATIONS

As well as considering the methods described above, several alternative designs were evaluated based on feasibility, construction, and practicality. These included articulated linkages, telescopic booms, and a suspension cable network.

1.4.1 SUSPENSION CABLE NETWORK

The method illustrated in Figure 1.6 has been named the Suspension Cable Network (S.C.N.). As the name implies, the microphone would be suspended from cables originating in each corner of the room. The cartesian coordinates and height from the floor would be controlled by motors that control the length of each cable.

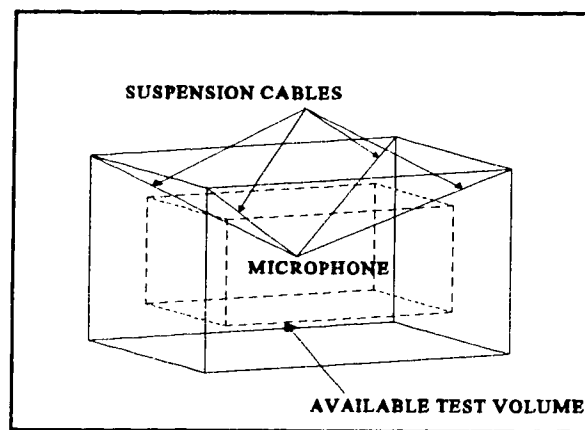


Figure 1.6: Suspension Cable Network

Although the changes in the linear cable weight and microphone mass would require changes in the software controlling such a system, the algorithm used would be straight forward and simple to apply. The input to the software could be as simple as the 3-D cartesian

coordinates of the desired microphone position. The system could attain any position in the rectangle inscribed by the cable origins, and any height between the floor and the cable origin height. In the illustrated case, the microphone could be positioned to virtually any location in the chamber.

The major drawback to this design is that the cable origins, as shown in Figure 1.6, would interfere with the placement of the diffuser panels, which are suspended from the ceiling, roughly diagonal across each corner of the chamber. The cables might also encounter the diffuser activation ropes.

To alleviate this constraint, placement of the cable origins at the mid-span of each side wall would result in attainable microphone positions, in relation to the available test volume, as shown in Figure 1.7. As shown, this limits accessibility to the available testing volume and is not desirable. Another concern with this solution is its applicability in the large reverberation chamber. Due to placement of diffuser panels across two of the sidewalls, and

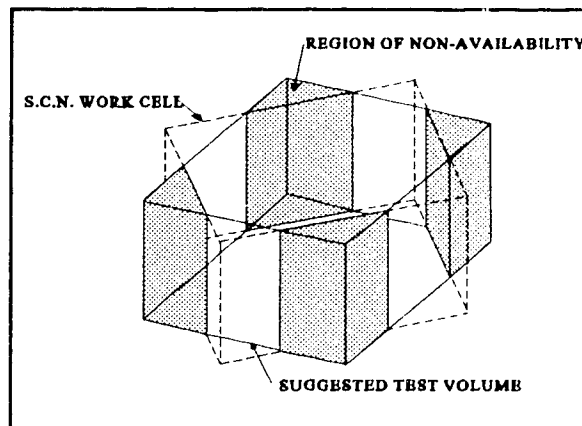


Figure 1.7: Alternative Cable Origin Limitations

each of the four corners, placement of cable origins at these locations would be inappropriate. Although the scope of this project is concentrated on the development of a positioning system for the small chamber only, it is desirable that the solution be appropriate for both chambers.

1.4.2 ARTICULATED LINKAGE

A common method of positioning an end effector in a 3-D work cell is the use of an articulated linkage manipulator. An articulating linkage consists of a series of members, connected by revolute joints. Figure 1.8 shows a common type of articulating linkage robot. The joint actuators may either be located directly at the joints, or located remotely, with a mechanical transmission system that delivers power to the joint.

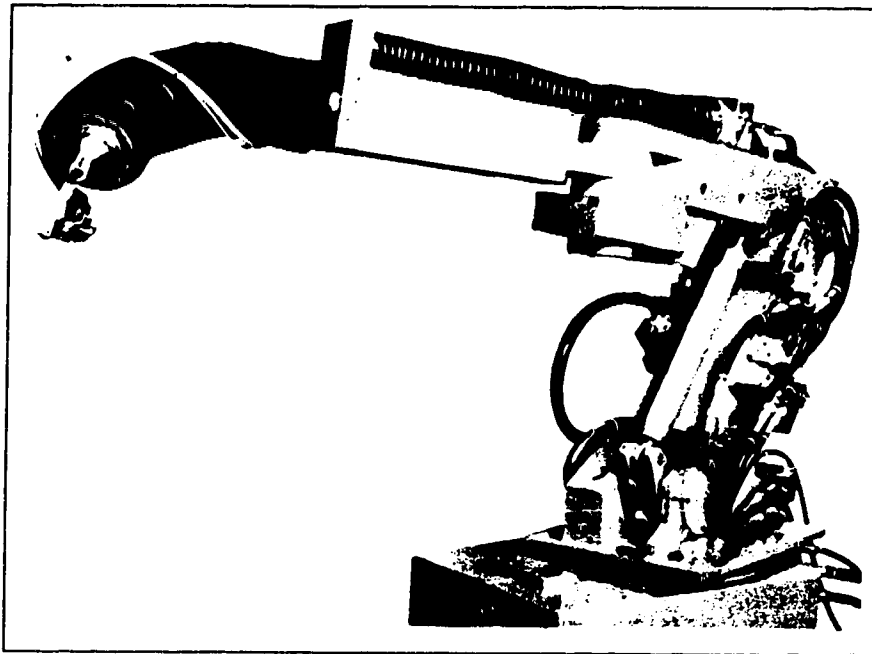


Figure 1.8: Articulated Linkage Manipulator

Serious consideration must be given to type of joint actuation chosen. Having individual actuators at the joints of a serial linkage results in a relatively heavy robot. The

weight of the actuator used to control one of the joints becomes a load for the actuator at the previous joint along the arm. Consequently, the required actuator torque and member cross section increase exponentially along the linkage.

The alternative would be to locate the actuators closer to the base of the linkage, and use cable systems or screws to transfer power to the member. This method can result in very complex cable or shafting systems and require a great deal of space to mount the actuators at the base, or more commonly on the first member, as the number of linkage members increases.

This design, by far, would provide the largest, and most desirable work cell, as the articulated linkage would be able to move around obstacles in the chamber. As the number of linkage members increases, the complexity of work cell also increases, giving a more unrestrained placement ability.

However, this same increase in placement ability corresponds to an increase in the complexity of the control algorithm. Not only must it ensure that the end effector never leaves the work envelope, but that none of the linkage members or joints leaves the work envelope.

1.4.3 TELESCOPIC BOOM

Another method of positioning, and the one adopted for M.E.A.N.U., uses linkage members with prismatic joints, such that each member has a single degree of freedom in relation to neighbouring members. The addition of a revolute base joint with two orthogonal axes of rotation results in the spherical geometry manipulator, shown in Figure 1.9.

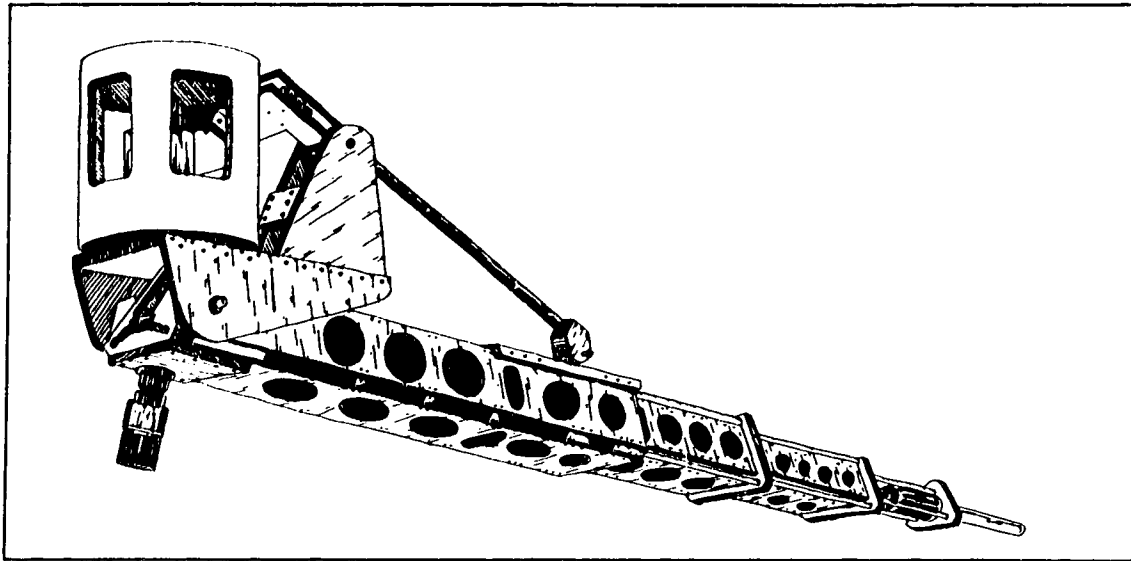


Figure 1.9: Spherical Geometry Manipulator

The positioning radius is achieved by a telescopic boom consisting of several members with progressively larger cross sections. This allows successive members to fit inside the previous one. Rather than actuating each member independently, a self-actuation scheme using cables, as shown in Figure 1.10, has been devised.

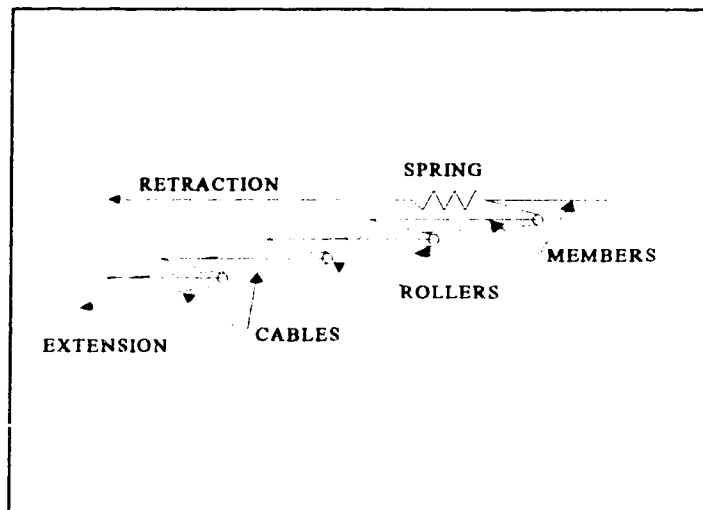


Figure 1.10: Boom Extension/Retraction Scheme

The two rotations of the base joint provide an azimuth control, and a boom elevation. The resulting control algorithm directly controls the robot in spherical coordinates. The work cell of such a manipulator is a hemispherical shell with the outer and inner radii corresponding to the maximum and minimum boom extensions.

While a drawback to this the design is the complex nature of the boom construction, the fact that the boom itself requires a single actuator is an advantage in terms of the control algorithm. The maximum and minimum boom extensions are designed such that the manipulator work cell meets or exceeds the available test volume. More importantly, it is not hindered by the presence of the diffuser panels as it requires unobstructed space only in the axial direction of the boom. Although this design does not provide the flexible work cell of an articulated linkage, it is acceptable in that it is not effected by obstacles above the end of the boom, as does the design used by the N.R.C. which was outlined in section 1.3.1.

The requirement of three actuators is an advantage over the articulated link method, which would require four actuators (for the manipulator shown in Figure 1.8). The telescopic boom construction is less complicated compared to the complexity required to actuate each member on an articulated linkage from a central location. Since the articulated linkage requires rotation between successive members, ultimately an activation torque must be applied. This could be accomplished by locating a servo at the joint, or supplying servo power to the joint through a power transmission system. These alternatives have drawbacks as discussed in Section 1.4.2. The relative motion required between the telescopic boom members requires that a force be applied to each member, however, this can be accomplished with a continuous cable activation system.

1.5 DESIGN OBJECTIVES

The objective of this project was to complete the fabrication and implement the microphone positioning system outlined in Section 1.4.3. Although the facility will require a manipulator in each chamber, the scope of this project included only the manipulator for the smaller of the two chambers.

The system should be able to attain any position in the chamber from any other position in under thirty seconds, as manual repositioning can be accomplished in this period. This requires that the boom extension and elevation axes be capable of moving through their range of motions in thirty seconds. The azimuth axis, or rotation in a horizontal plane, only has to rotate through a maximum of 180° , or half of its range of motion, to reach any point in the chamber from any starting point.

The manipulator should be capable of interfacing with the IBM® personal computer used to control the current testing equipment at M.E.A.N.U.. The control system should also allow for unattended command of the manipulator to permit a fully automated testing procedure in the future.

1.6 THESIS OUTLINE

Chapter 2 contains discussion and detailed analysis of the mechanical components. The chapter is divided into five major sections, one for each of the axes, and sections detailing the actuator selection and overall cost to construct the manipulator. Details include the determination of dynamic stresses and static deflections, as well as axis torque requirements.

Chapter 3 is a discussion of the final configuration of the system. Details of the control system will be presented, as well as the performance specifications. The test performance of the manipulator will be compared to the design estimates. Chapter 4 summarizes the design with comparisons to the design objectives.

As suggested in Chapter 1, the telescopic manipulator was chosen for the final design. The first assumption made before undertaking the actual design and fabrication of the mechanical components of the chosen manipulator system was that appropriate actuators would be available. It was further assumed that the actual size and type of actuator chosen would not affect the design of the major components.

In this chapter, details of the specific components of the manipulator are considered. The chapter is divided into five major sections, three of which deal with the major components of the manipulator indicated in Figure 2.1, and the final sections which include a discussion on the selection of the axis actuators, and an outline of the costs incurred.

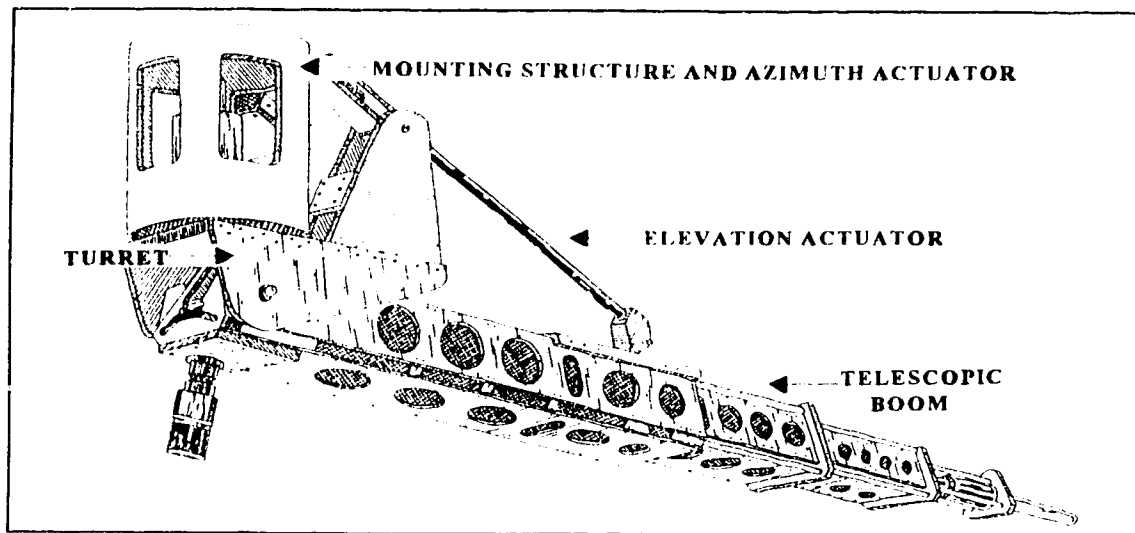


Figure 2.1: Major Manipulator Components

Structural elements of the telescopic boom and azimuth rotation were designed and fabricated as part of a previous project. The elements of this effort are included for completeness in the understanding of the final device, as well as an evaluation of the design of these components.

2.1 TELESCOPIC BOOM

The telescopic boom is by far the most complex component of the manipulator. This element was the portion where most of the design and fabrication effort occurred. Several factors, including retracted and deployed boom length, static and dynamic loading, and boom section geometry were considered before the final configuration was chosen.

2.1.1 RETRACTED BOOM LENGTH

As mentioned above, one of the design constraints required that the floor in the test chambers be kept free to accommodate specimens. As a result, the most appropriate mounting location for the manipulator was on the ceiling. Also, location of the manipulator origin in the center of the chamber would reduce the required length of the boom to reach all positions in the available test volume. Since this is also the location of the diffuser activation crank, a distance of 1m from the roof was allocated for a base structure.

The base structure was designed not only to provide a rigid mounting surface for the manipulator, but also allow for operation of the diffuser crank and activation ropes. With this structure in place, the origin of the manipulator is at the center of the top boundary of the testing volume as defined for sound power measurements. Mounting of the manipulator in this manner created a hemispherical region, of radius equal to that of the fully retracted boom, where it is not possible to attain positions with the manipulator.

To minimize this unavailable region, the retracted length of the boom should be as small as possible. This can be accomplished by decreasing the lengths of the individual boom sections and increasing the number of sections. While theoretically this increases the region serviced, it has an adverse effect on the weight and rigidity of the boom.

To estimate an acceptable minimum boom length, a nonavailable volume of less than 10% of the total available testing volume would not be significant. While the total available testing volume of the small chamber is 65 m^3 based on the cube-shaped region in Figure 2.2a, a more realistic volume, shown in Figure 2.2.b, is an elliptic cylinder. This shape avoids the diffuser panels and results in a total available volume of 51 m^3 . A hemisphere with 10% of this volume, or 5.1 m^3 , would therefore result in a minimum boom radius of 1.35 m.

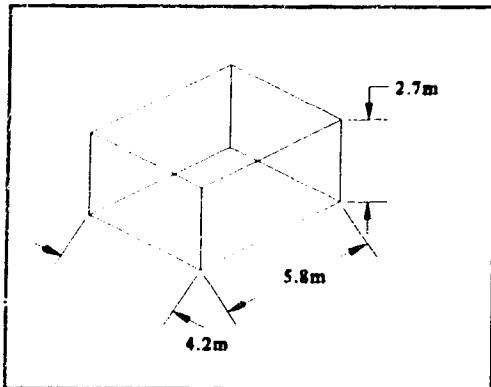


Figure 2.2.a: Available Test Volume Based on Cubic Region

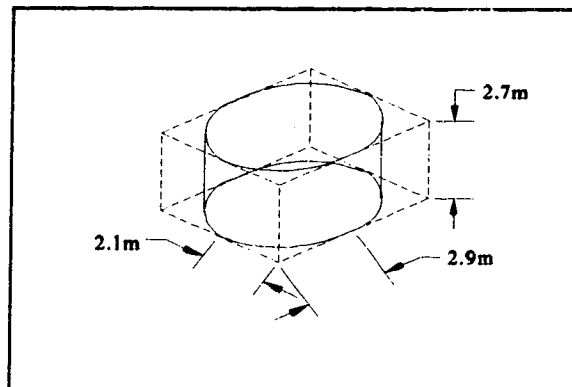


Figure 2.2.b: Available Test Volume Based on Elliptic Cylinder

2.1.2 DEPLOYED BOOM LENGTH

Figure 2.3 shows a schematic of the total available test volume for the small chamber without regard to the diffuser panels. This volume is based on sound power measurement standards that require a distance of 1m from major room surfaces. The minimum deployed

boom radius to attain all of the positions in this test volume is 4.46 m.

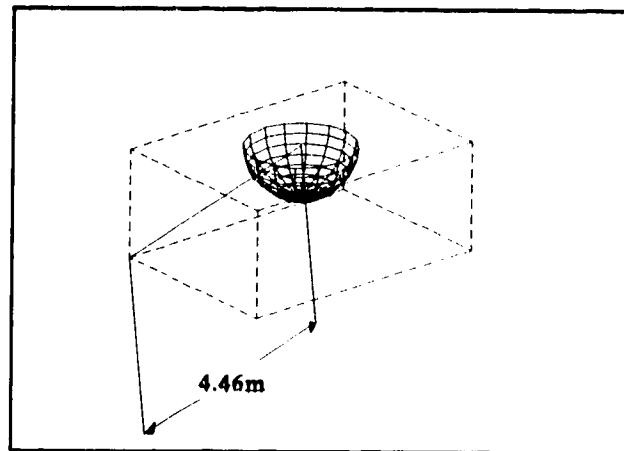


Figure 2.3: Required Boom Extension

The available test volume based on sound transmission and absorption is smaller than that based on sound power measurement standards, as a distance of 1.7 m from major room surfaces is required. In both cases, the presence of the diffuser panels further decreases the available test volume as a minimum distance of 0.5 m from the panels is required. The present configuration of the diffuser panels is such that the specified minimum deployed boom length exceeds that required to attain all points in the available test volume. Because of this, the specified boom length could be reduced, however, the diffuser panels may be reconfigured in the future to allow for use of a larger test volume. As a result, the 4.46 m dimension was used as a design value for the required deployed length.

2.1.3 MEMBER LENGTH

In determining the length and number of individual boom members, provision was made for an overlap between neighbouring members when the boom is fully extended. This overlap was required to provide two or more support bearing locations for each member.

As the overlap between members increases, the relative maximum extension decreases. This results in a reduction in the maximum deployed length of the entire boom. To accommodate for this reduction, either the individual member length could be increased (which would have the negative effect of increasing the retracted length of the boom) or the number of members in the boom could be increased. A decrease in the overlap between members would increase the bearing loads and bending stresses in the boom members. This could require an increase in the size or number of bearings required to support each member, or result in an increase in the cross-section sizes for the members.

With this overlap fraction, ol , the deployed boom length, L_{max} , for a boom consisting of a number of element members, n_{mem} , each with an overall length of L_{mem} , is given by the following equation:

$$L_{max} = L_{mem} ((n_{mem} - 1)(1 - ol) + 1) \quad (2.1)$$

This equation accounts for the fact that the base member does not move, so that its entire length is contributed to the extended length of the boom. The remaining members contribute all but their overlap to the deployed length. While (2.1) requires both the member length and the number of members, by rearranging the equation, the constraint values for the retracted and deployed length may be used to find the number of members required for a given overlap value, as:

$$n_{mem} = \frac{\frac{L_{max}}{L_{mem}} - ol}{(1 - ol)} \quad (2.2)$$

Using the design constraint values for extended and retracted boom lengths, 4.46 m and 1.35 m respectively, and an overlap value of 25%, the minimum number of boom members is 4.1. Therefore, using five boom members gives some flexibility in the specification of the overlap or the retracted length. Since a decrease in the retracted length increases the range of the boom, the retracted length is minimized while keeping the overlap at 25% of the individual member length.

Beyond the above considerations, the first member (most extended) requires a slight pre-extension to fit a microphone mounting bracket, and the last member will require extra length to accommodate both the cable actuation system and a single axis joint. Arbitrary values of 0.04 m for the pre-extension of the first member, and 0.15 m for the last member were allowed for these factors. By subtracting these from the minimum deployed boom length, an individual member length of 1.07 m can be found by rearranging equation (2.2) into the following form.

$$L_{mem} = \frac{L_{max}}{n_{mem}(1 - ol) + ol} \quad (2.3)$$

The retracted length L_{retr} will also contain the pre-extensions. For the above member length, the retracted length will be 1.26 m, 0.09 m less than the maximum retracted length desired.

2.1.4 BOOM CROSS-SECTION

The boom requires five members that fit inside each other, with sufficient clearance between members for deployment cables and linear motion shafts and bushings. Another consideration is that the boom be as compact as possible. The dominant concerns in selecting

the member cross-section were that the boom be as rigid as possible, while being lightweight to reduce deflections at its free end. The boom should also be rigid laterally as well as in the loading plane to decrease deflections as it is moved in its two planes of rotation.

The simplest cross-section to implement for the first boom member is a cylindrical one. The use of a 1" (25.4 mm) diameter section of hardened steel tubing allows for support using two low-friction recirculating ball bushings. These bushings are housed in the center of second member's cross-sections as shown in Figure 2.4. Also shown is the triangular arrangement of the 1/2" (12.7 mm) hardened steel guidance shafts that support the second member. This triangular arrangement is the basis for the triangular cross-sections of the remaining three members.

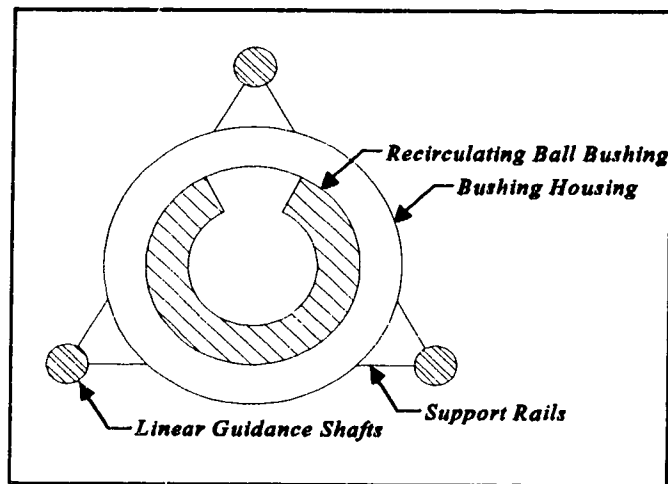


Figure 2.4: Linear Guidance Shafts and Bushing Arrangement on Second Member

The triangular arrangement of the guidance shafts is a compromise between the opposing criteria that the boom be as rigid as possible but also lightweight. A rigid boom is desirable to decrease deflections not only when the boom is at rest, but lateral deflections

which may occur as the boom undergoes an azimuth rotation. Such deflections could cause binding or interference between members if the boom is being extended or retracted during the azimuth rotation. A lightweight boom may increase deflections at the free end, but it more importantly eases the actuator and support requirements for the two rotation axes.

The lightest feasible boom construction would support the members with single guidance rails on the top and bottom of each member as shown in Figure 2.5.A. This would certainly be rigid in the plane of bending due to the weight of subsequent members and the microphone payload. However, the lateral stiffness would be relatively low compared to cross-sections based on triangular or rectangular shaft placement.

Conversely the most rigid cross-section would have the guidance shafts arranged at the corners of a square as shown in Figure 2.5.B. This configuration would also be close to twice as heavy as that shown in Figure 2.5.A. since it has twice as many guidance shafts. The compromise is to arrange the guidance shafts in an equilateral triangle as shown in Figure 2.5.C. This arrangement is not as rigid laterally as the square cross-section, but is not as heavy.

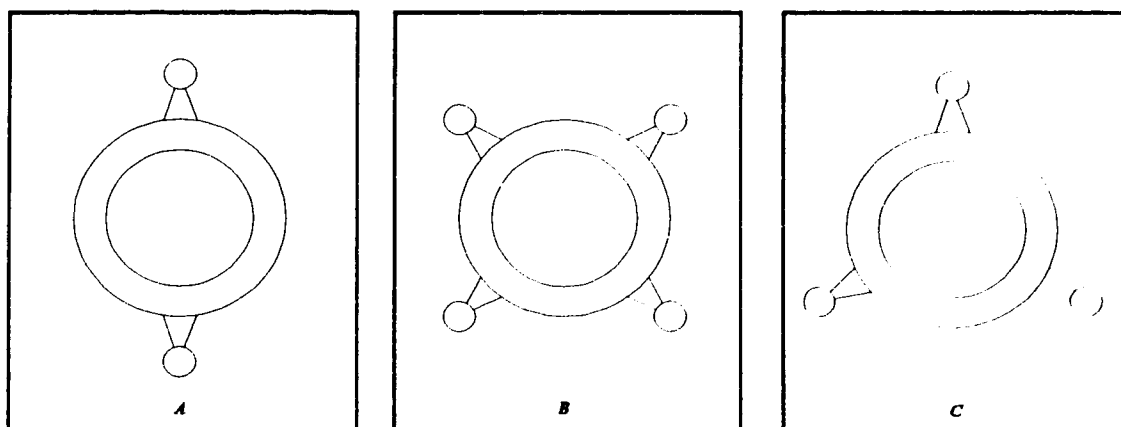


Figure 2.5: Alternative Member Cross-Sections

2.1.5 DYNAMIC MODELLING

The telescopic boom will not only undergo dynamic loading due to the translation of the element members, but will also from the azimuth and elevation rotations. The magnitude of the reactions at the member supports due to these rotations must be considered when selecting the support bushings.

The basis for the kinematic model used to determine the support reactions and dynamic stresses in the members is the acceleration function given by:

$$a(t) = a_{\max} \left(\frac{1}{2} - \frac{1}{2} \cos(2\pi \frac{t}{\tau}) \right) \quad (2.4)$$

The form of this function is also shown in Figure 2.6 and is meant to apply to motion in each of the three axes. The acceleration profile chosen is reasonable since it has a zero jerk value at the beginning and end of its interval. The acceleration interval is of length τ , generally assumed to be approximately 1 second.

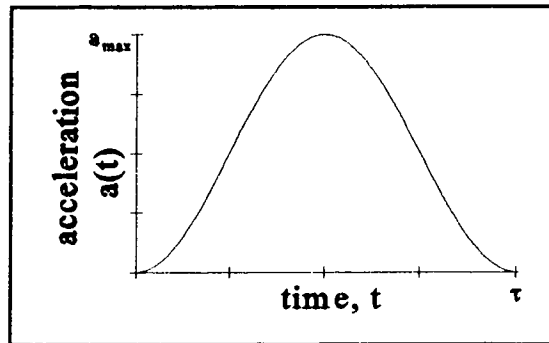


Figure 2.6: Acceleration Profile

The velocity profile corresponding to the acceleration function can be found by integrating (2.4) and assuming that the axis starts from rest to give:

$$v(t) = a_{\max} \left(\frac{1}{2} t - \frac{\tau}{4\pi} \sin\left(2\pi \frac{t}{\tau}\right) \right) \quad (2.5)$$

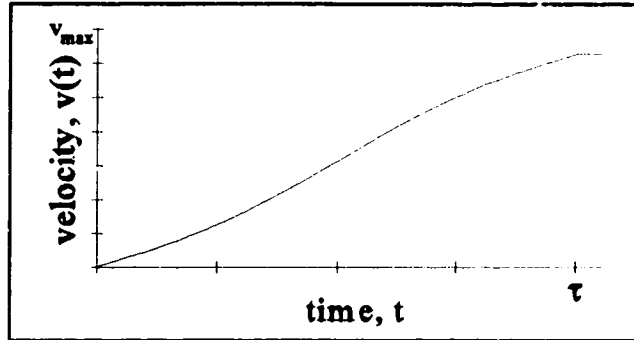


Figure 2.7: Velocity Profile

The form of (2.5) is shown in Figure 2.7. The value of the velocity at the end of the acceleration interval is the maximum velocity. By specifying the maximum velocity, the maximum acceleration can be determined from (2.5) for the time interval, τ , as:

$$a_{\max} = \frac{2v_{\max}}{\tau} \quad (2.6)$$

The maximum velocities for each of the three axes are determined by the requirement that moving from any point in the chamber to any other point should take less than 30 seconds. Due to the relative motion between boom members, each member will have different maximum velocities and accelerations. Since the relative velocities are the same between neighbouring members, the velocities of the members will be an integer multiple of the velocity of the member which extends the least amount. This member will have a velocity corresponding to moving 0.803 m (75% of its required length as discussed in 2.1.3) in 30

seconds or 0.02675 m/s. The range of motion for the remaining members, as well as the two rotational axes are given in Table 2.1. Also contained in Table 2.1 are the corresponding maximum velocities and accelerations.

| MANIPULATOR ELEMENT | RANGE | MAXIMUM VELOCITY | MAXIMUM ACCELERATION |
|-------------------------------|-----------------|------------------|----------------------------|
| BOOM MEMBER 4 | 0 - 0.803 m | 0.02677 m/s | 0.05353 m/s ² |
| BOOM MEMBER 3 | 0 - 1.606 m | 0.05353 m/s | 0.10708 m/s ² |
| BOOM MEMBER 2 | 0 - 2.409 m | 0.08031 m/s | 0.16062 m/s ² |
| BOOM MEMBER 1 | 0 - 3.212 m | 0.10708 m/s | 0.21416 m/s ² |
| AZIMUTH ROTATION (θ) | π radians | 0.10472 rad/s | 0.20944 rad/s ² |
| ELEVATION ROTATION (ϕ) | $\pi/2$ radians | 0.05236 rad/s | 0.10472 rad/s ² |

Table 2.1: Axis Accelerations

Figure 2.8 shows a member in global spherical coordinates undergoing acceleration in the three axes of motion. In Figure 2.8, " θ " is defined as the azimuth, or rotation in a horizontal plane, " ϕ " is defined as the elevation rotation, and " r " is the translation or boom deployment axis.

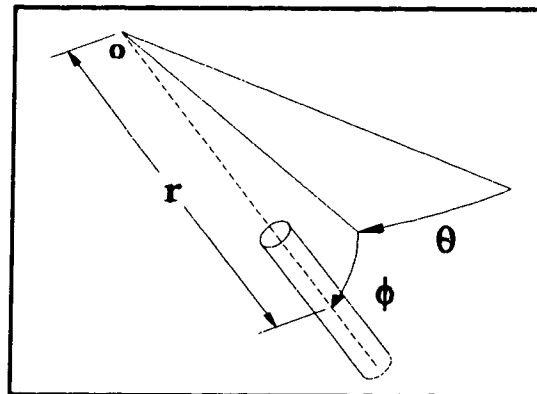


Figure 2.8: Global Spherical Coordinate System

The components of the acceleration of the mass center are given by:

$$a_r = \frac{d^2r}{dt^2} - r \left(\frac{d\phi}{dt} \right)^2 - r \cos^2 \phi \left(\frac{d\theta}{dt} \right)^2 \quad (2.7)$$

$$a_\phi = r \frac{d^2\phi}{dt^2} + 2 \frac{dr}{dt} \frac{d\phi}{dt} + r \left(\frac{d\theta}{dt} \right)^2 \sin \phi \cos \phi \quad (2.8)$$

$$a_\theta = r \cos \phi \frac{d^2\theta}{dt^2} + 2 \left(\frac{dr}{dt} \cos \phi - r \frac{d\phi}{dt} \sin \phi \right) \frac{d\theta}{dt} \quad (2.9)$$

One condition for the maximum radial and transverse acceleration components is that the boom be horizontal. This maximizes the third term in (2.7) and the Coriolis term in (2.9). This also eliminates the product containing the rotational velocity squared in (2.8) and the product of the rotational velocities in (2.9), however, the magnitudes of these terms were found to be negligible compared to the tangential accelerations. Applying the $\phi = 0$ condition to (2.7), (2.8), and (2.9) result in the following equations:

$$a_r = \frac{d^2r}{dt^2} - r \left(\frac{d\phi}{dt} \right)^2 - r \left(\frac{d\theta}{dt} \right)^2 \quad (2.10)$$

$$a_\phi = r \frac{d^2\phi}{dt^2} + 2 \frac{dr}{dt} \frac{d\phi}{dt} \quad (2.11)$$

$$a_\theta = r \frac{d^2\theta}{dt^2} + 2 \frac{dr}{dt} \frac{d\theta}{dt} \quad (2.12)$$

While the maximum radial acceleration occurs when the boom is fully extended and the translational acceleration is negative, it is not clear when the transverse acceleration components (2.11) and (2.12) will be at their maximums. One condition is that the boom is

fully extended, maximizing the tangential acceleration. The Coriolis component of the transverse acceleration is a maximum when the member's radial velocity is maximum. Since the boom members requires some deceleration time, assumed to be 1 second for design purposes, the velocity would not be at its maximum in the fully extended position. Using these conditions, however, will over-estimate the maximum transverse accelerations for design purposes.

Another condition for the maximum transverse acceleration is that the tangential and Coriolis components be in the same direction. Rather than considering all of the possible permutations of the rotational acceleration and velocity and the translational direction, these quantities were assumed to be positive for design considerations. By substituting Equations (2.4) and (2.5) into (2.11) and (2.12), the transverse accelerations are given as:

$$a_{\phi}(t) = r(a_{\phi_{max}}(\frac{1}{2} - \frac{1}{2} \cos(2\pi \frac{t}{\tau})) + 2(\frac{2}{\tau}v_{max}v_{\phi_{max}}(\frac{1}{2}t - \frac{\tau}{4}\pi \sin(2\pi \frac{t}{\tau}))) \quad (2.13)$$

$$a_{\theta}(t) = r(a_{\theta_{max}}(\frac{1}{2} - \frac{1}{2} \cos(2\pi \frac{t}{\tau})) + 2(\frac{2}{\tau}v_{max}v_{\theta_{max}}(\frac{1}{2}t - \frac{\tau}{4}\pi \sin(2\pi \frac{t}{\tau}))) \quad (2.14)$$

By differentiating (2.13) with respect to time, the point during a one second acceleration interval at which the acceleration is a maximum is found from:

$$\frac{da_{\phi}}{dt} = ra_{\phi_{max}}\pi \sin(2\pi t) + \frac{dr}{dt}a_{\phi_{max}}(\frac{1}{2} - \frac{1}{2}\cos(2\pi t)) + 2v_{max}v_{\phi_{max}}(1 - \cos(2\pi t)) = 0 \quad (2.15)$$

By inspection, $t = 1/2$ is a solution to (2.15). By substituting appropriate values for the first member and an acceleration period of 1 second, the actual rotational accelerations during the acceleration interval are given by equations (2.16) and (2.17).

$$a_{\phi}(t) = r(0.10472(\frac{1}{2} - \frac{1}{2} \cos(2\pi t)) + 0.02243(\frac{1}{2}t - \frac{1}{4}\pi \sin(2\pi t))) \quad (2.16)$$

$$a_{\theta}(t) = r(0.20944(\frac{1}{2} - \frac{1}{2} \cos(2\pi t)) + 0.08971(\frac{1}{2}t - \frac{1}{4}\pi \sin(2\pi t))) \quad (2.17)$$

The maximum transverse accelerations are found by evaluating (2.16) and (2.17) at $t = 1/2$ seconds:

$$a_{\phi_{max}}(r) = (0.10472 r + 0.00561) \frac{m}{s^2} \quad (2.18)$$

$$a_{\theta_{max}}(r) = (0.20944 r + 0.02242) \frac{m}{s^2} \quad (2.19)$$

The radial acceleration will be a maximum when the azimuth and elevation rotations are at their maximum velocities and the member is undergoing its maximum retraction acceleration. Realistically, the boom could never undergo such a loading condition as the elevation angle and boom radius would not be at their limits of travel once these axes are activated. However, since this loading condition does over-estimate the maximum radial acceleration, this condition was used to determine the maximum dynamic deployment cable tensions. The maximum radial acceleration becomes:

$$a_r(t) = (a_{retraction} - r(a_{\phi_{max}} + a_{\theta_{max}}))(\frac{1}{2} - \frac{1}{2} \cos(2\pi t)) \quad (2.20)$$

Evaluated at $t = 1/2$ seconds, the maximum acceleration will be:

$$a_{r_{max}}(r) = -a_{retraction} - r(a_{\phi_{max}} + a_{\theta_{max}}) \quad (2.21)$$

Substituting appropriate values from Table 2.1 gives:

$$a_{r_{max}}(r) = -a_{r_{max}} - 0.31416r \quad (2.22)$$

2.1.6 MEMBER LOADING

The members were designed and fabricated starting with the most extended member. The first member consists of a tubular steel shaft with a nominal diameter of 1" (25.4 mm). The shaft length of 1.11 m accounts for the nominal length of the shaft (1.07 m) and a 0.04 m extension to accommodate a microphone mounting bracket. Two recirculating ball bushings support the member. Figure 2.9 is a free body diagram of the member undergoing acceleration in the three component directions of motion.

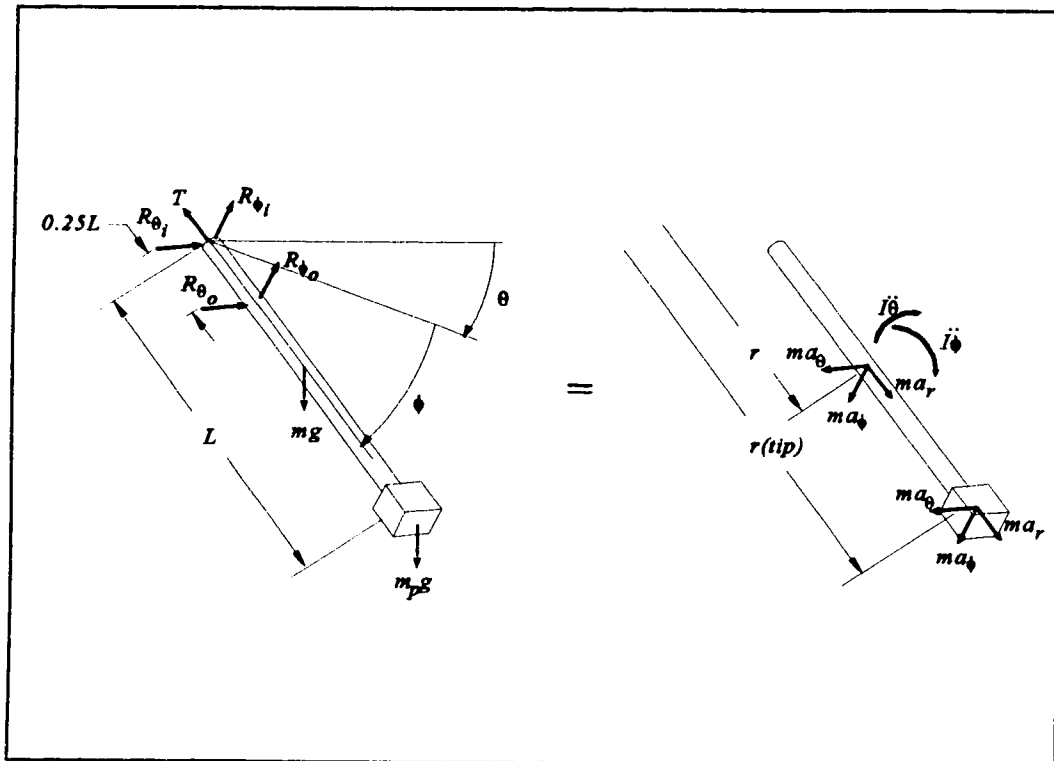


Figure 2.9 : Free Body Diagram of Most Extended Member with Microphone

The figure represents the boom in its fully extended position. The support reactions are located at the tail end of the member (T , R_{ϕ} , R_{θ}) and at 25% of the nominal length (0.27 m) from the end support (R_{ϕ} , R_{θ}). The first member also includes a 25 N load at its tip ($m_p g$), which represents the microphone payload, as well as its own weight (mg).

The dynamic loading due to the microphone payload attached to the first member can be determined by evaluating the radial and transverse accelerations from Equations (2.18), (2.19) and (2.22) at the maximum tip radius of 4.46 m. Substituting this radius into the appropriate equations results in the following values:

$$a_{\phi_{np}} = 0.473 \frac{m}{s^2} \quad (2.23)$$

$$a_{\theta_{np}} = 0.957 \frac{m}{s^2} \quad (2.24)$$

$$a_{r_{np}} = 1.615 \frac{m}{s^2} \quad (2.25)$$

Assuming that the microphone has negligible rotatory inertia about its centroidal axes, and that the boom elevation is horizontal, the equations of motion provide the maximum reactions for a 25 N payload as:

$$R_{\phi_{pay}} = -(-m_{pay} a_{\phi_{np}} + m_{pay} g) = -25.7 \text{ N} \quad (2.26)$$

$$R_{\theta_{pay}} = m_{pay} a_{\theta_{np}} = 2.4 \text{ N} \quad (2.27)$$

$$R_{r_{pay}} = m_{pay} a_{r_{np}} = -4.1 \text{ N} \quad (2.28)$$

Note that the magnitude of the reaction given by (2.26) is a maximum when the elevation transverse acceleration is negative. Applying these reactions to the tip of the first

member results in the free body diagram of the first member as shown in Figure 2.10.

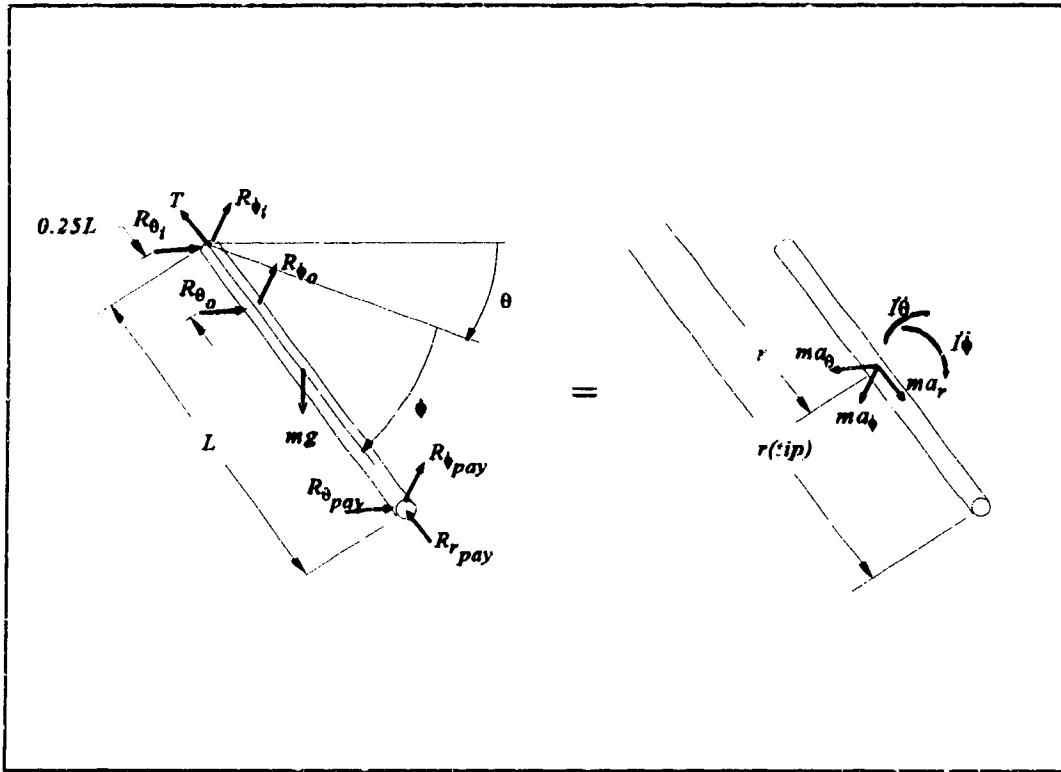


Figure 2.10 : Alternate Free Body Diagram of First Member

The accelerations at the mass center of the first member can be determined by evaluating equations (2.18), (2.19) and (2.22) at a radius of 3.91 m. The accelerations are:

$$a_{\phi_1} = 0.415 \frac{m}{s^2} \quad (2.29)$$

$$a_{\theta_1} = 0.841 \frac{m}{s^2} \quad (2.30)$$

$$a_{r_1} = 1.443 \frac{m}{s^2} \quad (2.31)$$

Summing forces for each axis and applying Newton's Second Law results in the three equations of motion as follows:

$$-R_{\phi_1} - R_{\phi_0} - R_{\phi_{py}} + m_1 g = m_1 a_{\phi_1} \quad (2.32)$$

$$-R_{\theta_1} - R_{\theta_0} - R_{\theta_{py}} = m_1 a_{\theta_1} \quad (2.33)$$

$$-T - R_{r_{py}} = m_1 a_{r_1} \quad (2.34)$$

Summing moments about the center of gravity for the two rotations yields two more equations:

$$0.5L(R_{\phi_1} - R_{\phi_{py}}) + 0.25LR_{\phi_0} = I_1 \frac{d^2\phi}{dt^2} \quad (2.35)$$

$$0.5L(R_{\theta_1} - R_{\theta_{py}}) + 0.25LR_{\theta_0} = I_1 \frac{d^2\theta}{dt^2} \quad (2.36)$$

Solving the above equations for the desired reactions yields the following:

$$R_{\phi_0} = -4 \frac{I_1 d^2\phi}{L dt^2} - 4R_{\phi_{py}} + 2m_1 g - 2m_1 a_{\phi_1} \quad (2.37)$$

$$R_{\phi_1} = -R_{\phi_0} - R_{\phi_{py}} + m_1 g - m_1 a_{\phi_1} \quad (2.38)$$

$$R_{\theta_0} = -4 \frac{I_1 d^2\theta}{L dt^2} - 4R_{\theta_{py}} - 2m_1 a_{\theta_1} \quad (2.39)$$

$$R_{\theta_1} = -R_{\theta_0} - R_{\theta_{py}} - m_1 a_{\theta_1} \quad (2.40)$$

$$T = -m_1 a_{r_1} - R_{r_{py}} \quad (2.41)$$

The case hardened steel tubing used for the first boom member has a nominal outside diameter of 1" (25.4 mm) with a published weight per unit length of 0.158 lbs/inch (27.8 N/m). For the specified member length of 1.11 m the mass of the first member is 30.8 N. The mass moment of inertia about the center of mass can be approximated to that of a slender rod, which is given by:

$$I_1 = I_{\phi_a} = I_{\theta_a} = \frac{1}{12} m_1 L^2 = 0.323 \text{ kg-m}^2 \quad (2.42)$$

Using these values for the mass and mass moment of inertia, along with the center of mass acceleration values from (2.29), (2.30) and (2.31), payload reactions from (2.26), (2.27) and (2.28), and angular accelerations from Table 2.1, the support reactions as found from equations (2.37) through (2.41) are given by the following :

$$R_{\phi_s} = 167.2 \text{ N} \quad (2.43)$$

$$R_{\phi_i} = -109.4 \text{ N} \quad (2.44)$$

$$R_{\theta_s} = -14.9 \text{ N} \quad (2.45)$$

$$R_{\theta_i} = 10.0 \text{ N} \quad (2.46)$$

$$T = -8.6 \text{ N} \quad (2.47)$$

The resultant transverse loading at each bearing location is the vector sum of each of the transverse components:

$$\overline{R}_i = \overline{R}_{\theta_i} + \overline{R}_{\phi_i} \quad (2.48)$$

$$\overline{R}_o = \overline{R}_{\theta_o} + \overline{R}_{\phi_o} \quad (2.49)$$

For the values given above, the resultant loadings and directions are given as:

$$\overline{R}_i = -109.8 \text{ N } \angle 5.2^\circ \quad (2.50)$$

$$\overline{R}_o = 167.9 \text{ N } \angle 5.0^\circ \quad (2.51)$$

The direction is in degrees counterclockwise from the vertical in a plane normal to the radius. With the maximum dynamic load given by (2.51) the bearing requirements may be determined.

For subsequent members, each approximated as slender rods, the support loads can be determined by applying the resultant loads from the previous member at the appropriate locations. The free body diagram shown in Figure 2.11 applies to the second, third, and fourth members. Summing forces and moments for the free body diagram, the reactions for these member can be obtained from the following:

$$R_{\phi_o}(n) = -4 \frac{I_n}{L_n} \frac{d^2\phi}{dt^2} - 2m_n a_{\phi_n} + 2m_n g + 4R_{\phi_o}(n-1) + R_{\phi_i}(n-1) \left(2 + \frac{L_{n-1}}{L_n} \right) \quad (2.52)$$

$$R_{\phi_i}(n) = -m_n a_{\phi_n} + m_n g + R_{\phi_o}(n-1) + R_{\phi_i}(n-1) - R_{\phi_o}(n) \quad (2.53)$$

$$R_{\theta_o}(n) = -4 \frac{I_n}{L_n} \frac{d^2\theta}{dt^2} - 2m_n a_{\theta_n} + 4R_{\theta_o}(n-1) + R_{\theta_i}(n-1) \left(2 + \frac{L_{n-1}}{L_n} \right) \quad (2.54)$$

$$R_{\theta_i}(n) = -m_n a_{\theta_n} + R_{\theta_o}(n-1) + R_{\theta_i}(n-1) - R_{\theta_o}(n) \quad (2.55)$$

$$T(n) = -m_n a_{r_n} \quad (2.56)$$

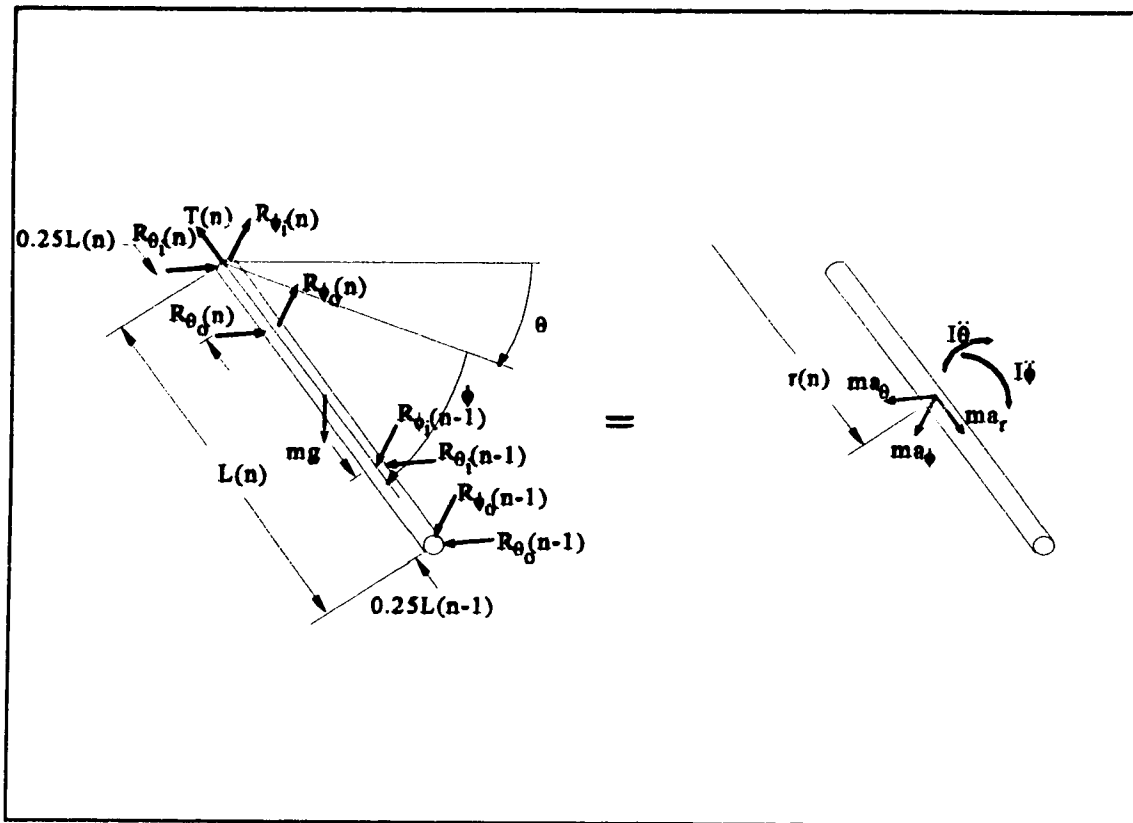


Figure 2.11: Free Body Diagram of Subsequent Member

The last member is supported by a pin at its tail end which allows the member to rotate in the plane of the elevation rotation. The last member is also supported by a reaction from the elevation actuation system at the member's tip. Since these reactions do not affect the bearing selection and member construction for the telescopic portion of the boom, they will be appropriately discussed in section 2.2 below.

A summary of the individual member accelerations and reaction components can be found in Appendix A. The support reactions for the members as constructed are given in Table 2.2. These reactions allow for appropriate linear ball bushings to be selected.

| BOOM MEMBER | INBOARD REACTION R_i N ccw from vertical | OUTBOARD REACTION R_o N ccw from vertical |
|--------------------|--|---|
| 1 | -109.8 \angle 5.2° | 167.9 \angle 5.8° |
| 2 | -334.9 \angle 4.8° | 443.7 \angle 4.7° |
| 3 | -749.2 \angle 4.4° | 945.5 \angle 4.3° |
| 4 | -1447.1 \angle 3.9° | 1751.8 \angle 3.8° |

Table 2.2: Summary of Member Support Reactions and Directions

2.1.7 SUPPORT BEARING SELECTION

The bearings used to support each of the boom members were purchased from Thomson Industries. The selection of the actual bearing components was performed using calculations and specifications outlined in "Linear motion technology guide.", published by Thomson Industries, Inc. [6].

As previously mentioned, the first member consists of a tubular shaft. The Thomson designation of this shaft is a one inch (nominal) O.D. Tubular 60 Case hardened and ground shaft. The shaft itself is manufactured using bearing-quality, high carbon alloy steel and then case hardened to a Rockwell C Hardness of 58 - 63 through a minimum depth of 0.080 inches.

The shaft is supported by a Thomson Super Ball Bushing bearing at each of the inboard and outboard bearing locations. The specification of the bearings used is SUPER-16-OPN, where the "OPN" suffix refers to an open type bushing. These bearings have a normal rolling load rating of 780 pounds (\approx 3.5 kN). From the analysis in Section 2.1.6, the maximum transverse load on this member will be 167.9 N. From the Thomson catalog, the travel life

expectancy of these bearings can be found from the load correction factor K_L given by:

$$K_L = \frac{\text{Load Capacity required}}{\text{Rolling Load Rating} \times K_H} \quad (2.57)$$

The load correction factor, K_{H1} , can be determined from the chart in Figure 2.12 for Rockwell C Hardness of 58, which is the lower bound for the specified hardness range.

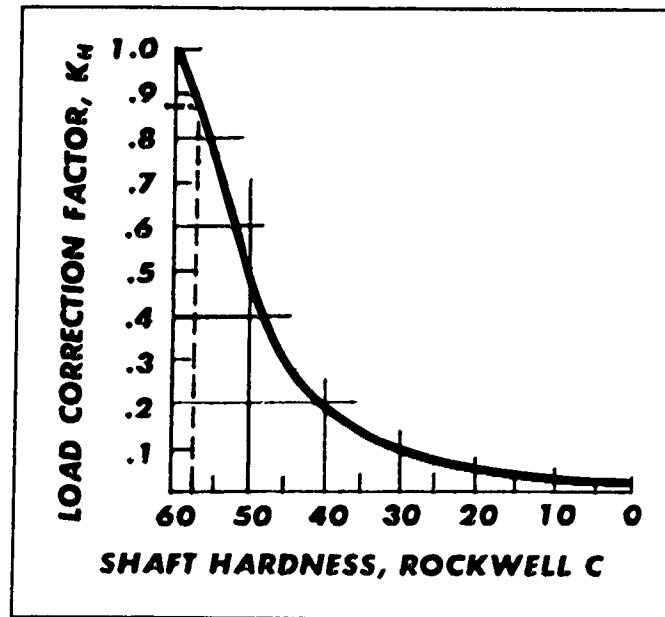


Figure 2.12: Load Correction Factor for Linear Guidance Rails

From Figure 2.12, the load correction factor is approximately 0.87. Using this with the load capacity of 167.9 N and the rolling load capacity of 3478 N, the load correction factor for the first member is:

$$K_L = \frac{167.9}{3478 \times 0.87} = 0.055 \quad (2.58)$$

This figure, however, only specifies travel life for load correction factors in excess of 0.1. As a result, the travel life is assumed to be greater than the longest travel life specified, or 50.8 million metres (2000 million inches).

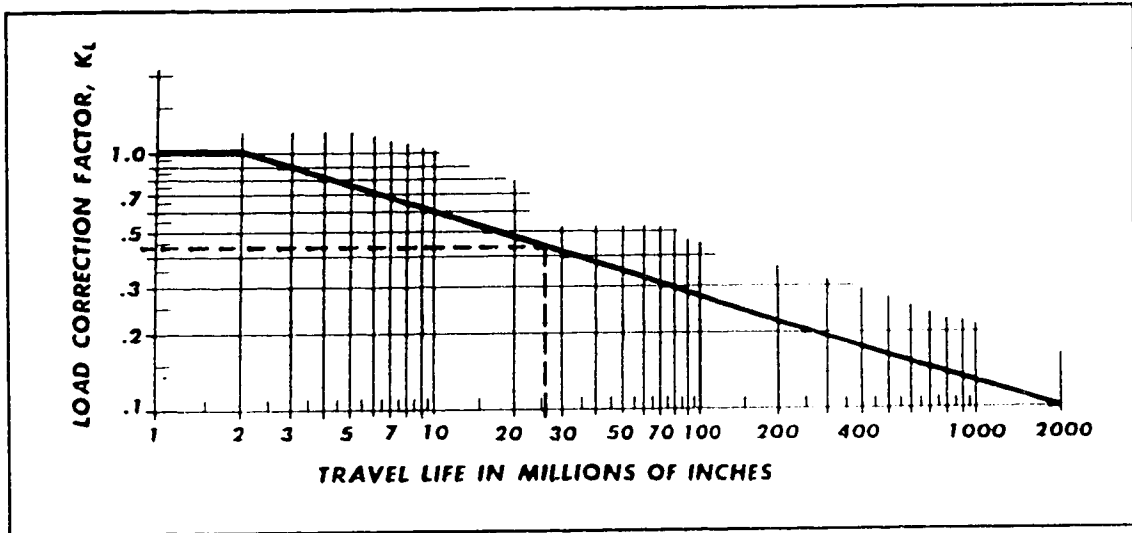


Figure 2.13: Load Correction Factor Based on Service Travel Life

Each of the remaining members are supported by three 1/2" Class "PD" 60 Case shafts, with a weight per unit length specification of 0.055 lbs/inch (0.98 kg/m). These shafts all run in SUPER-8-OPN bearings, with a rolling load capacity of 180 lbs (\approx 800 N).

At both the inboard and outboard bearing locations the members are supported by the three rails. The support loads determined in Section 2.1.6 for each location are assumed to be distributed equally between the three rails. There may also be more than one bearing at each location.

| MEMBER | INBOARD BEARING LOCATION | | | OUTBOARD BEARING LOCATION | | |
|--------|--------------------------|------------------|-------|---------------------------|------------------|-------|
| | # of BEARINGS | LOAD CAP. REQ'D. | K_L | # of BEARINGS | LOAD CAP. REQ'D. | K_L |
| 1 | 1 | 109.8 N | 0.04 | 1 | 167.9 N | 0.06 |
| 2 | 1 | 111.6 N | 0.16 | 1 | 147.9 N | 0.21 |
| 3 | 1 | 249.7 N | 0.36 | 2 | 157.5 N | 0.23 |
| 4 | 2 | 241.2 N | 0.35 | 2 | 292.0 N | 0.42 |

Table 2.3: Bearing Loads and Load Correction Factors for Boom Support Bushings

From Table 2.3, the most critically loaded bearings are those supporting the outboard reaction on the fourth member. By locating $K_L = 0.42$ on Figure 2.13, a travel life of approximately six hundred thousand metres is found. To put this in perspective, for a full range extension, the member moves 0.83 m. The travel life then corresponds to approximately eight hundred thousand extensions. With a nominal sixteen extensions per test, this corresponds to about fifty thousand tests before the bearings and shafts should be replaced. This should be adequate for the purposes of M.E.A.N.U.

It should be noted that the above endurance calculations are for dynamic or rolling loads. Thomson Industries does not give specific static load ratings for the bearings used here but does mention that they are slightly higher than the rolling load ratings. Further, the static load data that is provided only to indicate the maximum safe non-brinelling load. Brinelling occurs in ball bearings when a static load applied is sufficient to dimple the running surface, greatly reducing the dynamic life of the bearing. Since that loading used to calculate the dynamic endurance limits for the support bearings, is conservatively high, and the endurance is acceptable, the static loading on the bearings is also acceptable.

2.1.8 SUPPORT BEARING DETAILS

The geometry of the Thomson Super Ball Bushing support bearings require that they be installed in a cylindrical housing. The bearings supporting the first member are housed in a cylindrical aluminum section with an appropriate inside diameter based on specifications from the Thomson catalogue. This arrangement has been shown previously in Figure 2.4 in Section 2.1.4.

The smaller bearings supporting the remainder of the members are also installed in cylindrical housings. The housings are available from Thomson as Super Ball Bushing pillow blocks Type SPB - OPN (for single bearings) or Type TWN - OPN (for double bearing sets). The assemblies are shown in Figure 2.14 as supplied from Thomson.

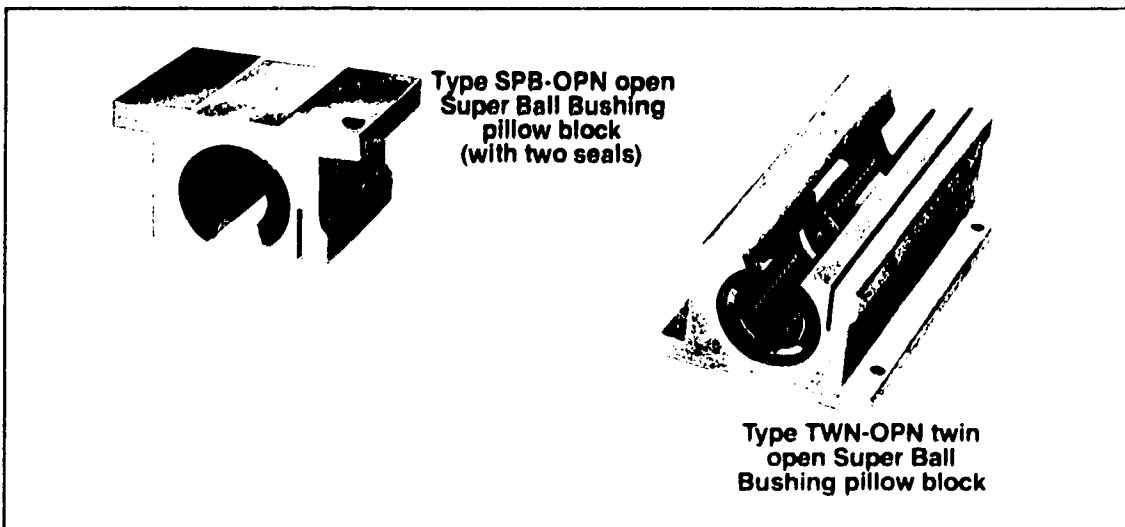


Figure 2.14: Thomson Super Ball Bushing Bearing Pillow Block Assemblies as Supplied

As shown, the pillow blocks have a rectangular cross-section. To adapt these to the triangular cross section of the subsequent members, the flanges were machined off and the corners chamfered 30° relative to the top of the pillow block, as shown in Figure 2.15. Also

shown in the figure are the linear guidance shafts and rails supporting the current member, as well as the structure supporting the pillow blocks.

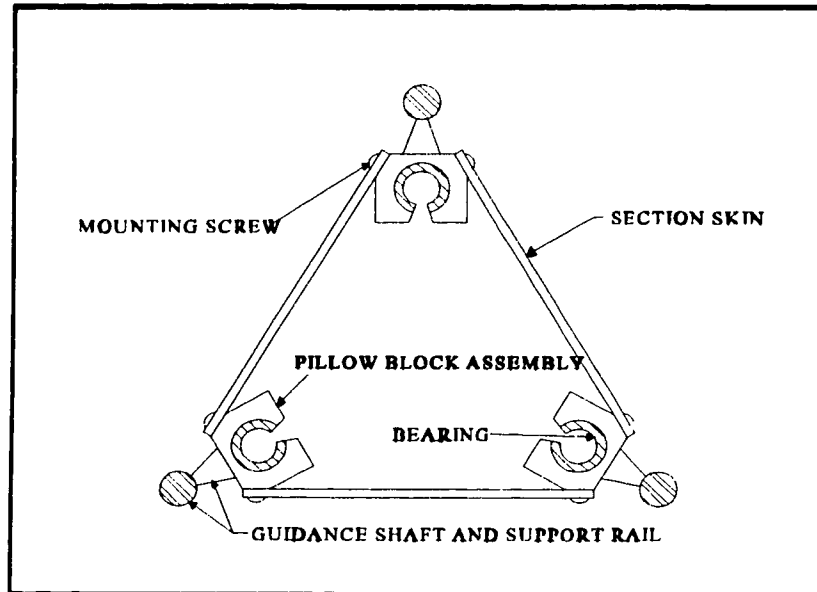


Figure 2.15: Schematic of Bearing Pillow Block and Support Shafts and Rails

Another detail shown in Figure 2.15 are the screws used to secure the section skins to the pillow blocks and rail assembly. As there are only two pillow block assemblies along the length of each member, several rail and skin mounts were fabricated to hold the members together. The geometry of these mounts are similar to the pillow blocks, and are placed every 12 cm.

Although the fifth, or base boom member has yet to be discussed, it is appropriate to discuss its cross-section in terms of the support bearing housing details. The cross-section of the fifth member is similar to the third and fourth members, but since there are no subsequent members, it lacks the bearing shaft - support rail assembly.

2.1.9 DYNAMIC MEMBER STRESSES

To determine the bending stresses in the members due to the dynamic loading, it is necessary to determine the second moment of the cross section of each member. This is complicated by the use of different materials in the construction of the members, and by non-uniformities in the aluminum member skins, namely various sized holes for weight reduction and access to bearings and cable connections.

The first member is not affected by the above considerations, since it is simply a tubular section which is uniform along its length. The second moment of area of the member, as shown in Figure 2.16, is given by:

$$\bar{I} = \frac{1}{4}\pi(R_o^4 - R_i^4) \quad (2.59)$$

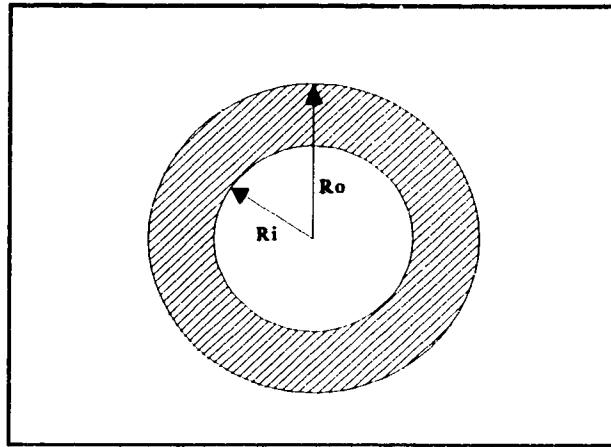


Figure 2.16: Cross-Section of First Member

The cross-sectional properties of the remaining four members is discussed in detail in Appendix B.

For the first member, as supplied, the outside radius, R_o , is 0.5" (nominal) and the inside radius, R_i , is 0.3" (nominal). Converting to S.I. units and substituting into equation (2.59) the second moment of area is:

$$\bar{I} = \frac{1}{4}\pi(12.7^4 - 7.6^4)mm^4 = 17.8 \times 10^3 mm^4 \quad (2.60)$$

The dynamic loading on the first member in the planes of the azimuth and elevation rotations is shown in Figures 2.17 A and B respectively. The loading shown is for the boom in the horizontal position. Also shown in Figure 2.17 are the shear force and bending diagrams for the loading shown. Appendix C contains diagrams for the subsequent members.

The maximum bending stress will occur at the position with the largest bending moment. In the case of the first member, this corresponds to the location of the outboard support bearing, in the plane of the elevation rotation. The normal stress due to bending can be found from:

$$\sigma = \frac{My}{I} \quad (2.61)$$

where y is the distance from the neutral bending axis, M is the magnitude of the bending moment, and I is the second moment of area about the neutral axis. For the values found above, the maximum normal stress in the first member is:

$$\sigma = \frac{30.4kNmm \times 12.2mm}{17.8 \times 10^3 mm^4} = 20.8MPa \quad (2.62)$$

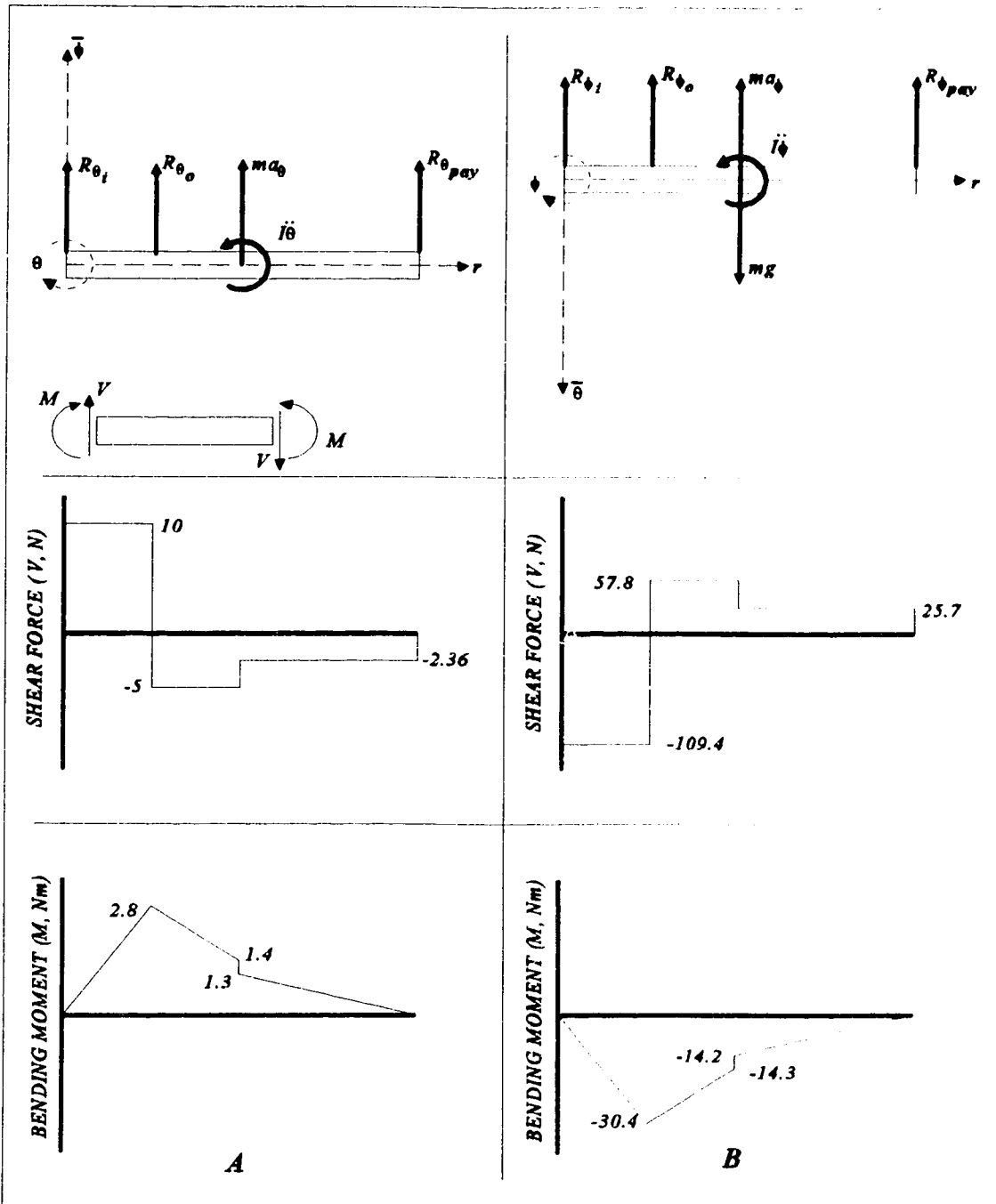


Figure 2.17: Shear Force and Bending Moment Diagrams for Transverse Dynamic Loading of First Member

In all cases, the shear stresses are assumed to be negligible. It is also assumed that the members undergo only pure bending so that the stress state is either uniaxial tension or compression.

For cases of uniaxial tension, most failure criterion state that yielding will occur if the normal stress exceeds the tensile yielding stress, S_y . The yield stresses used for design purposes were 317 MPa for steel (AISI 1015), and 275 MPa for aluminum (alloy 6061-T6). The criterion for comparing relative stress magnitudes is the factor of safety, N , as defined in (2.63):

$$N = \frac{\textit{Tensile Yield Stress of Material}}{\textit{Induced Stress}} \quad (2.63)$$

For the first member, the factor of safety is:

$$N_1 = \frac{317\text{MPa}}{20.8\text{MPa}} = 15.9 \quad (2.64)$$

The analysis for the subsequent members can be found in Appendix B. The results are summarized in Table 2.4. The high value of the safety factors indicates the likelihood of yielding is low. A more critical failure mode would be the fatigue of the screws and skins.

| MEMBER | SAFETY FACTOR, N |
|--------|------------------|
| 1 | 15.9 |
| 2 | 25.2 |
| 3 | 13.8 |
| 4 | 16.6 |
| 5 | 24.3 |

Table 2.4: Summary of Dynamic Loading Safety Factors

2.1.10 STATIC DEFLECTIONS

The deflection of the boom assembly under static loading is of interest as the absolute positioning accuracy will be within the limits of the static deflections. The static loading on the individual boom members is due to the microphone payload and the weight of the members. The support reactions can be determined from the equations for the dynamic reaction components, in Section 2.1.6, by setting the acceleration and velocity terms to zero. This analysis can be found in Appendix A.

Rather than analyzing each member separately, and combining the individual deflections and slopes, the entire boom will be considered. Figure 2.18 shows the boom model used.

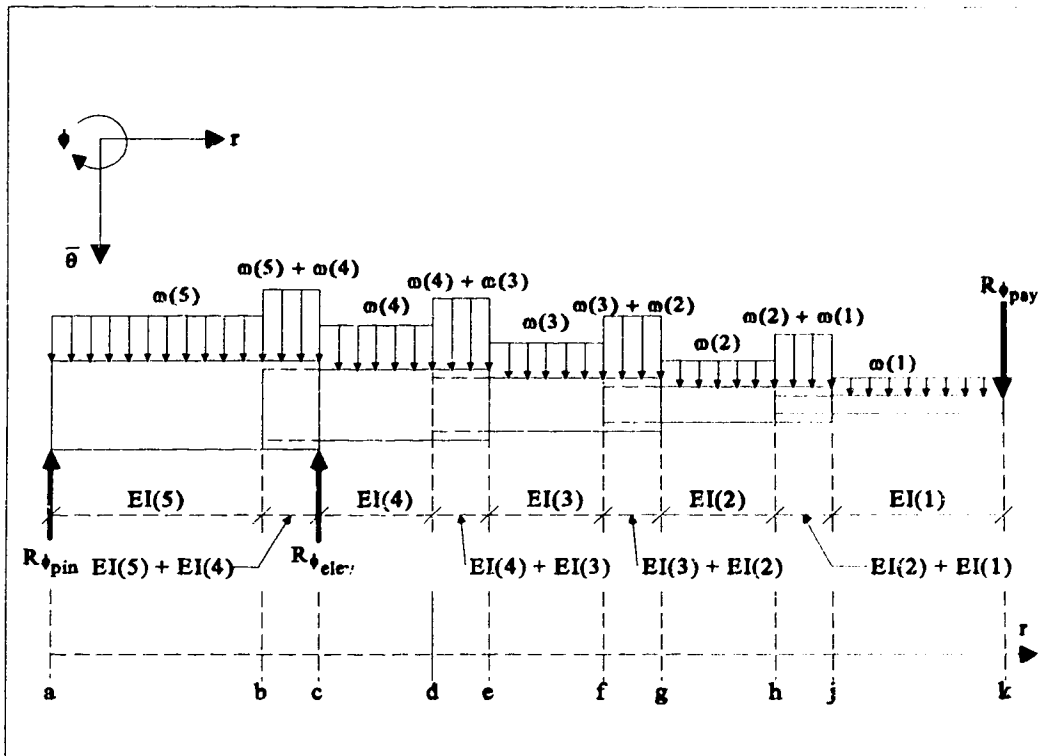


Figure 2.18: Static Deflection Model

The linear weights of the individual boom members are represented by the distributed loads, $\omega(n)$. Note that at the regions where the members overlap, the linear weights are superimposed. A simplifying assumption is that the flexural rigidity, $EI(n)$, of overlapping members also directly adds. This simplification is equivalent to assuming that the members are rigidly attached in the overlap region. Although the support bearing cannot be assumed to be rigid, there are no stiffness specifications for the type of bearing used. This assumption will under-estimate the deflection of the boom, but will be compared to the actual boom deflection in Chapter 3. A summary of the flexural rigidity and linear weight values is given in Table C.2 in Appendix C.

Figure 2.18 contains two unknown reactions, namely the external pin and tip reactions on the fifth member. The magnitude of these reactions due to each loading can be found by performing a static analysis. The values of these reactions considering only the weight of the members are:

$$R_{\phi_{pin}} = -194.68 N \quad (2.65)$$

$$R_{\phi_{dr}} = 576.9 N \quad (2.66)$$

The reactions considering both the weight of the members and the payload reaction are:

$$R_{\phi_{pin}} = -263.4 N \quad (2.67)$$

$$R_{\phi_{dr}} = 670.6 N \quad (2.68)$$

The deflections due to the individual loadings were determined by integrating the governing differential equation of the elastic curve. This was performed for the loading with

and without the payload reaction. The differential equation governing the elastic curve of the boom, in general, is:

$$\frac{d^2y}{dr^2} = \frac{M(r)}{EK(r)} \quad (2.69)$$

Integrating once with respect to r , the slope at any point on the elastic curve is given by:

$$\alpha(r) = \int_0^r \frac{M(\rho)}{EK(\rho)} d\rho + C_1 \quad (2.70)$$

Integrating with respect to r again, the deflection of the elastic curve is given by:

$$\delta(r) = \int_0^r d\rho \int_0^\rho \frac{M(\rho)}{EK(\rho)} d\rho + C_1 r + C_2 \quad (2.71)$$

In the specific case of the boom model in Figure 2.18, the flexural rigidity is not constant over the length of the boom, so that the integrations in equations (2.70) and (2.71) were split up over the intervals where the flexural rigidity is constant. The integral for the slope at the free end of the boom is then:

$$\begin{aligned} \alpha(r) = & \int_0^b \frac{M(\rho)}{EI_5} d\rho + \int_b^c \frac{M(\rho)}{EI_5 + EI_4} d\rho + \int_c^d \frac{M(\rho)}{EI_4} d\rho \\ & + \int_d^e \frac{M(\rho)}{EI_4 + EI_3} d\rho + \dots + \int_j^k \frac{M(\rho)}{EI_1} d\rho + C_1 \end{aligned} \quad (2.72)$$

It can be shown that the equation describing the bending moment for the loading shown in Figure 2.18 is given by:

$$M(r) = R_{\phi_{pr}} r + R_{\phi_{dr}} r - \frac{1}{2} \omega_5 (r^2 - \langle r - c \rangle^2) - \frac{1}{2} \omega_4 (\langle r - b \rangle^2 - \langle r - e \rangle^2) - \frac{1}{2} \omega_3 (\langle r - d \rangle^2 - \langle r - g \rangle^2) - \frac{1}{2} \omega_2 (\langle r - f \rangle^2 - \langle r - j \rangle^2) - \frac{1}{2} \omega_1 \langle r - j \rangle^2 \quad (2.73)$$

By virtue of the singularity functions, (2.73) is valid for any point along the length of the boom. Substituting (2.73) into (2.72) would then allow for the evaluation of the slope at any point along the boom.

By integrating the result of (2.72) numerically over the length of the boom will provide the boom deflection along the length of the boom.

The plots in Figures 2.19 and 2.20 are the corrected slope and deflection of the boom for loading due to the weight of the members only. Figures 2.21 and 2.22 are the corrected slope and deflection of the boom including the payload.

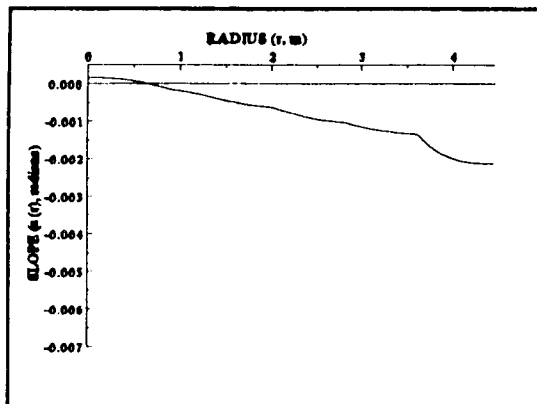


Figure 2.19: Deformed Boom Slope with Boundary Conditions Applied for Loading Due to Member Weight

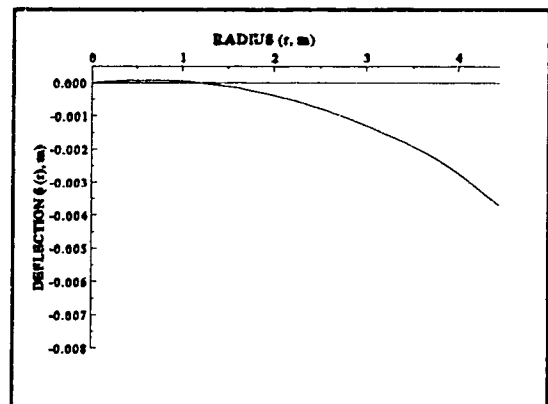


Figure 2.20: Boom Deflection with Boundary Conditions Applied for Loading Due to Member Weight

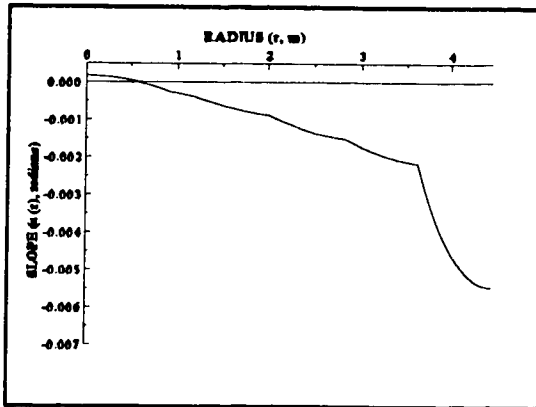


Figure 2.21: Deformed Boom Slope with Boundary Conditions Applied for Loading Due to Member Weight and Payload

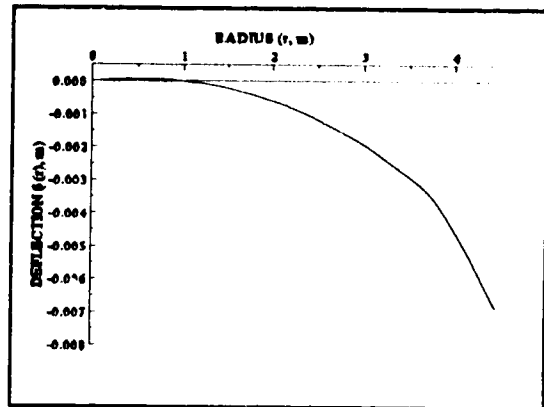


Figure 2.22: Boom Deflection with Boundary Conditions Applied for Loading Due to Member Weight and Payload

As shown in the appropriate figure above, the deflection of the boom predicted by this model under the design payload of 25 N is approximately 7 mm. This model does not, however, take into account the rigidity of the linear ball bushings used to support the members. Although this could be accounted for in the flexural rigidity values in the regions where the members overlap, the manufacturer does not provide such information.

Another factor affecting the actual deflection of the boom is the rigidity of the elevation mechanism and azimuth turret. The amount that these elements contribute to the overall deflection of the boom is difficult to estimate and has not been considered in this study.

2.1.11 CABLE ACTIVATION SYSTEM

A schematic of the cable activation system between the first and second members is shown in Figure 2.23. As the deployment cable is pulled through a distance Δr , the first member extends the same distance from the second member. In relation to the reference line AA, the retraction cable length also increases by the same amount. This idea was extended to include all of the members.

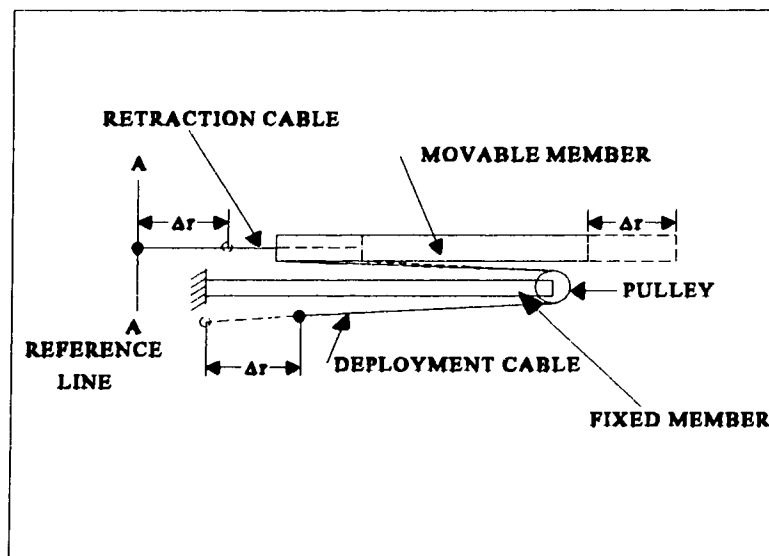


Figure 2.23: Cable Activation System Between First and Second Members

Figure 2.24 shows a schematic of the first three members. Note that the deployment cable for the first member is fixed to the third member. As the deployment cable for the second member is pulled through a distance of Δr , the second member extends the same distance from the third member. Since the deployment cable for the first member is attached to the third member, it will also be pulled through a distance of Δr , causing the first member to extend this amount from the second member. The overall increase in length of the

arrangement is $2\Delta r$. Extending this concept to the boom configured with five members, the overall increase in length would be $4\Delta r$.

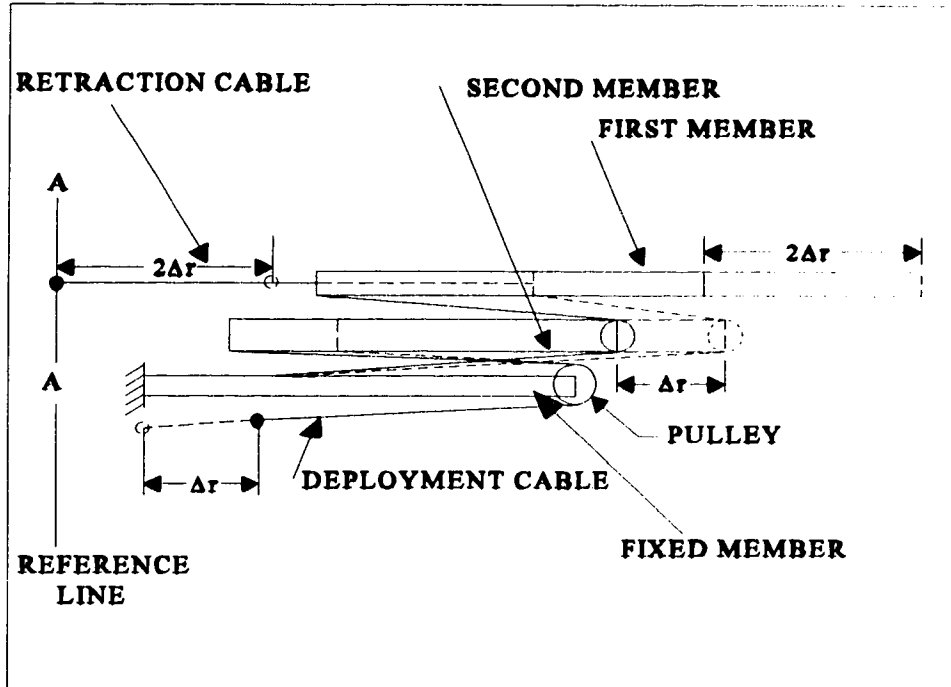


Figure 2.24: Cable Activation System Between First, Second, and Third Members

To move the fourth member to its maximum extension from the fifth member, the amount of cable that must be withdrawn is simply:

$$\Delta r_4 = 0.75 L_4 = 0.81 \text{ m} \quad (2.74)$$

The length that retraction cable increases for this manoeuvre is then:

$$\Delta r_{\text{retr}} = 4 \Delta r_4 = 3.24 \text{ m} \quad (2.75)$$

The boom is deployed by reeling the deployment cable for the fourth member onto a drum and unreeling the retraction cable from another drum. Since there is exactly a four to one ratio between the amount of cable to be reeled and unreeled, these two drums can be located on the same shaft, with an appropriate ratio of diameters.

The length of cable of diameter Φ_{cable} that is reeled onto a drum with a diameter of Φ_{drum} in one turn of the drum is given by:

$$L = \pi (\Phi_{drum} + K \Phi_{cable}) \quad (2.76)$$

where K is a constant that is based on the cable type and diameter. For the special case of $K = 1$, (2.76) can be interpreted to state that the center line of the cable remains one cable radius from the drum. This may not always be true.

The cable used is designated as 7 x 7 - 1/16 inch diameter cable. A schematic of the cable cross-section is shown in Figure 2.25.

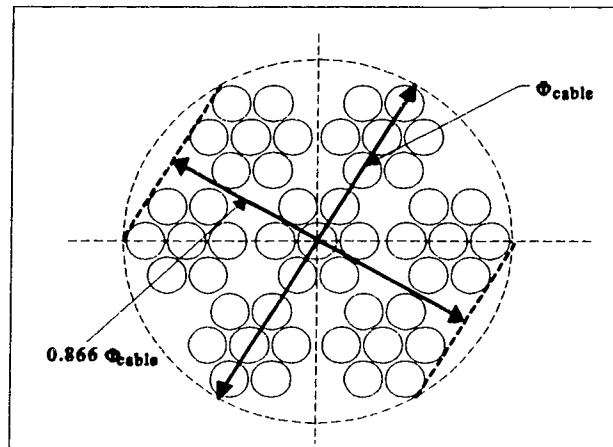


Figure 2.25: Cross-Section of 7 x 7 Cable

As shown in Figure 2.25, the cable consists of six strands wound around a seventh. Each strand consists of six wires wound around a seventh. As a note, the cable used is regular lay, meaning that the wires in the strands follow a helical path along the length of cable in the opposite direction to the helical path that the strands follow.

As shown in Figure 2.25 the actual diameter of the cable varies between $\frac{\sqrt{3}}{2} \Phi_{cable}$ and Φ_{cable} . Using the average value for the cable diameter, K becomes 0.933.

However, if (2.76) represents the length of deployment cable taken up per drum rotation, then the required length of retraction cable that must be unreeled is:

$$L_{retract} = 4L_{deploy} = 4\pi(\Phi_{drum_d} + K\Phi_{cable}) = \pi(\Phi_{drum_r} + K\Phi_{cable}) \quad (2.77)$$

If the cable constant K is independent of the diameters of the drums, solving for the diameter of the retraction drum gives:

$$\Phi_{drum_r} = 4\Phi_{drum_d} + 3K\Phi_{cable} \quad (2.78)$$

As constructed, the deployment drum has a diameter of 23.8 mm. With a cable diameter of 1.59 mm, the required diameter of the retraction drum is :

$$\Phi_{drum_r} = 4(23.8\text{ mm}) + 3(0.933)(1.59\text{ mm}) = 99.7\text{ mm} \quad (2.79)$$

For the above deployment drum diameter, the number of drum rotations for the full deployment or retraction can be found using:

$$n = \frac{L}{\pi(\Phi_{deploy} + K\Phi_{cable})} \quad (2.80)$$

where L is the range of motion of the fourth member (0.81 m). For this value, the number of drum rotations is:

$$n = \frac{0.81}{\pi (0.0238 + 0.933 \times 0.0016)} = 10.2 \text{ rotations} \quad (2.81)$$

Although an effort has been made to ensure that the ratio of the change in cable lengths remains very close to four to one, variability in the diameters of the drums due to the machining process, and variations in the actual cable diameter cannot be completely determined. As a measure to accommodate variations in the drum ratio, a spring loaded cable tensioning element has been added to the cable activation system.

Figure 2.26 is a cut-away schematic of the first member. As shown, the retraction cable is attached to one end of a threaded rod. The threaded rod passes through a number of Belleville washers, which act as springs. The washers are located in a region of the first member that has been machined out to a larger inside diameter. The cable system can be pretensioned by holding the nut on the threaded rod with a deep socket, and turning the rod with a screwdriver. The amount of cable variation that can be taken up through this arrangement is approximately 50 mm.

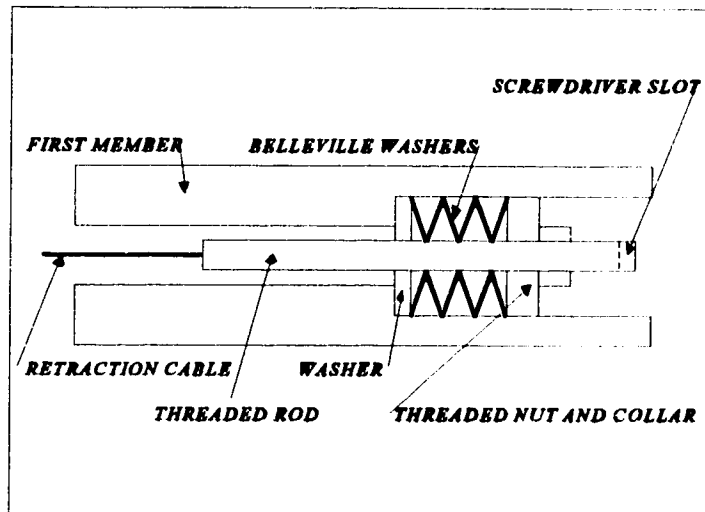


Figure 2.26: Schematic of Cable Tensioning Element

2.1.12 CABLE TENSION

The maximum cable tensions will occur when the boom is at its vertical elevation. The maximum radial accelerations as found in Section 2.1.6 are used to determine the maximum cable tensions. Although the deployment/retraction accelerations are for a different position, they are the absolute maximum accelerations that the boom members will undergo and will provide a conservative estimate of the cable tensions.

As shown in the free body diagram in Figure 2.27, the first member is connected to the retraction cable and its own deployment cable. Summing forces in the radial direction gives equation (2.82).

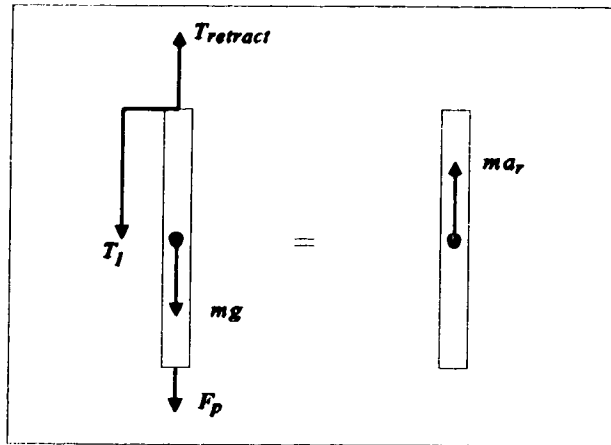


Figure 2.27 : Free Body Diagram of First Member

$$T_{retract} = m_1(g + a_r) + T_1 + F_p \quad (2.82)$$

The second member has a free body diagram as shown in Figure 2.28. The member is acted on by its deployment cable, by the deployment cable of the first member which runs over a sheave at the tip of the second member, and by the reaction due to the microphone payload, F_p . Summing forces in the radial direction gives Equation (2.83).

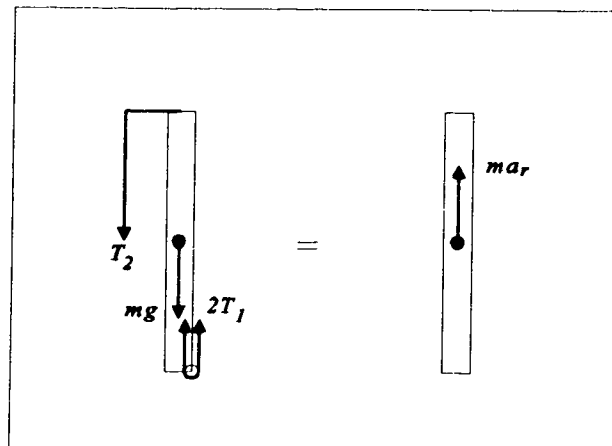


Figure 2.28 : Free Body Diagram of Second Member

$$2T_1 = m_2(g + a_{r_2}) + T_2 \quad (2.83)$$

The third member is acted on by its own deployment cable, the deployment cable from the second member and the deployment cable from the first member, which is anchored to the third member. Its free body diagram is shown in Figure 2.29, which provides equation (2.84).

$$2T_2 = m_3(g + a_{r_3}) + T_3 + T_1 \quad (2.84)$$

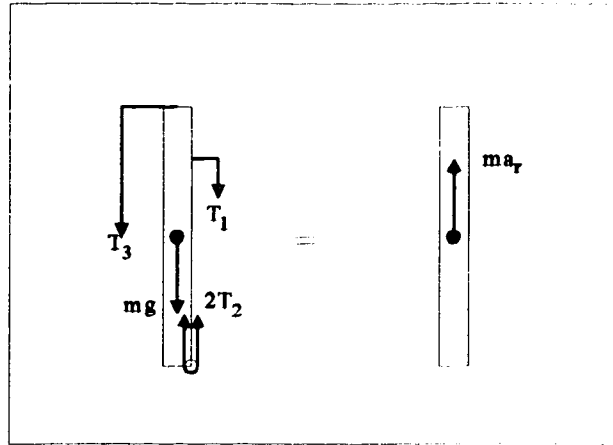


Figure 2.29 : Free Body Diagram of Third Member

The free body diagram for the fourth member would look the same as Figure 2.29 above, except with different numbered cable tensions. The equation it would yield is:

$$2T_3 = m_4(g + a_{r_4}) + T_4 + T_2 \quad (2.85)$$

The system of equations given by (2.82) through (2.85) is indeterminate since there are five unknowns in the four equations. Although it is not intuitively obvious, the

deployment cable for the fourth member is redundant. Figure 2.30 shows a schematic of the entire boom with and without the presence of the fourth deployment cable.

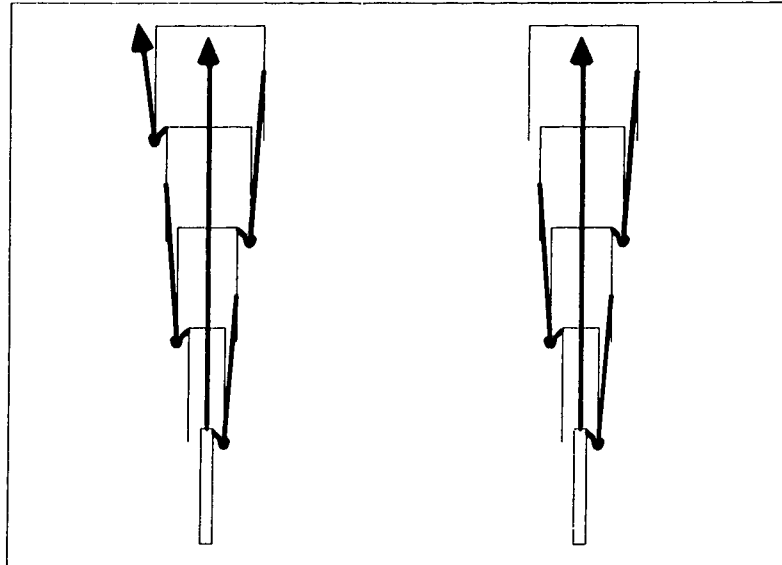


Figure 2.30 : Schematic of Cable Arrangement With and Without the Fourth Deployment Cable

As shown in Figure 2.30, the removal of the fourth deployment cable does not change the position of any of the boom members. This does not, however, indicate that the fourth member deployment cable is unnecessary. In the position shown the members will attain their positions solely by the weight of the members themselves. In a horizontal position the friction in the linear guidance bushings inhibits the relative motion of certain members and their deployment cables lose their tension. This can result in binding and interference as the clearance between the members is approximately 7 mm. The presence of the fourth member deployment cable preserves a pre-tension on all cables and forces the relative motion between members when gravity is not sufficient (i.e. horizontal boom positions). The initial tension is approximately 30 N.

Using this value, equations (2.82) and (2.85) result in a determinate system. Solving for the cable tensions gives:

$$T_{retract} = m_1(g + a_{r_1}) + \frac{3}{4}m_2(g + a_{r_2}) + \frac{1}{2}m_3(g + a_{r_3}) + \frac{1}{4}m_4(g + a_{r_4}) + \frac{1}{4}T_4 + F_p \quad (2.86)$$

$$T_1 = \frac{3}{4}m_2(g + a_{r_2}) + \frac{1}{2}m_3(g + a_{r_3}) + \frac{1}{4}m_4(g + a_{r_4}) + \frac{1}{4}T_4 \quad (2.87)$$

$$T_2 = \frac{1}{2}m_2(g + a_{r_2}) + m_3(g + a_{r_3}) + \frac{1}{2}m_4(g + a_{r_4}) + \frac{1}{2}T_4 \quad (2.88)$$

$$T_3 = \frac{1}{4}m_2(g + a_{r_2}) + \frac{1}{2}m_3(g + a_{r_3}) + \frac{3}{4}m_4(g + a_{r_4}) + \frac{3}{4}T_4 \quad (2.89)$$

Using the values from Appendix A, the cable tensions are:

$$T_{retract} = 204.8 N \quad (2.90)$$

$$T_1 = 140.3 N \quad (2.91)$$

$$T_2 = 191.0 N \quad (2.92)$$

$$T_3 = 167.2 N \quad (2.93)$$

$$T_4 = 30 N \quad (2.94)$$

The stresses in the cable as it bends around a sheave or drum can be considered as an equivalent tension at the point of bending. The tension in the cable does not actually increase, but the value may be used for evaluation of the cable loading. "Machinery's Handbook" [7] gives the equivalent tension as:

$$T_B = \frac{EkQd_{cable}^3}{\Phi_{sheave}} \quad (2.95)$$

where E is the modulus of elasticity for the cable (82 GPa), k is a constant related to the diameter of the component wire (0.106), Q is an area correction factor based on the cable type (0.437 for 7x7 cable), d_{cable} is the cable diameter (1.6 mm nominal), and Φ_{sheave} is the pitch diameter of the sheave or drum. The smallest pitch diameter is approximately 15 mm. This corresponds to an equivalent tension of:

$$T_B = \frac{82 \times 10^9 \times 0.106 \times 0.437 \times (1.6 \times 10^{-3})^3}{15 \times 10^{-3}} N = 1037N \quad (2.96)$$

This tension can be added to the cable tensions to get their effective tensions.

The breaking strength of the cable used is not readily available. However, the breaking strength of 1/4 " nominal cable, regular lay 7x7, is approximately 25 kN. If the cable strength is based on the cross-sectional area for the nominal diameter, 1/16" nominal cable would have a breaking strength one sixteenth that of the 1/4" cable. The breaking strength is therefore assumed to be approximately 1600 N.

The maximum cable tension from the above analysis is in the third deployment cable, with an effective magnitude of 1228 N. The safety factor for this cable is 1.30, which is quite low. The commonly recommended range is between 3 and 4. However, the analysis of the bending loads is specified for significantly larger cables of 1/4" (6.4 mm) nominal diameter and above. The above analysis may not be appropriate for small diameter cables.

2.1.13 ACTIVATION TORQUE

The maximum retraction torque can be determined from the maximum retraction cable tension and the fourth deployment cable tension. Figure 2.31 is a free body diagram of the deployment/retraction drum assembly. If the angular acceleration of the drum assembly

is neglected, summing moments about the drum center gives equation (2.97).

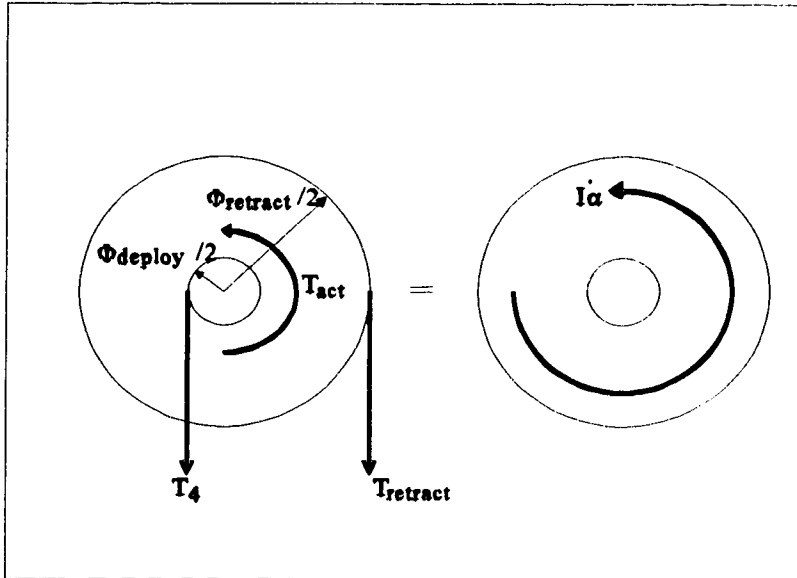


Figure 2.31: Free Body Diagram of Drum Assembly

$$T_{act} = \frac{T_{retract} \Phi_{retract} - T_4 \Phi_{deploy}}{2} \quad (2.97)$$

Using the above values, the activation torque is:

$$T_{act} = \frac{204.8N \times 0.0997m - 30N \times 0.0238m}{2} = 9.9 Nm \quad (2.98)$$

The torque in (2.98) is the minimum that must be provided by the actuator for the deployment axis. As constructed, the boom has significant friction due to the number of bearings, bearing seals and variations in the distance between rails. The actual maximum activation torque was measured using a torque wrench to be approximately:

$$T_{act} = 30Nm \quad (2.99)$$

2.1.14 EFFECTIVE INERTIA

One important characteristic required when selecting the axis actuators is the effective inertia or load inertia. This is distinguished from the mass moment of inertia of the boom members in that the effective inertia is the apparent inertia at the point that the actuator applies power to the axis. In the case of the telescopic boom, the actuator is located at the deployment/retraction drum assembly. Since the members move linearly towards or away from the drum assembly, they have no rotatory inertia about the drum assembly. The effective inertia of each member is then given by:

$$I_{e_n} = m_n \delta_n^2 \quad (2.100)$$

where δ_n is the distance that member "n" travels for a one radian rotation of the drum assembly.

The distance that the fourth member moves for a one radian rotation of the drum can be found from the amount of cable reeled in or out for one drum rotation, as given in (2.76).

Multiplying by an appropriate factor gives:

$$\delta_4 = \pi (\Phi_{deploy} + K \Phi_{cable}) \times \frac{1}{2 \pi \text{ radians}} \quad (2.101)$$

Since the distance that the subsequent members travel is related to the motion of the fourth member, a general relationship can be given as:

$$\delta_n = \pi (\Phi_{deploy} + K \Phi_{cable}) \times \frac{5 - n}{2 \pi \text{ radians}} \quad (2.102)$$

Equation (2.102) is valid for n as the member number, which ranges between one and four.

Using (2.102), the effective inertia can be found for the individual members by:

$$I_{e_n} = m_n \delta_n^2 = m_n \left(\pi (\Phi_{deploy} + K \Phi_{cable}) \times \frac{1}{2 \pi \text{ radians}} \right)^2 \quad (2.103)$$

The total inertia due to member translation is then:

$$I_{e_{trans}} = \sum_{n=1}^4 m_n \left(\pi (\Phi_{deploy} + K \Phi_{cable}) \times \frac{5-n}{2 \pi \text{ radians}} \right)^2 \quad (2.104)$$

Using values from the previous section and Appendix A, this contribution to the effective inertia is:

$$I_{e_{trans}} = 25.5 \times 10^3 \text{ kgmm}^2 \quad (2.105)$$

The inertia of the drum assembly must also be accounted for in the effective inertia. The drum assembly consists of the deployment and retraction drums, as discussed in the previous section, and the 1/2" (nominal) shaft that supports them. The drums were fabricated from T6061-T6 aluminum, and the shaft is mild steel. The rotatory inertia of a cylinder is given by:

$$I_{e_{cylinder}} = \frac{1}{2} m r^2 \quad (2.106)$$

If the cylinder height and material density are known, (2.106) becomes:

$$I_{e_{cylinder}} = \frac{1}{2} \rho \pi h r^4 \quad (2.107)$$

Using a height of 27 mm for the drum heights with a density of $2.7 \times 10^{-6} \text{ kg/mm}^3$, and 291 mm for the shaft height with a density of $7.9 \times 10^{-6} \text{ kg/mm}^3$, the total inertia from the

drum assembly is:

$$I_{e_{\text{drum}}} = 716.6 \text{ kgmm}^2 \quad (2.108)$$

The overall effective inertia of the telescopic boom relative to the drum assembly is the sum of (2.105) and (2.108):

$$I_{e_{\text{boom}}} = 26.2 \times 10^3 \text{ kgmm}^2 \quad (2.109)$$

2.2 BOOM ELEVATION

The last boom member is supported by a pin at its tail end and by a linear actuator at its tip, as shown in Figure 2.32. The pin and linear actuator are both supported by the turret assembly, which allows the boom and elevation components to be rotated in the azimuthal plane.

In this section, details of the turret and linear actuator are discussed.

2.2.1 SUPPORT REACTIONS

The free body diagram of the fifth member, shown in Figure 2.32, can be analyzed in a manner similar to that in Section 2.1.6 to determine the pin and elevator reactions. Since the pin is parallel to the direction that the azimuthal reaction (R_θ) would be, this reaction is replaced with a moment about the tail end of the member. Physically, this moment is assumed to arise from reactions on the pin and will be discussed further in a section to follow.

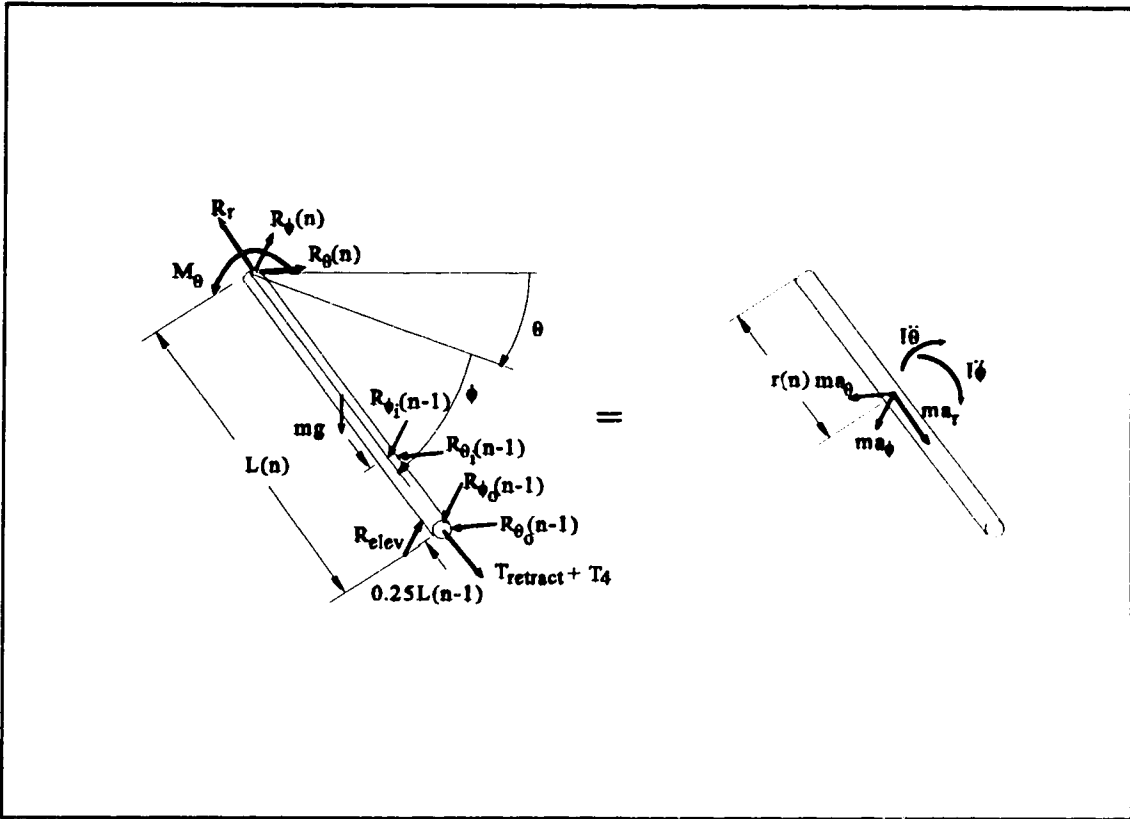


Figure 2.32: Free Body Diagram of Last (Fixed) Member

The reactions in the plane of the elevation rotation can be determined from the following equations:

$$R_{elev} = -\frac{I_5}{L_5} \frac{d^2\phi}{dt^2} + R_{\phi_s}(4) + \frac{L_5 - \frac{1}{4}L_4}{L_5} R_{\phi_i}(4) + \frac{m(g - a_\phi)}{2} \quad (2.110)$$

$$R_\phi = -m a_{\phi_s} + R_{\phi_s}(4) + R_{\phi_i}(4) + mg - R_{elev} \quad (2.111)$$

Using values from Appendix A, these reactions are:

$$R_{elev} = 680.9N \quad (2.112)$$

$$R_y = -262.5 N$$

(2.113)

These reactions will vary based on the boom deployment radius, however, the elevation reaction is a maximum for the configuration analyzed.

2.2.2 LINEAR ACTUATOR LOADING

The basis of the linear actuator used to rotate the boom in a vertical plane is a ball screw. A schematic of the linear actuator as installed is shown in Figure 2.33. The screw is supported by trunnion pins, which are housed in support flanges attached to the azimuth turret. The ball nut is attached by an external thread onto a length of pipe which is pinned to the tip of the last member. As the screw is rotated, the ball nut moves along the screw, changing the distance between the tip of the last member (B) and the position of the trunnion pin (C).

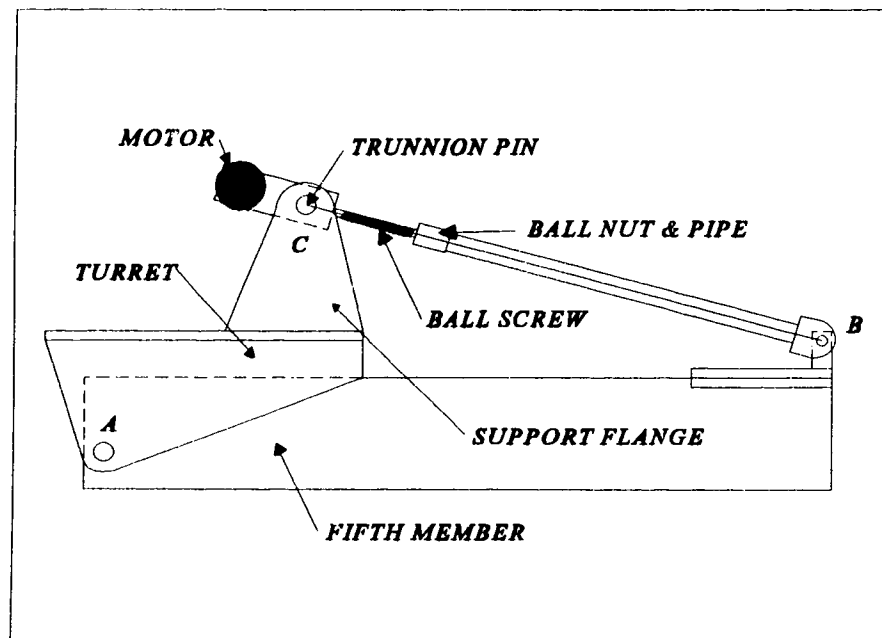


Figure 2.33: Elevation Assembly

The trunnion pins and the tip pin assembly allow the linear actuator to rotate as the boom rotates. Figure 2.34 defines the geometry of the triangle defined by points A, B, and C in Figure 2.33.

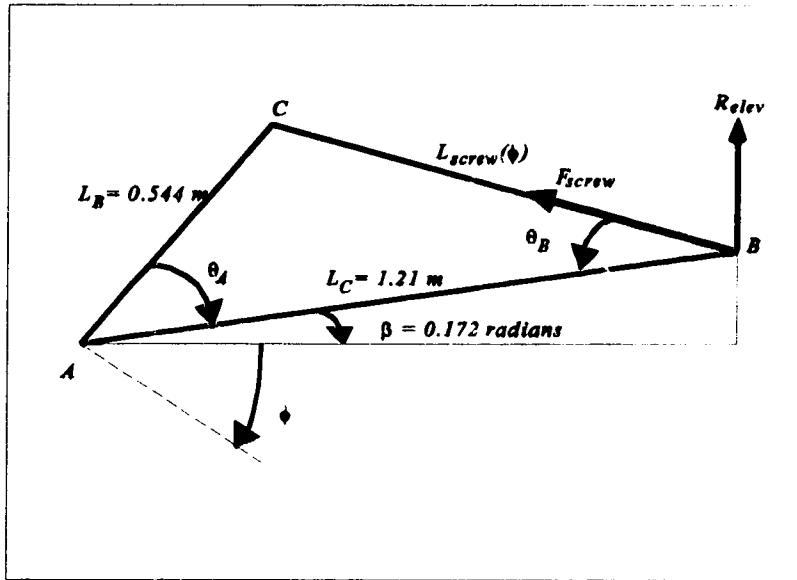


Figure 2.34: Elevation Assembly Geometry

The total force that the screw must exert on the pin at location "B" can be found from:

$$F_{screw}(\phi) = \frac{R_{elev}(\phi)}{\sin(\theta_B(\phi) - \beta)} \quad (2.114)$$

The angle $\theta_B(\phi)$ can be found using the law of sines as:

$$\theta_B(\phi) = \sin^{-1}\left(\frac{L_B \sin\theta_A(\phi)}{L_{screw}(\phi)}\right) \quad (2.115)$$

For any elevation angle, ϕ , the screw radius is obtained, using the cosine law, as:

$$L_{screw}^2(\phi) = L_B^2 + L_C^2 - 2L_B L_C \cos(\theta_A(\phi)) \quad (2.116)$$

where $\theta_A(\phi)$ is given by:

$$\theta_A(\phi) = \theta_A(\phi = 0) + \phi \quad (2.117)$$

Based on the position of the trunnion pin as constructed, $\theta_A(\phi = 0)$ is 0.703 radians.

Substituting this value as well as L_B and L_C from Figure 2.34, (2.116) becomes:

$$L_{screw}^2(\phi) = (1.771 - 1.341 \cos(0.703 + \phi)) m^2 \quad (2.118)$$

Substituting (2.117) and (2.118) into (2.115) yields:

$$\theta_B(\phi) = \sin^{-1} \left(\frac{0.544 \sin(0.703 + \phi)}{\sqrt{1.771 - 1.341 \cos(0.703 + \phi)}} \right) \quad (2.119)$$

The tensile force in the screw is then:

$$F_{screw}(\phi) = \frac{R_{elev}(\phi)}{\sin^{-1} \left(\frac{B \sin(0.703 + \phi)}{\sqrt{1.771 - 1.341 \cos(0.703 + \phi)}} \right) - 0.172} \quad (2.120)$$

It would be computationally intensive to determine the actual elevation force requirement, $R_{elev}(\phi)$, for any elevation angle using the method outlined in Section 2.1.6. Recognising that the maximum elevation force requirement will always occur with the boom fully extended, and that the force required to overcome inertia is very small compared to the force required to support the mass of the boom, a simplifying assumption can be made. This assumption is that the entire mass of the boom is concentrated at the radial mass center of the boom, and that the acceleration of the mass center is due to angular acceleration in the plane of the elevation rotation only. Figure 2.35 shows the simplified boom geometry.

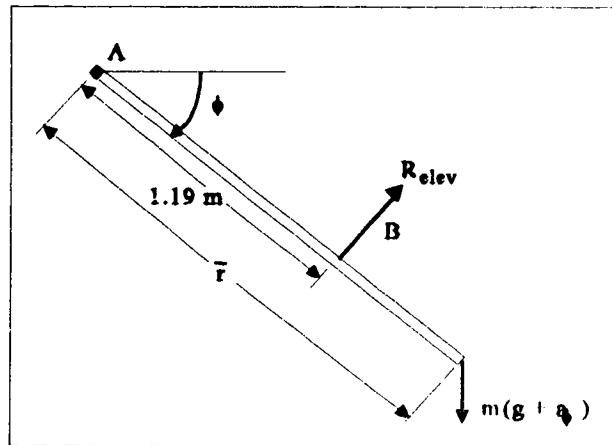


Figure 2.35: Simplified Boom Geometry

The mass center of the fully extended boom can be determined by:

$$\bar{r} = \frac{\sum_{n=1}^5 m_n \bar{r}_n}{\sum_{n=1}^5 m_n} \quad (2.121)$$

The acceleration of the mass center is given by :

$$a_{\phi \bar{r}} = \bar{r} \frac{d^2 \phi}{dt^2} \quad (2.122)$$

Substituting known values from Appendix A into (2.121) and (2.122) gives:

$$\bar{r} = 1.802 m \quad (2.123)$$

$$a_{\phi \bar{r}} = 0.193 \frac{m}{s^2} \quad (2.124)$$

Based on the simplified geometry, the elevation reaction can be found from:

$$R_{elev}(\phi) = \frac{1.80}{1.19} m(g + a_{\phi_r}) \cos(\phi) = 694.0 \cos(\phi) N \quad (2.125)$$

Substituting (2.125) into (2.120) results in the plot of the axial screw force as shown in Figure (2.36).

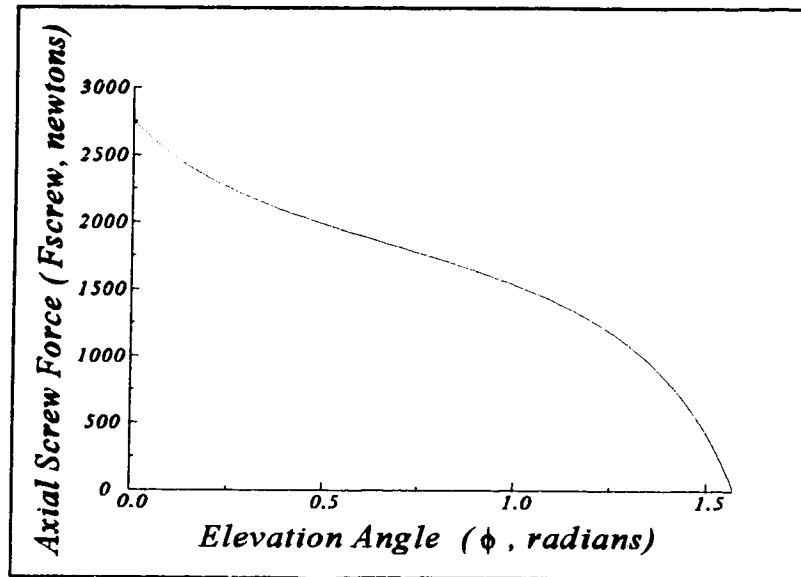


Figure 2.36: Axial Screw Loading

As shown in Figure 2.36, the maximum load is approximately 2750 N.

2.2.3 BALL BEARING SCREW

The ball bearing screw used was a Warner Electric GN-0705 screw and ball nut. The screw has a nominal root diameter of 0.750" (19.1 mm) and a thread pitch of five threads per inch (5.1 mm thread pitch). The ball nut has external threads on one end that allow it to be threaded into a 1" (nominal) schedule 80 steel pipe. An aluminum sleeve was fitted to the inside of the pipe to prevent wear between the steel screw and internal pipe surface.

Using method similar to those in Section 2.1.7, the estimated service life of the screw for the maximum axial load in Figure 2.36 is in excess of five million cycles. The maximum dynamic load capacity of the screw is over three times the expected dynamic load, and the maximum static loading before brinelling would occur is over 14 times greater than the expected static load. Brinelling can occur if the static load carried by the ball bearings is sufficient to dimple the screw surface.

The required screw length can be found from the difference in actuator lengths, as given in equation (2.118), at the extents of the elevation rotation. The actuator length for the horizontal boom position is:

$$L_{screw}(\phi = 0) = \sqrt{1.771 - 1.341 \cos(0.703)} = 0.865 \text{ m} \quad (2.126)$$

And for the vertical position, the actuator length is:

$$L_{screw}(\phi = \frac{\pi}{2}) = 1.624 \text{ m} \quad (2.127)$$

The required screw length is then:

$$L_{required} = 0.76 \text{ m} \quad (2.128)$$

The value given in (2.128) is the amount of screw travel required. The actual length of the screw must also include the length of the ball nut (70 mm) as well as an additional length to ensure that the ball nut does not extended past the end of the screw (25 mm). The actual screw length used was 0.86 m.

Using the screw pitch of 5.1 mm, the number of screw rotations for the full range of motion is:

$$n = \frac{0.76 \text{ m}}{5.1 \frac{\text{mm}}{\text{thread}}} = 149.6 \text{ rotations}$$

2.2.4 ACTIVATION TORQUE

The torque required to activate the ball screw based on the axial load is given by:

$$T_{act} = \frac{1}{2\pi} \frac{F_{screw} p}{\epsilon} \quad (2.129)$$

where p is the thread pitch (5.1 mm per thread), and ϵ is the screw efficiency which accounts for frictional losses between the balls and the screw thread. According to Wagner Electric specifications [7], the screw efficiency is between 90% and 95%. Using a maximum axial load of 2750 N, the activation torque requirement is:

$$T_{act} = \frac{1}{2\pi} \frac{2750 \text{ N} \times 5.1 \times 10^{-3} \text{ m}}{0.9} = 2.47 \text{ Nm} \quad (2.130)$$

2.2.5 EFFECTIVE INERTIA

The effective inertia of the elevation axis includes terms arising from the lead screw and the telescopic boom. The rotatory inertia of the ball screw is given by:

$$I_{BS} = \frac{1}{2} m_{BS} r_{BS}^2 = \frac{\pi}{2} r_{BS}^4 L_{BS} \rho_{steel} \quad (2.131)$$

where r_{BS} is the pitch radius of the ball screw (9.5 mm), L_{BS} is the overall length of the ball screw (0.93 m including end journals), and ρ_{steel} is the density of steel (7700 kg/m³). These

values give the ball screw inertia as:

$$I_{BS} = 90.9 \text{ kgmm}^2 \quad (2.132)$$

The effective inertia of the boom, I_{BOOM} , can be determined from the mass moment of inertia of the boom about the tail pin . If the ball screw is treated as a rotational reduction, the effective inertia of the boom is then:

$$I_{BOOM_{effective}} = I_{BOOM} \left(\frac{d\phi}{d\alpha} \right)^2 \frac{1}{\epsilon} \quad (2.133)$$

where $d\phi/d\alpha$ is the change in the boom elevation angle due to a rotation of the screw.

This reduction can be found by inverting equation (2.118) to obtain the following form:

$$\phi(L_{screw}) = \cos^{-1} \left(\frac{1.771 - L_{screw}^2}{1.341} \right) - 0.703 \quad (2.134)$$

The length of the actuator is given by :

$$L_{screw} = L_{screw}(\phi = 0) + \frac{\alpha}{2\pi p} \quad (2.135)$$

where alpha is the total rotation through which the ball screw has been turned. Evaluating (2.118) at $\phi = 0$, and using the thread pitch of the screw, the actuator length is:

$$L_{screw} = 0.865m + 0.808 \times 10^{-3} \alpha \frac{m}{rad} \quad (2.136)$$

Substituting (2.136) into (2.134) gives:

$$\phi(\alpha) = \cos^{-1}(0.763 - 1.043 \times 10^{-3} \alpha - 0.487 \times 10^{-6} \alpha^2) - 0.703 \quad (2.137)$$

Differentiating once with respect to α :

$$\frac{d\phi}{d\alpha} = \frac{1.043 \times 10^{-3} + 0.974 \times 10^{-6} \alpha}{\sqrt{1 - (0.763 - 1.043 \times 10^{-3} \alpha - 0.487 \times 10^{-6} \alpha^2)^2}} \quad (2.138)$$

The rotatory inertia of the boom can be found by:

$$I_{BOOM} = \sum_{n=1}^5 (I_n + m_n \overline{r_n^2}) \quad (2.139)$$

where I_n is the centroidal member inertia, m_n is the member mass, and $\overline{r_n^2}$ is the distance from the boom tail pin to the mass center of the member. Using the values in Appendix A, the boom inertia was found to be:

$$I_{BOOM} = 174 \text{ kgm}^2 \quad (2.140)$$

The plot in Figure 2.37 shows the behaviour of equation (2.133) using (2.138), (2.140), and a screw efficiency of 90%. The effective inertia varies in a non-linear manner in a range of 1285 kgmm² at a vertical elevation, and 414 kgmm² at $\phi = 0.39$ radians. Accounting for the screw inertia from (2.132) gives values for the effective inertia as:

$$505 \text{ kgmm}^2 < I_{BOOM, \text{effective}} < 1376 \text{ kgmm}^2 \quad (2.141)$$

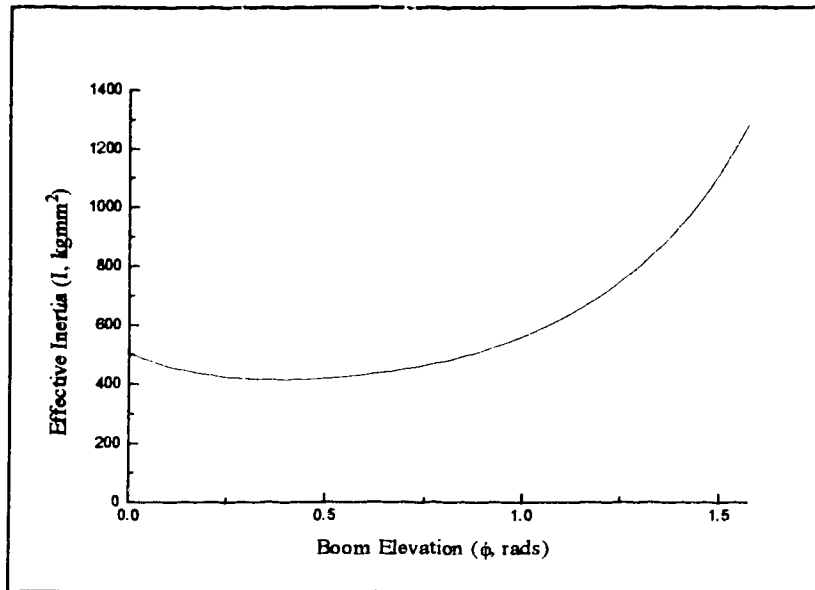


Figure 2.37: Effective Boom Inertia for Elevation Axis

2.2.6 ELEVATION TRUNNION SUPPORT FLANGES

Figure 2.38 shows a drawing of the trunnion support flanges used to support the linear actuator. Also shown is the loading at the trunnion pin location and the assumed reaction at the base of the support flanges.

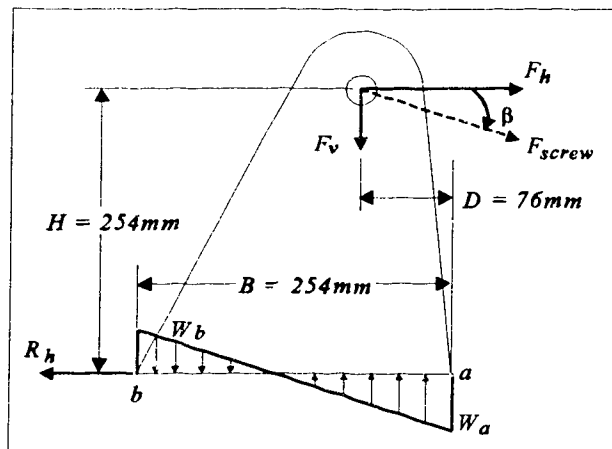


Figure 2.38: Trunnion Support Flange Loading

The value of the distributed load between "a" and "b" is given by:

$$W(r) = W_a + \frac{W_b - W_a}{B} r \quad (2.142)$$

Summing horizontal forces yields:

$$R_h = F_h = F_{screw} \cos(\beta) \quad (2.143)$$

Similarly, summing forces in the vertical direction gives:

$$\int_a^b W(r) dr = -F_v = -F_{screw} \sin(\beta) \quad (2.144)$$

where W_a is positive in the same direction as F_v . Evaluating (2.144) using (2.142) gives:

$$\frac{(W_a + W_b)B}{2} = -F_{screw} \sin(\beta) \quad (2.145)$$

Summing moments about position "a" gives:

$$\int_a^b W(r)r dr = F_{screw} H \cos(\beta) - F_{screw} D \sin(\beta) \quad (2.146)$$

Once again using (2.142), (2.146) becomes:

$$\frac{(2W_b + W_a)B^2}{3} = F_{screw} (H \cos(\beta) - D \sin(\beta)) \quad (2.147)$$

Using $\beta = 0.235$ radians, and $F_{\text{screw}} = 2750$ N, the unknown values in Figure 2.38 can be found to be:

$$R_h = 2675N \quad (2.148)$$

$$W_a = -39.3 \frac{kN}{m} \quad (2.149)$$

$$W_b = 34.3 \frac{kN}{m} \quad (2.150)$$

Each support flange is attached to the turret base web with 9 - 5/16" x 18 N.C. Grade 8 socket head capscrews, which are evenly spaced along the bottom of the flange. Each flange was fabricated from 1" nominal (25.4 mm) T6061-T6 aluminum plate. The minimum required capscrew preload to prevent separation of the joint in the tensile region is given by Juvinal [8] as:

$$F_i = \frac{k_j}{k_c + k_j} F_{\text{external}} \quad (2.151)$$

where F_i is the preload, k_c and k_j are the capscrew and joint stiffnesses, and F_{external} is the external load on the joint.

The capscrew and joint stiffnesses are given by:

$$k_{\text{comp}} = \frac{A_{\text{comp}} E_{\text{comp}}}{t} \quad (2.152)$$

where A_{comp} is the cross sectional area of the joint component, E_{comp} is the stiffness of the joint component, and t is the joint thickness. In this case, the joint thickness is the thickness of the

turret base web, which is 3/8" (9.5 mm) nominal T6061-T6 aluminum. The cross-sectional area of the capscrew is based on the root diameter of the thread, which is 7.6 mm. The cross-sectional area of the joint is given by:

$$A_j \approx d^2 + 0.68 dt + 0.65 t^2 \quad (2.153)$$

where d is the shank diameter of the capscrew. For the capscrews used, d is 5/16" (7.9 mm) nominal. Using these values, with elasticity moduli of 72 GPa for aluminum, and 207 GPa for steel, equation (2.151) becomes:

$$F_t = 0.568 F_{external} \quad (2.154)$$

The maximum tensile external load occurs at the capscrew location closest to edge "b" in Figure 2.38. An approximation of the loading at each location is the average load over one interval on either side of the capscrew. Since the nine capscrews are evenly spaced, there are ten capscrew intervals along the length of the flange base. The loading at the capscrew closest to edge "b" is then:

$$F_{external_{max}} = (W(B) + W(B - 2\frac{B}{10})) \frac{B}{10} \quad (2.155)$$

where B is the value given in Figure 2.38.

Using equation (2.142) to evaluate the distributed load, the maximum tensile load is:

$$F_{external_{max}} = 1369 N \quad (2.156)$$

Since this load is shared between the two flanges, the actual load at the capscrew location is

half the value in (2.156). Using this value, the required capscrew preload can be found from (2.154) to be:

$$F_t = 389N \quad (2.157)$$

If the shearing force on the joint, R_n , is assumed to be born by the capscrews rather than friction in the joint, and the shearing force is distributed uniformly over the 18 capscrews, the shearing load on each capscrew is:

$$F_{shear} = 149N \quad (2.158)$$

The stresses in the capscrew due to (2.157) and (2.158) are:

$$\sigma = \frac{F_t}{A_t} = \frac{389N}{33.8 \times 10^{-6}} = 11.5MPa \quad (2.159)$$

$$\tau = 4.4MPa \quad (2.160)$$

where A_t is the tensile area of the thread. The equivalent tensile stress in the capscrews using distortion energy is:

$$\sigma_e = \sqrt{\sigma^2 + 3\tau^2} = 13.8MPa \quad (2.161)$$

Compared to the proof stress of 650 MPa for the capscrews used, this seems to be a safe loading condition. However, the increase in equivalent tensile loading of the bolt due to shear loading of the joint can't be ignored.

A common practice is to initially torque the capscrews to their proof load, since for separating loads the capscrew load cannot be increased significantly unless the joint separates, and for joint shearing loads, the increased tension in the capscrew increases the friction in the joint, which bears a large portion of the shearing load. In this case, however, an initial torque which loads the capscrew to approximately half of its proof load is sufficient to prevent joint separation and at the same time insure that the capscrew does not fail if the shearing load is born by the capscrews rather than joint friction. The initial torque to required to provide an initial tensile stress of half the proof load is given by:

$$T = 0.09A_t S_p d = 16Nm \quad (2.162)$$

where S_p is the proof load and d is the nominal shank diameter. The factor in (2.162) accounts for friction in the threads and between the capscrew head, as well as the thread geometry. As installed, the capscrews were initially torqued to a value between 10 and 20 Nm.

2.3 AZIMUTH ROTATION

The boom is supported at its tail end by a pin that allows rotation in the plane of elevation. This pin also imparts a moment on the boom to rotate it in the azimuthal plane. The turret assembly is attached to a slewing bearing that allows rotation in the azimuthal plane. Details of the slewing bearing and the azimuth rotation are discussed in this section.

2.3.1 SUPPORT REACTIONS

Figure 2.39 shows a top view of the pin assembly and the force couple that facilitates the azimuthal rotation.

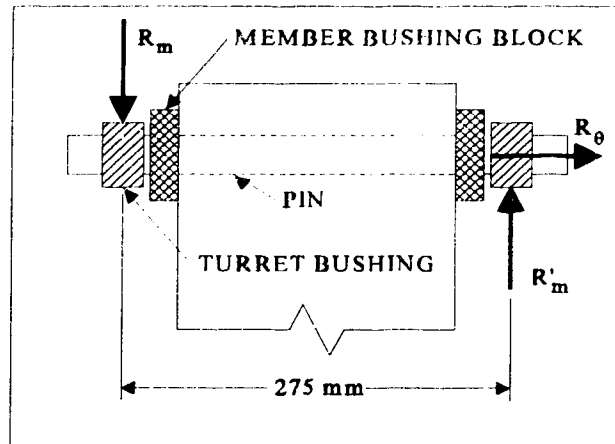


Figure 2.39: Azimuth Support Couple.

From the free body diagram of the last member, shown in Figure 2.32, the support couple, M_θ , and reaction, R_θ , can be determined from the following equations:

$$R_\theta = -m a_{\theta_5} + R_{\theta_0}(4) + R_{\theta_1}(4) \quad (2.163)$$

$$M_\theta = -I_5 \frac{d^2\theta}{dt^2} - \frac{m a_{\theta_5} L_5}{2} + R_{\theta_0}(4)L_5 + R_{\theta_1}(4)(L_5 - \frac{1}{4}L_4) \quad (2.164)$$

Evaluating these equations using values from Appendix A gives:

$$R_\theta = 18.0N \quad (2.165)$$

$$M_\theta = -47.8 Nm \quad (2.166)$$

The value of the moment given in (2.166) is the required activation torque of the azimuth axis. It can be shown that the pin reaction couple will have magnitudes of :

$$R_m = R'_m = 173.8N \quad (2.167)$$

2.3.2 BOOM TRUNNION SUPPORT FLANGES

The boom tail pin is supported by two flanges that run the length of the azimuth turret. The flanges, constructed from 3/8" (9.5 mm) T6061-T6 aluminum plate, are attached to the turret base web with 14 10-24 socket head screws spaced every 25 mm to 75 mm. Figure 2.40 shows support flanges with the combined loading at the pin from the elevation azimuth rotations.

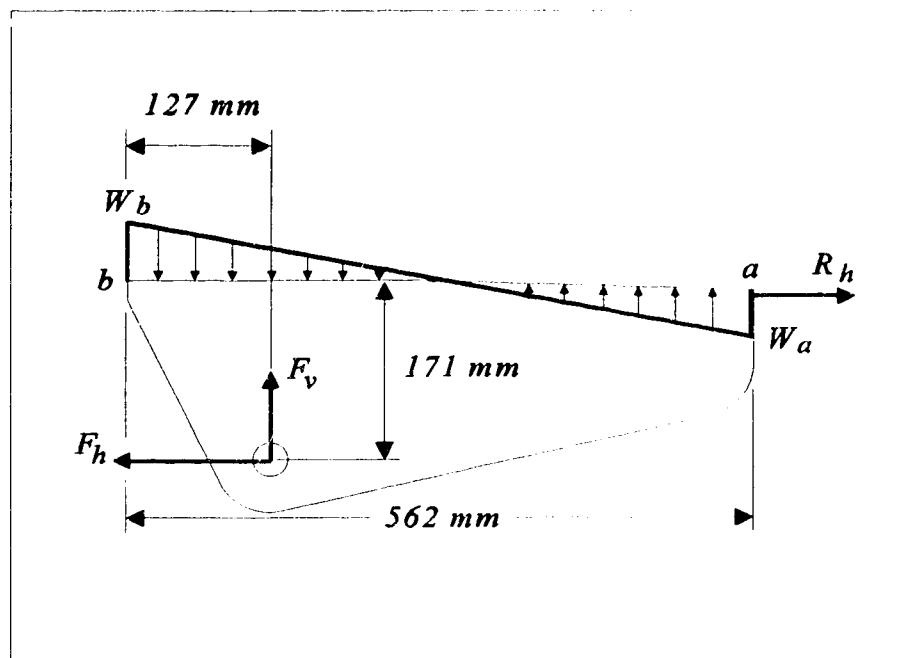


Figure 2.40: Boom Trunnion Flange Loading

The vertical force on the boom pin, F_v , was found previously in (2.113). The horizontal force, F_h , is the combination of the horizontal load on the boom at the elevation actuator, given in (2.148), and the force couple that rotates the boom in azimuthal plane, given in (2.167).

Using the method outlined in Section 2.2.6, the values defining the distributed reaction can be found to be:

$$W_a = 5.72 \frac{kN}{m} \quad (2.168)$$

$$W_b = -6.65 \frac{kN}{m} \quad (2.169)$$

In Section 2.2.6, the joint in question was under a separating tensile load. In this case, the joint between the boom support flanges and the turret web is subjected to a shearing load. The shearing load is composed of the horizontal reaction, R_h , and the vertical distributed, $W(r)$. The approximate shear loading due to the vertical distributed load can be found from the average load over two screw intervals, as outlined in Section 2.2.6. The horizontal load can be assumed to be uniformly distributed between all the screws in each flange.

The screw locations which undergo the maximum shearing force are the locations closest to the edges of the flange. These locations are approximately 12 mm from the flange edges. The screw spacing near edge "a" in Figure 2.40 is approximately 75 mm whereas the spacing near edge "b" is 25 mm.

The maximum shear force can be shown to occur at the screw location closest to edge "a", with an approximate value of:

$$F_{shear_{max}} = 280 N \quad (2.170)$$

This corresponds to a shear stress of approximately 25 MPa. The screws were torqued to approximately 3 Nm, which induces stresses in the screws to half their proof load.

2.3.3 AZIMUTH SLEWING RING

The azimuth turret is supported by a slewing ring, which allows the turret to rotate in a horizontal plane. This method of supporting a boom requiring an azimuth rotation is quite common in the design of cranes. Slewing rings are large sized bearings, and in general are distinguished from conventional roller bearings by the presence of threaded holes in the inner and outer bearing races used to secure the bearing to both the load it carries and the base structure.

The slewing ring used was manufactured by Gear Products Inc., and has the official designation of : Rotation Bearing 449 - 03054 - 1. The diameter of the bolt pattern on the inner race is 175 mm. The azimuth turret base web is mounted on this race. Figure 2.41 shows the loading on the azimuth turret, and the assumed distributed normal support load at the location of the inner race of the slewing ring.

Using the method outlined in Section 2.2.6, the distributed load is defined by:

$$W_a = 139.1 \frac{kN}{m} \quad (2.171)$$

$$W_b = -134.8 \frac{kN}{m} \quad (2.172)$$

The maximum tensile load on any of the capscrews which fix the turret base web to the inner race of the slewing ring occurs at location "a" in Figure 2.41. The value of this tensile load is:

$$F_a = 926N \quad (2.173)$$

For this value the 5/8" - 11 N.C. bolts should be initially torqued to at least 20 Nm to ensure that joint separation does not occur.

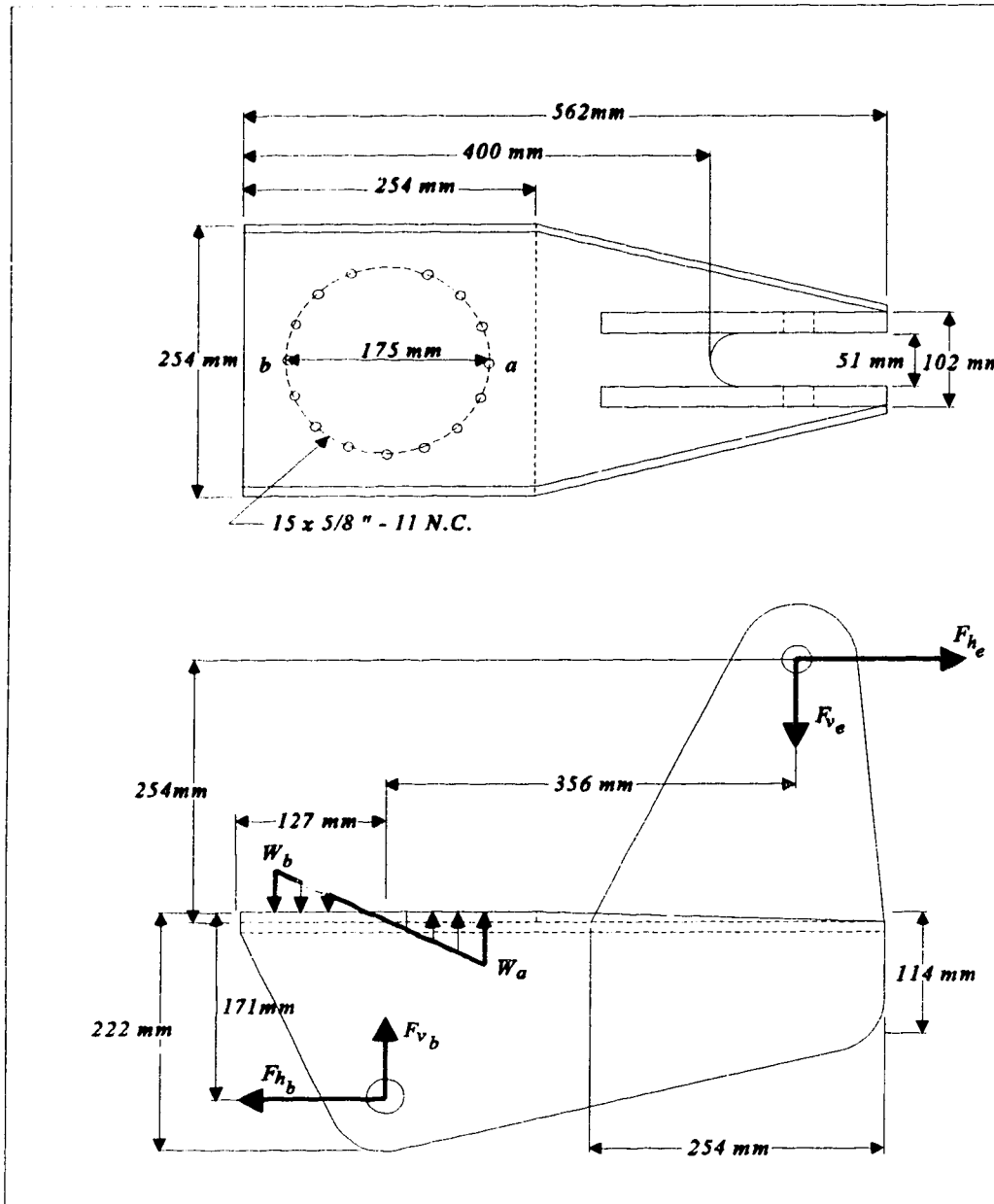


Figure 2.41: Azimuth Slewing Ring Loading

The resultant moment about the slewing ring axis due to the distributed load is given by:

$$M_{SR} = \int_a^b W'(r)r dr \quad (2.174)$$

where $W(r)$ is the function defining the distributed load with respect to the center of the bearing. The form of $W'(r)$, where $r = 0$ is the center of the bearing, is given by:

$$W'(r) = W\left(r + \frac{r_b - r_a}{2}\right) = W_a + (W_b - W_a)\left(\frac{r}{B} + \frac{1}{2}\right) \quad (2.175)$$

Using (2.175) in (2.174), the resultant moment is:

$$M_{SR} = 700 Nm \quad (2.176)$$

In a similar manner, the axial load on the slewing ring may be determined to be:

$$F_{SR} = 377 N \quad (2.177)$$

Although bearing specifications for the slewing ring used were unavailable, a comparable model produced by SKF can be shown to have an estimated service life in excess of one million rotations based on the loading given by (2.176) and (2.177). The static and dynamic load rating for the ring is 15 kN, far greater than the expected loading. For this reason, the slewing ring used is deemed adequate.

2.3.4 MANIPULATOR MOUNTING STRUCTURE

The mounting structure must accommodate the diffuser activation system as well as providing a rigid surface from which to suspend the manipulator. The structure consists of a dodecahedral cylinder which encloses the activation crank. The diffuser activation ropes pass through rectangular holes in alternating sides of the dodecahedron, and are supported by rollers on either side of the holes, as shown in Figure 2.42.

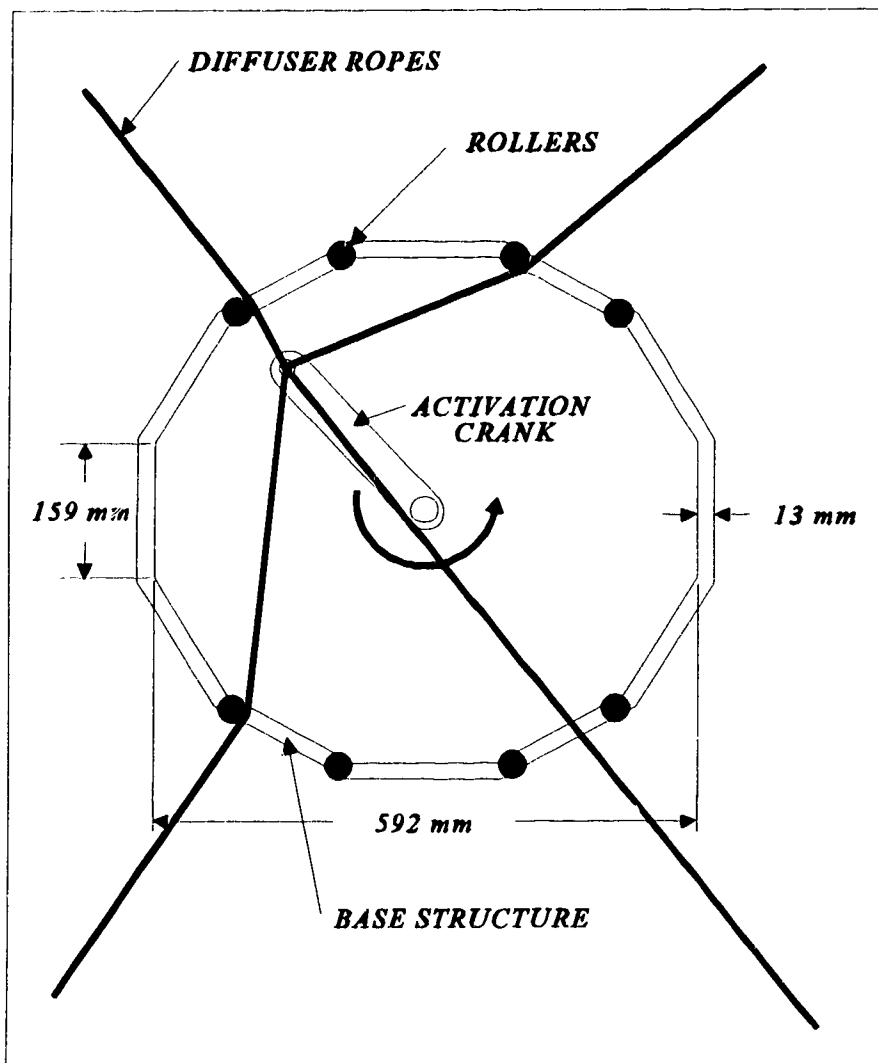


Figure 2.42: Dodecahedral Mounting Structure Details

Figure 2.43 is a photograph of the mounting structure as installed. The dodecahedral cylinder is suspended from the ceiling by twelve 1" - 8 N.C. studs through a flange at the top of the cylinder. The stud holes pass through the concrete ceiling slab and a mating flange on the roof. Although the stud size and number used were more than sufficient to support the expected loading, allowance was made to accommodate the possibility that the stud location coincided with one of the several cables running the length of the core floor slabs used in the roof. If this circumstance occurred, one or more of the studs could be left out. As installed, the small chamber has ten studs while the large chamber has the full twelve.

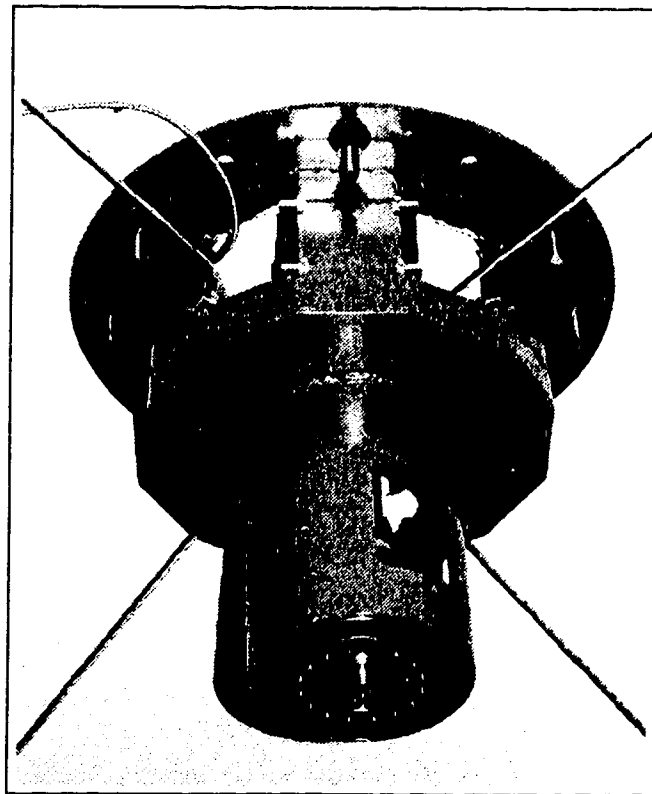


Figure 2.43: Mounting Structure As Installed

At the bottom of the cylindrical section is an internal flange and column, at the bottom of which the slewing ring is mounted. The column is comprised of a length of 12" (305 mm) schedule 40 steel pipe. The length of the column positions the boom pin at 1 m from the ceiling, and allows clearance between the bottom flange of the dodecahedral section, and the elevation trunnion flanges.

The column is assembled in two sections, with internal flanges, to allow access to the azimuth drive reduction and actuator. The column has several rectangular holes along its length to access the bolts securing the slewing ring and column sections.

2.4 AXIS ACTUATION

Selection of the actuator type depends on many factors, but a major concern is the type of control system to be used. Control systems can be roughly separated into two classes: open and closed loop. Any control system may be comprised of elements of each class.

An open loop control system sends motion control information to an actuator, but does not monitor the actual performance of the actuator. A closed loop system monitors the actuator by measuring the actuator output, comparing it to the input, and adjusting the actuator input to compensate for the difference.

The simplest and most cost effective system to implement is the open loop system. Noting that an open loop system can be changed into a closed loop system if the necessity arises, this is the system implemented for the manipulator.

In general, two types of axis actuators are feasible for this application, electrical and hydraulic. Both types lend themselves to computer control, and the physical size of the actuators required to provide the essential power is not inhibitive in either case. However,

hydraulic actuators are not appropriate for applications involving open-loop control. For that matter, the only common electrical actuators suitable for open-loop operation are stepper motors.

This section deals with the selection of the appropriate sized stepper motors. A more detailed discussion of the control system is located in Chapter 3. Figure 2.44 shows the location of the individual axis motors and drive reductions.

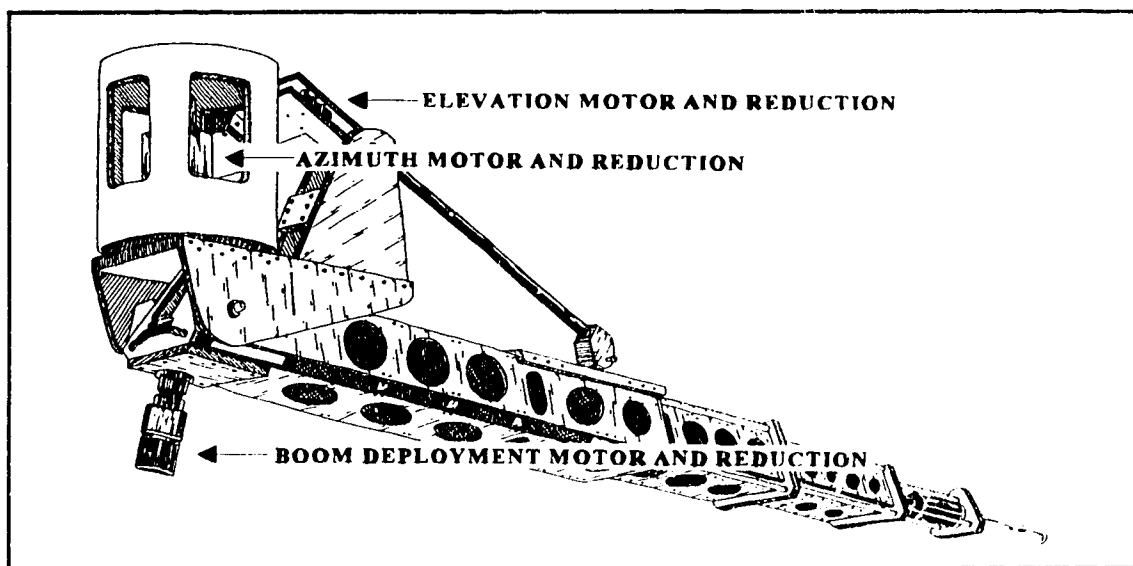


Figure 2.44: Axis Actuator Locations

2.4.1 SELECTION CRITERIA

Two factors must be considered when selecting the appropriate sized stepper motors. The most obvious consideration is that the motor be capable of supplying the desired torque in the speed range required. Figure 2.45 shows the output torque - speed characteristics typical of stepper motors.

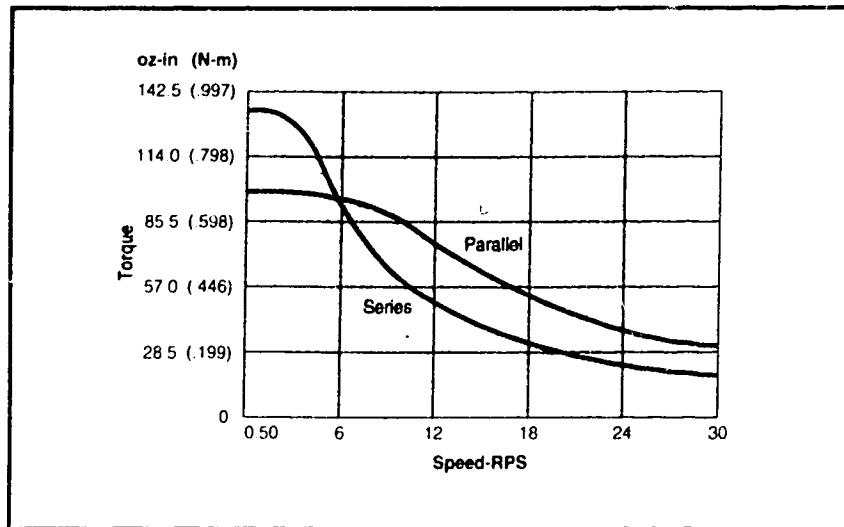


Figure 2.45: Stepper Motor Torque vs. Speed Characteristics

As shown above, the output torque drops off at higher speeds. The low speed torque is higher if the motor windings are wired in series, and higher for parallel connections at moderate speeds. Connection of the motor winding in parallel also heats up the stepper significantly more than series windings, which reduces the period of time that they can be run at high speeds.

The other major consideration when selecting steppers is the ratio between the rotor inertia of the stepper and the effective inertia of the driven load. If the rotor inertia is relatively high, resonances caused by the operation of the stepper motor can become more pronounced. These resonances can cause the motor to stall, which is difficult to account for in an open loop system.

Alternatively, if the rotor inertia is relatively low, the motion of the load dominates the system. This results in longer acceleration/deceleration intervals, as rapid changes in speed may not occur properly, causing lost steps. Most stepper motor manufactures suggest

selection of motors with rotor inertias of between one tenth and one quarter of the effective load inertia, although some sources give values as high as 1:1.

Table 2.5 is a summary of the activation torque, maximum rotational speed input, and effective inertia for each axis from previous sections.

| AXIS | EFFECTIVE INERTIA $I_{\text{effective}}$, kg-mm ² | ACTIVATION TORQUE $T_{\text{activation}}$, N-m | MAXIMUM INPUT SPEED ω_{max} , RPS |
|------------|--|--|--|
| DEPLOYMENT | 26.2×10^3 | 30 | 0.32 |
| ELEVATION | 505 - 1376 | 2.47 | 4.99 |
| AZIMUTH | 174×10^6 | 47.8 | 0.017 |

Table 2.5 ; Summary of Axis Actuation Characteristics

2.4.2 ACTUATOR DRIVE REDUCTIONS

From specifications supplied by several stepper motor manufacturers, the largest commonly available stepper motor could supply a maximum low speed torque of approximately 32 Nm, and has a rotor inertia of approximately 6150 kg-mm². If for no other reason than to alter the effective load inertia and torque requirements for the azimuth axis, the use of drive reductions between the axis and stepper motor must be considered.

A further important consideration is that a drive reduction will increase the positioning resolution. One revolution of a common stepper motor is divided into two hundred steps, each step consisting of a 1.8° rotation. In the case of a directly driven azimuth rotation, this severely limits the number of positions that can be attained.

A criterion in selecting the appropriate drive reduction is that the stepper motor requirements be small enough to ensure that the motion of the axes is not inhibited, especially in the case of the elevation rotation. The presence of the support column and the flange on

the bottom of the dodecahedral cylinder limit the clearance available for a motor at the trunnion end of the ballscrew.

Another minor consideration is that the steppers for all three axes be of the same approximate size. This provides the possibility of exchanging motors between axes if the situation arises that the performance of a particular motor is substandard. Temporarily exchanging the motors can eliminate, or pinpoint, a number of components during the troubleshooting process.

A final consideration is that the drive reductions selected for the azimuth and deployment have a small backlash value. This is especially important since the deployment and azimuth axes have the potential for the direction of the actuating force to reverse. Any backlash in these system results in lost motor steps when a direction change occurs. Since the control system is of the open loop variety, these losses cannot be accounted for.

As a result of the above consideration, different types of drive reductions were selected for the azimuth and deployment axes than for the elevation axis. The elevation axis reduction is a conventional gear-type drive reduction. The azimuth and deployment axes use Harmonic Drive reducers.

2.4.3 HARMONIC DRIVE REDUCERS

Harmonic Drive reducers are gear type reducers that provide zero backlash without the complexity required in conventional zero backlash gearsets. These reducers are also capable of providing high ratio reductions and high torque capacities in a single stage without the component mass and physical size of conventional gear reduction units. This type of reduction is commonly applied in industrial robotics. Figure 2.46 shows the three constituent

components of the Harmonic Drive.

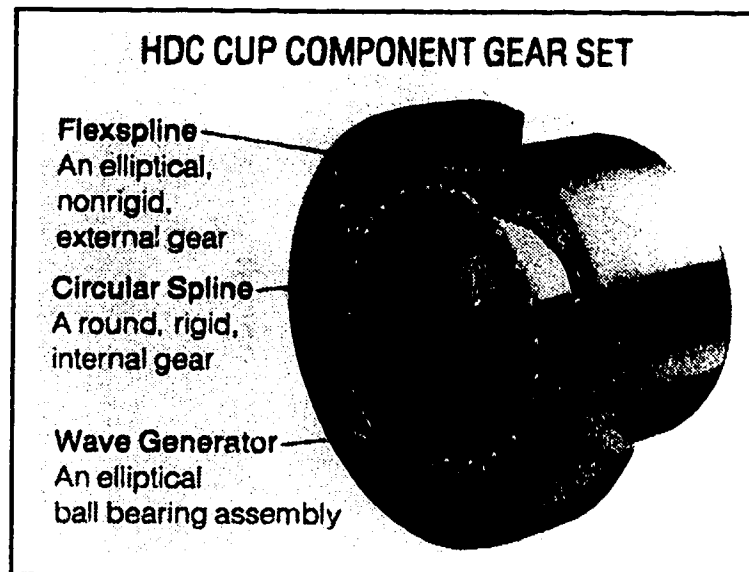
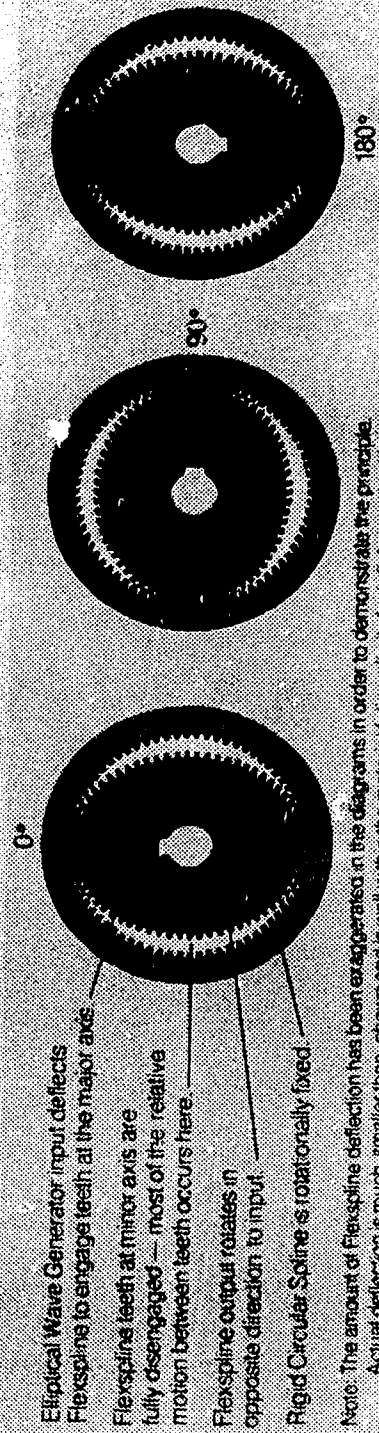


Figure 2.46 : Harmonic Drive Components

Harmonic Drives are comprised of three concentric elements: an elliptical plug/ball bearing assembly (wave generator), a flexible cup with an external spline (flexspline), and a rigid ring with an internal spline (circular spline or ringspline). The flexspline normally has two less teeth than the ringspline. Since the spline teeth have the same pitch, the flexspline has a slightly smaller diameter than the ringspline. The wave generator has a major diameter which is larger than the flexspline diameter by the difference of the flexspline and ringspline pitch diameters.

When the three components are assembled, the wave generator deflects the flexspline so that its teeth mesh with the ringspline teeth at both ends of the major axis. The teeth at the ends of the minor axis move radially inward to provide clearance between the flexspline and ringspline. Figure 2.47 shows the principle of operation for Harmonic Drives.

PRINCIPLE OF OPERATION



Elliptical Wave Generator input deflects Flexspine to engage teeth at the major axis.
 Flexspine teeth at minor axis are fully disengaged — most of the relative motion between teeth occurs here.
 Flexspine output rotates in opposite direction to input.
 Rigid Circular Spine is rotationally fixed.

Note: The amount of Flexspine deflection has been exaggerated in the diagrams in order to demonstrate the principle. Actual deflection is much smaller than shown and is well within the material fatigue limits for normal service life.

Figure 2.47 : Principle of Harmonic Drive Operation

Since the flexspline has two fewer teeth than the ringspline, as the wave generator is rotated through half a turn, relative motion occurs between the flexspline and the ringspline in the direction opposite to input rotation. A full rotation produces relative motion of two spline teeth. The effective reduction ratio is half the number of teeth on the flexspline.

The Harmonic Drive reductions for the azimuth and deployment axes were selected on the basis of the maximum output torque ratings, which are specified according to the flexspline diameter. Based on the torque requirements given in Table 2.5, appropriate sized drive units were selected.

2.4.4 REDUCTION RATIOS AND MOTOR SELECTION

The criteria for choosing the size of stepper motor is based on the axis characteristics, which are affected by the drive reduction. Since the choice of the drive reduction ratio should adjust the axis characteristics to closely match the performance characteristics of a particular motor, these selections are normally performed at the same time. This section discusses the selection process for each of the three axes.

2.4.4.1 Elevation Axis

Based on the selection criteria in section 2.4.1, and the characteristics of the elevation axis given in Table 2.5, an appropriate motor would be able to supply a torque of at least 2.5 Nm at a rotational speed of 5 RPS and have a rotor inertia in a range between 50.5 and 344 kgmm². The performance of a potential choice is shown in Figure 2.48. The motor has a rotor inertia of 187 kgmm².

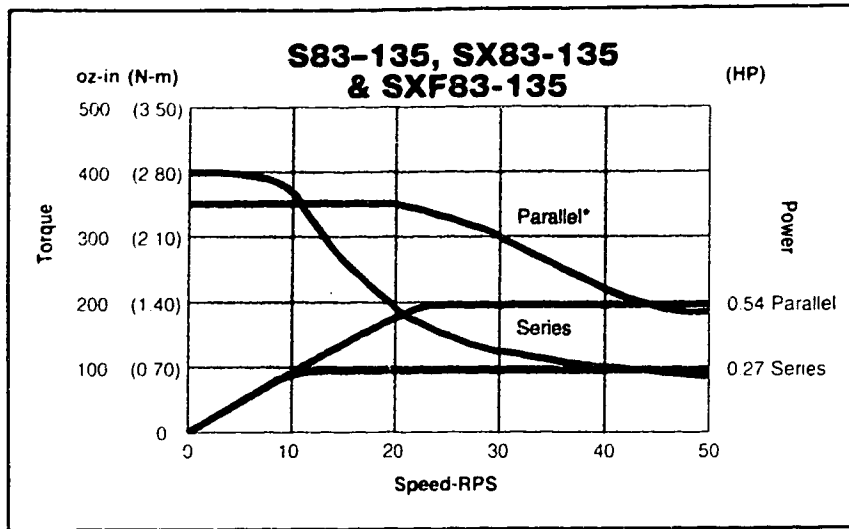


Figure 2.48: Performance Curve for Compumotor S83 - 135 Stepper Motor

As shown above, the motor could supply an adequate torque at the desired speed. However, there is not a large margin of error to accommodate for unaccounted losses in the system.

Applying a drive reduction with a ratio "R" with a mechanical efficiency of "ε" and a known moment of inertia $I_{reduction}$ would have the following effect on the axis characteristics:

$$I'_{required} = \frac{I_{required}}{R^2} + I_{reduction} \quad (2.178)$$

$$T'_{required} = \frac{T_{required}}{\epsilon R} \quad (2.179)$$

$$\omega'_{max} = R \omega_{max} \quad (2.180)$$

For a 2:1 reduction with an efficiency of 80% and an inertia of 50 kgmm², the axis characteristics become:

$$177 < J'_{\text{effective}} < 394 \text{ kg-mm}^2 \quad (2.181)$$

$$T'_{\text{required}} = 1.54 \text{ N-m} \quad (2.182)$$

$$\omega'_{\text{max}} = 9.98 \text{ RPS} \quad (2.183)$$

According to the values in (2.181), a rotor inertia in the range of 17.7 to 98.5 kgmm² is required. The next smallest motor to the one discussed above has a rotor inertia of 123 kgmm². This corresponds to approximately a third of the maximum effective load inertia which is slightly higher than most manufacturers recommend. The performance of this motor is shown in Figure 4.49.

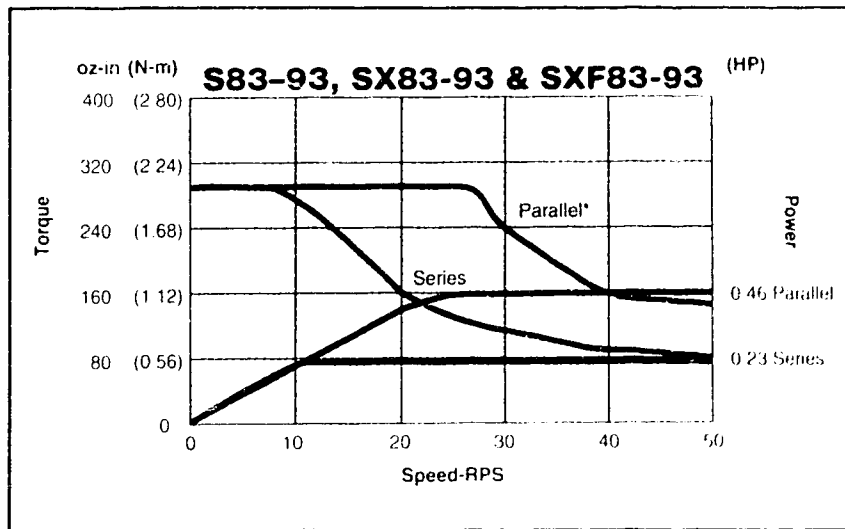


Figure 2.49: Performance Curves for Compumotor S83 - 93 Stepper Motor

As illustrated above, the motor has a larger excess torque margin than the previous motor. It can be shown that the next smallest motor to this one has a rotor inertia in the

desired range, however cannot supply the required torque. It is for these reasons that this is the motor selected for the elevation axis. If the higher rotor inertia value presents a problem in the actual performance of the axis, load inertia in the form of a flywheel can be added to the actuator, most likely at the tail shaft of the motor.

2.4.4.2 Azimuth Axis

The maximum reduction ratio available for the Harmonic Drive reductions is 200:1, with a mechanical efficiency of 70%. Applying this as the reduction value to the information given in Table 2.5 results in a required rotor inertia in the range of 435 to 1090 kgmm². The required output torque is 0.34 Nm at a maximum speed of 3.4 RPS.

The torque requirement can be provided by the smallest of stepper motors with an acceptable margin for error, however, the rotor inertia requirement can only be provided by significantly larger and more costly stepper motors. Figure 2.50 shows the performance curve for the next largest motor, with a rotor inertia of 805 kgmm², to that in Figure 2.48.

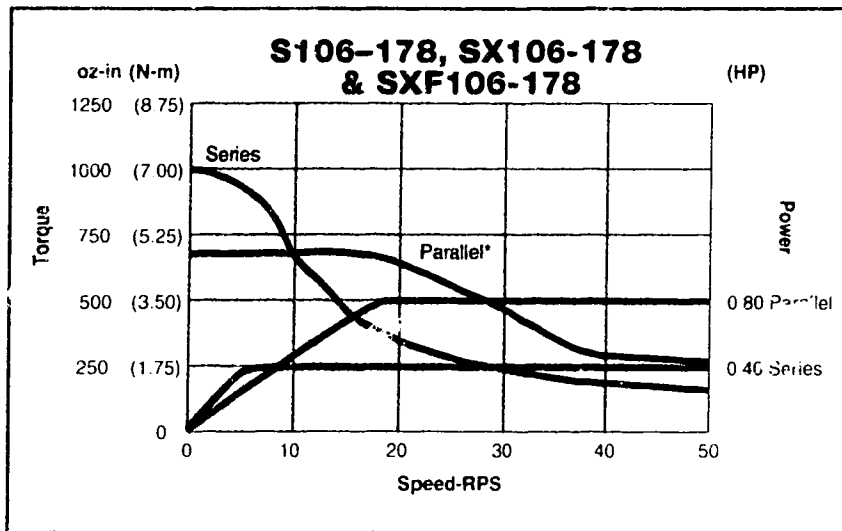


Figure 2.50: Performance Curve for Compumotor S106 -178 Stepper Motor

As shown above, the torque requirement is approximately twenty times less than the potential. Since this axis requires a relatively low torque at a low speed, and the acceleration interval of one second is relatively long, the rotor inertia criterion may be relaxed in this case to allow the use of a smaller, more cost effective motor. As a result, the motor whose performance curve is shown in Figure 2.48 was selected.

2.4.4.3 Boom Deployment Axis

The criterion for selecting the reduction for the deployment axis was to maximize the positioning resolution. As a result, the ratio selected was 160:1. The appropriate rotor inertia for this reduction is between 0.10 and 0.26 kgmm², and the torque requirement is 0.27 Nm at a rotational speed of 51.2 RPS.

The rotational speed requirement is above the maximum recommended speed by 2.4%. However, since this limitation only increases the positioning time by 0.72 seconds, this relaxation of the maximum move time is acceptable.

The low rotor inertia requirement cannot be met even by the smallest of conventional steppers. This fact coupled with the relatively high torque requirement at the maximum speed of 50 RPS demands the use of a flywheel with a larger motor.

The motor whose performance is shown in Figure 2.48 was selected on the basis that a large torque margin at top speed will be the limiting factor for this axis. A flywheel with a rotatory inertia of approximately 1800 kgmm² was mounted on the tail shaft of the motor to give the axis an effective inertia close to ten times the rotor inertia of 187 kgmm². This effective inertia was chosen to reduce the effect of high speed resonance typical of stepper motors. The implications of these decisions will be discussed in Chapter 3.

2.4.5 POSITIONING RESOLUTION

Based on the drive reduction values and the axis characteristics, the resolution for one step in each of the three axes for the boom in the fully extended position are given in Table

2.6. From these values, the overall resolution is 0.50 mm.

| AXIS | RESOLUTION (δ , mm) |
|------------|-----------------------------|
| AZIMUTH | 0.70 |
| ELEVATION | 0.18 |
| DEPLOYMENT | 0.011 |

Table 2.6: Full Step Axis Resolutions

In Chapter 2, the design of the specific machine components was discussed in detail. Also, the axis actuators were specified as stepper motors, allowing the control system to be of the open loop variety. Usually, an open loop system can be converted to a closed loop system by the addition of feedback devices that monitor the motor performance, normally velocity and position. As a result, an appropriate starting point is the implementation of an open loop control system.

The control system selected for this application is a Compumotor PC-23 motion control system. This chapter is divided into sections dealing with the details of the control system used, the performance of this system with the manipulator, and the overall cost of the manipulator.

3.1 CONTROL SYSTEM ELEMENTS

Figure 3.1 shows the typical elements of an open loop motion control system for an application with one axis of motion. Additional axes can be added to the system at the location shown. Each of the control system elements will be discussed in this section.

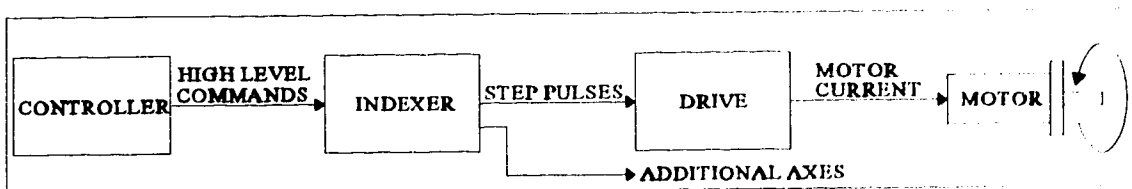


Figure 3.1: Motion Control System Elements

3.1.1 CONTROLLER

In general terms, the controller provides an interface between the user and the control system. The controller also manages the desired task that the application performs. This involves communicating to the indexer the desired motion, at the appropriate moment.

Commonly available controllers may be integrated into a personal computer, may be "stand alone" such that no other peripheral devices are required, or a combination of the two. A true stand alone controller can be easily programmed to control repetitive tasks, but for use in more complex applications where the required motion can change due to unrelated factors, these controllers normally have the potential of communication with other devices. Although a stand alone controller would allow operation of the M.E.A.N.U. manipulator without any peripheral devices, the testing procedure is already controlled by a personal computer. It was for this reason that a PC based controller was selected.

The Compumotor PC-23 controller is designed as a peripheral inserted into a single expansion bus slot on an IBM® PC. The PC-23 is capable of controlling three axes simultaneously, with provision for encoder inputs to operate the system in a closed loop manner. The PC-23 also has the ability to interrupt the host computer under user defined circumstances, and furnishes an input for a two-axis joystick. As well as six limit switch inputs to provide open loop position information for each axis, the controller also provides six programmable Transistor-Transistor Logic (TTL) outputs. The TTL outputs can provide either a low signal of less than 0.8 volts or a high signal of between 2.5 and 5 volts. Although only one of the TTL outputs has a planned use for the manipulator itself, the remaining outputs could prove useful for other applications in the M.E.A.N.U. testing procedure.

The controller is also capable of providing system status information, such as the motor position according to an internal counter, limit switch status, and configuration information. Although precise values for the motor position would require components associated with closed loop systems, the position according to the command inputs is recorded.

The PC-23 motion control system was chosen for the following reasons. Since the PC-23 controller relies on a user supplied microprocessor and display, it is more cost effective. The PC-23 is also capable of controlling the three manipulator axes simultaneously, with provision for closed loop control if necessary. Other controllers with similar features were available, however, most were capable of controlling either two or four axes. Application of these controllers was found to be more expensive.

The controller can be operated using any of the commonly used programming languages, such C, Fortran, or QuickBASIC. The control algorithm must be developed by the user, although several commonly used subroutines are supplied with the system. A terminal emulation program was also supplied with the system, but was limited in its usefulness.

3.1.2 INDEXER

The indexer is the component that provides the pulse information that controls the motor drivers. The series of indexer pulses is altered according to the desired acceleration, velocity or position. In a closed loop system, the indexer has the added task of monitoring the performance of the motors, and adjusting the output pulses accordingly. Figure 3.2 is a diagram of the indexer system.

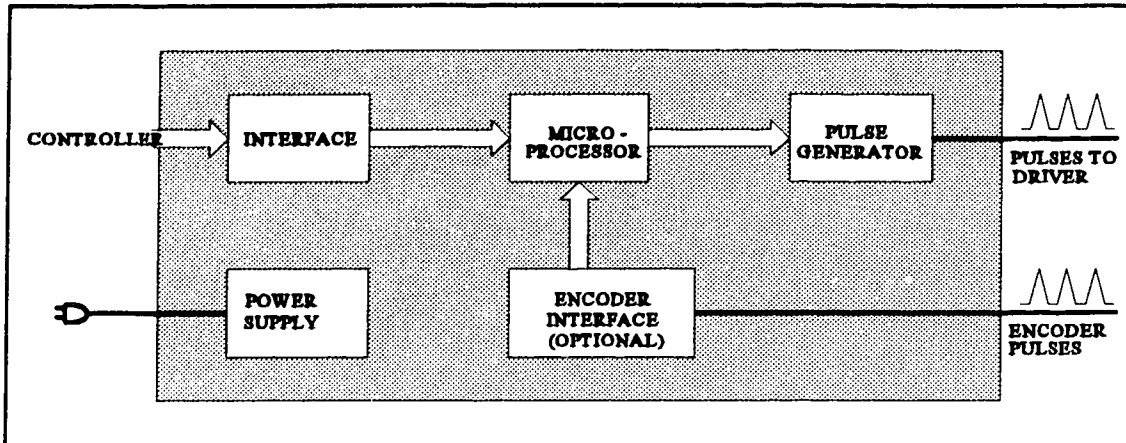


Figure 3.2: Indexer System Diagram

Whereas the controller is operated using common programming languages and practices, the indexer receives information in the form of an executable code. This code, termed X-code by Compumotor, is specific to the manufacturer. The code consists of approximately one hundred commands that govern all the features of the control system.

The PC-23 indexer is capable of supplying step pulse output frequencies between 250 Hz and 2 MHz and can change the output frequency at rates between 250 Hz/second and 25 MHz/second. The indexer can provide simultaneous signals in the above frequency ranges to three separate axes. These frequency ranges are capable of accelerating the axes to their design objective values.

3.1.3 MOTOR AND MOTOR DRIVE

The motor drive amplifies the indexer output to the higher D.C. voltages and currents required to operate the motors. As mentioned previously, the motors are standard 1.8° stepper motors.

The motor drivers selected were Compumotor S Series Microstepping drivers. Microstepping drives subdivide the basic motor step by proportioning the current to the motor windings. Microstepping has the effect of smoothing out roughness during low speed operation and reducing motor resonances at high speeds. Since the full steps are divided into a number of increments, the positioning resolution of the motor is greatly increased. The S Series drives selected are capable of sixteen different microstepping resolutions of up to 50,800 steps/rev.

3.1.4 END-OF-TRAVEL SWITCHES

Each of the manipulator axes is fitted with momentary contact switches, which are engaged at the limits of the axis motion. These switches send a signal to the indexer, when engaged, to indicate that the axis is at its limit of travel. Depending on the initialization of the indexer and controller, this could have the effect of quickly decelerating the particular axis to a stop, stopping all the axes, or interrupting the host computer.

The deployment and elevation axes each have two separate switches, which are located at the clockwise and counterclockwise limits of motor travel. The azimuth rotation has a single limit switch which represents both the clockwise and counterclockwise end of travel. This gives the azimuth axis virtually a full rotation for its range of motion.

The azimuth rotation cannot be allowed to rotate more than one full rotation in either direction, as the cables supplying the motor current interfere with rotations greater than approximately a rotation and a half. This limitation could be alleviated through the use of "slip rings" in the supply and signal lines. Slip rings are electrical connectors that allow wires to twist through a virtually unlimited number of rotations without breaking contact. In this

application, the slip rings would most likely be mounted on the azimuth web at the center of the slewing ring. Although this location is occupied by the azimuth actuator coupling, making slip ring installation difficult, the possibility of corrupting the stepper motor drive signals is the reason they are not used.

3.2 SYSTEM OPERATION

The system currently is operated either by a terminal emulation program, which was supplied with the controller, or through a program written especially for the manipulator and M.E.A.N.U. control system. The M.E.A.N.U. manipulator control program reads the X-code commands from a data file and sends them to the indexer. The commands are separated into blocks that contain the information for one or two moves at a time. The program must then receive an external input, either from the operator or from another program, which allows the information for the next move to be sent to the indexer. A listing of the control program and a sample command file are located in Appendices D and E respectively.

The terminal emulator program is a direct interface to the indexer, which allows commands to be written directly to the indexer. The emulator environment allows single commands to be executed, as well as easy access to the indexer status output capabilities. Although use of the terminal emulator would not be appropriate for repositioning the manipulator during the testing procedure, it is effective in the planning of the manipulator path and the testing positions during command file generation, and in executing single manipulator motions to correct for errors.

3.3 SYSTEM PERFORMANCE

The system performance was evaluated in terms of positioning time, positioning accuracy, manipulator deflection, and overall reliability. The actual manipulator performance is compared to the design objectives in the following sections.

3.3.1 POSITIONING TIME

The system performance was evaluated based on the comparison between the design objective that the manipulator be capable of reaching any point in the manipulator's work cell from any other point in under thirty seconds. Table 3.1 summarizes the maximum velocities that the axis motors must run to travel through their full range of motion in thirty seconds.

| AXIS | ROTATIONAL SPEED (ω_{max} , RPS) |
|------------|--|
| AZIMUTH | 3.4 |
| ELEVATION | 9.98 |
| DEPLOYMENT | 51.3 |

Table 3.1: Required Motor Speeds

The drivers for the azimuth and elevation axis motors were left at their factory preset microstepping resolutions of 50,000 steps/revolution. This setting is the second highest of the sixteen settings. For this resolution, the maximum speed capability is 40 RPS. Since these motors are relatively slow moving, the high resolution will smooth the operation of the axes.

The deployment axis requires a rotational speed of 51.3 RPS, so a motor resolution of 25,000 steps/revolution was chosen. This resolution setting provides a maximum speed of 80 RPS although operation of stepper motors above 50 RPS is not recommended.

The motor drivers also have a feature that allows the waveform of the driving current to be adjusted. The waveform can be a pure sine, or a pure sine which is attenuated by up to

10% of its third harmonic. The factory default setting is -4% and was not readjusted.

Although the PC-23 controller has provision for a customized velocity profile during the acceleration interval, the default profile is a linear ramp up. The target motor acceleration values, according to the design specifications, should accelerate the axes to their maximum velocities in one second. The magnitudes of the accelerations are then the same as the magnitudes of the maximum velocities. These magnitudes are also half the magnitudes used in the calculation of the dynamic loading, as given by equation (2.6).

As installed, the elevation and rotation axes are capable of being operated at their maximum speeds with reliable performance. The axes were run simultaneously through their full range of motion in both directions at their design maximum speeds during no less than one hundred consecutive trials. In no cases did the axes stall.

The deployment axis, however, performed in a far less satisfactory manner. Although certain regions in the range of motion can occasionally be performed at speeds as high as 40 RPS, a reliable speed for the full range of motion was found at 30 RPS, with a low acceleration of 15 RPS². Although the acceleration interval is acceptable, the speed is slightly less than 60% of the design objective. This speed allows full range motion of the deployment axis in approximately 50 seconds.

Based on the assumption that the microstepping resolution may affect the high speed performance, the motor was tested with a resolution of 50,000 steps/rev. The behaviour of the motor did not appear to improve. The reliable speed was found to be the same or slightly less. Although decreasing the resolution below 25,000 steps/rev was also a possibility, the performance did not vary significantly.

The implication of the limited performance of the deployment axis under several different motor operational characteristics is that the appropriate motor was not selected. This could be a result of flaws in the analysis of the axis properties, motor selection criteria, or inconsistencies in the axis itself. The consequences of this decision will be discussed in more detail in Section 3.3.4.

3.3.2 POSITIONING ACCURACY

Although under microstepping operation, the resolution of the axes is significantly higher than that of a standard 1.8° stepper motor, the positioning resolution does not increase from that calculated in Chapter 2. This is due to the fact that the stepper motors cannot be energized during sound tests, as they emit sound even when stationary. Since microstepping artificially increases the step resolution by proportioning the current between the windings, the motors should return to one of the actual step positions when not energized.

If the motor moves to the closest natural detent when de-energized, and returns to the proper microstep when re-energized, de-energizing the motors would not result in any lost motor steps. However, this does not account for loads on the motor at the location at which it is de-energized. In the case of the elevation and deployment axes, the loading due to gravity is always in the same direction, and would tend to increase the distance from the home position. The home position chosen for the manipulator is horizontal with the boom fully retracted. The end of travel switches provide a useful reference for this position.

Consider the case where the elevation or deployment axes stop one microstep from a natural step, but on the downhill side. When the motor is de-energized, the permanent magnets in the stepper motor may not provide sufficient torque to settle the motor at the

closest step, although it is very close. If the motor actually stops one full step away, when the motor is re-energized and returns to a position one microstep downhill, a full step has been lost. However, if the motors on these axes always settle at the natural detent downhill from their stopping position and always move to the microstep downhill from the detent, this results in one lost full step for each of the previous positions. These lost steps are not a problem if they occur consistently, since they could be accounted for.

Consider now the azimuth axis, which is not affected by gravity. Assuming a uniform load at the stopping position, the motor should settle at the closest natural detent when de-energized, and return to the original position when re-energized. However, if the stopping position is at the microstep closest to the center between full steps, the motor could settle at one of two different positions. Upon re-energizing, the motor seeks a position between two full steps, but may now be a full step from the original position, but the direction is not known. This makes it impossible to account for lost full steps as they occur.

If one full step was lost due to previous positioning at each location, the actual deviation would not be significant after eight or ten positions, and would be well within the tolerances for the testing performed. The steps lost due to de-energizing the motors is not the only source of positioning error. Steps lost during the movement of the manipulator axes is also an area of concern.

The positioning accuracy was tested by moving the manipulator through a complex series of motions, including full range, full speed movements with at least two resting positions for each axis. The axes were then returned to their home position at maximum speed. The home position at which the axes apparently stopped, according to the PC-23

indexer's internal position counter, was recorded. This was performed fifteen times for two separate trials. During the first trial the motors were not de-energized at any point. The motors were de-energized at two positions during the second trial. The motors are de-energized at two positions to accommodate the possibility that one of the positions corresponds to a full step, or close to it, such that the motor might tend to return to the closest detent. This could give a low indication of the steps lost or gained. The number of microsteps lost or gained for each run are recorded in Appendix F.

The method used to evaluate the positioning accuracy is based on the assumption that the manipulator axes always return to an actual home position with an absolute precision of one microstep. Table 3.2 gives the microstepping resolution of the axes based on 50,000 microsteps/revolution for the azimuth and elevation axes and 25,000 microsteps/revolution for the deployment axis.

| AXIS | MICROSTEP RESOLUTION ($\delta_M, \mu\text{m}$) |
|------------|--|
| AZIMUTH | 2.80 |
| ELEVATION | 1.88 |
| DEPLOYMENT | 0.088 |

Table 3.2: Microstepping Axis Resolutions

The ability of axes to return to their limit switches within the given resolutions is not only unlikely, but would be difficult to measure based on the magnitudes. Any inconsistency in the axis operation could result in a discrepancy in the home position. Another consideration is that the CPU speed of the host PC would affect the rate at which the switches are polled, and thereby affect the final position. Without more detailed information on the PC-23 control system, however, this factor cannot be taken into account when evaluating the trial results.

Another assumption is that the control system does not alter the position count for its own purposes, and that it records the actual number of pulses that are actually sent, rather than the number that should be sent under the circumstances. Without a listing of the indexer logic and qualifications to interpret it, this assumption would be formidable to affirm. More than likely, however, any artificial corrections in the indexer count would not be of a large magnitude.

Figure 3.3 shows a plot of the azimuth axis losses for each of the first trial runs. The negative values suggest an apparent loss of steps, and positive values indicate a gain. Statistically, the average of the magnitude discrepancy is 172 microsteps with a 95% confidence limit of ± 42 microsteps. The actual average is -66.4 ± 100 microsteps. The maximum deviation is 256 microsteps.

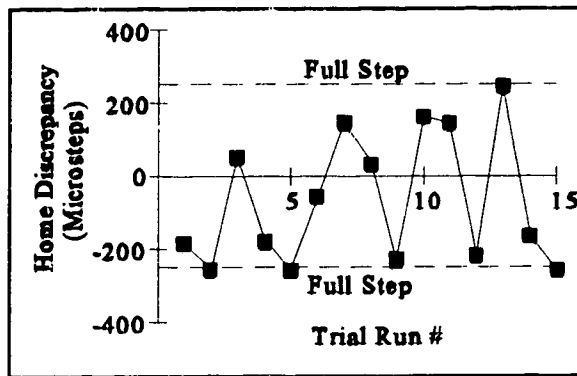


Figure 3.3: Apparent Home Position for Azimuth Axis - First Trial

Although a pattern may be developing in the above plot, the average magnitude of the homing discrepancy is less than a full step of 250 microsteps. Since the actual average is much less than the average magnitude, there does not appear to be an overall trend to the step discrepancies in terms of lost or gained steps.

The maximum deviation of 256 steps is slightly more than a full step. The occurrence of lost full steps can be explained by the occurrence of motor stalling. During the acceleration interval, the motor may not respond to the pulse information sent from the indexer. If the motor assumes the natural detent position for a long enough period, the information intended to move it a full step may be lost. If the motor remains on the natural detent, a full motion stall will occur and the motor will not rotate. If the motor only stalls for one cycle and starts moving, one full step will be lost.

The loss of microsteps, and in fact the loss of full steps, can be attributed to variations in the actual homing position. In the case of the azimuth performance, the small overall discrepancy in positioning accuracy is acceptable under the axis characteristics. The fact that the discrepancies tend to alternate indicates that lost steps are occurring in a more or less random manner.

Figure 3.4 shows the azimuth axis step losses for the second trial. The trend still appears to be random, but within a smaller range. With the exception of one point, all the positions are within the bounds of one full step.

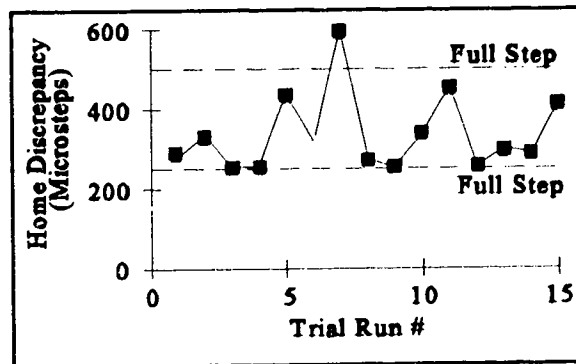


Figure 3.4: Apparent Home Position for Azimuth Axis - Second Trial

The above figure shows that fourteen times out of fifteen, between one and two full steps will be gained during repositioning. This behaviour was unexpected in the azimuth axis as the dynamic loading on the actuator is opposite to the direction of travel. The expected performance, as discussed above, would have the azimuth losing a full step, but in either direction, and possibly tending to lose a full step more often than not. The fact that the axis is gaining at least a full step (i.e., the axis does not have to travel as many steps to return home than to leave) indicates that there may be loading on the axis that has not been accounted for.

If the results of the above tests are interpreted such that the azimuth can be positioned with reliability to within two full steps in either direction, the maximum tip deflection would be ± 1.4 mm. Since the discrepancy is not significant, investigation into the circumstances under which it occurs was not undertaken.

The performance of the elevation and deployment axes during the trials are shown in the following two figures. The horizontal dashed lines are spaced in increments of four and twelve full steps for the elevation and deployment axes respectively.

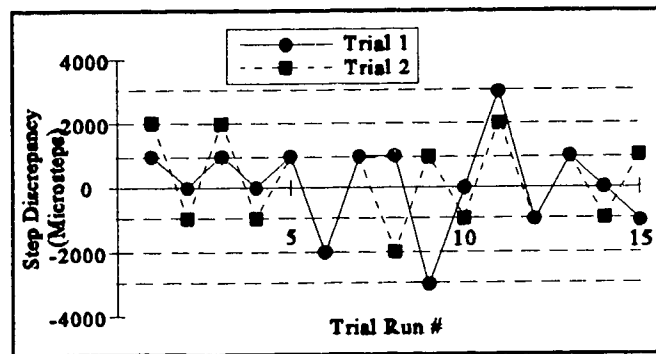


Figure 3.3: Apparent Home Position for Elevation Axis - Both Trials

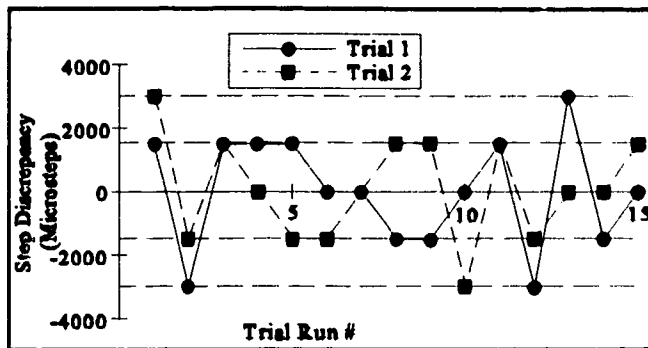


Figure 3.6: Apparent Home Position for Deployment Axis - Both Trials

In contrast to the azimuth axis, the elevation and deployment axes appear to lose or gain groups of full steps. The deployment axis had a maximum discrepancy of ± 24 full steps. This corresponds to tip motion range of ± 0.26 mm. The elevation axis loses or gains a maximum of 12 full steps, and the tip discrepancy is ± 2.16 mm.

The loss of full steps, as discussed above, can occur due to high acceleration rates, or backlash in the system. The gain of full steps, however, is peculiar, since the loading on these axes is always in the same direction. As a result, the step gain is probably arising from deviations in the homing position or could be an effect of the CPU speed of the host computer.

Another peculiar trend is that the axes always lose a fixed number of microsteps, regardless of the full step discrepancy. In the case of the elevation, one microstep is always lost, and six are lost consistently by the deployment axis. This could be a result of magnetic hysteresis in the motors. The manufacturer states that the magnetic hysteresis, which occurs with direction changes, is in the area of 0.03° . This corresponds to approximately four microsteps for the elevation axis, and two microsteps for the deployment axis.

During movement through the programmed path used for the trials, each axis changes direction three times. As a result, a loss of twelve microsteps by the elevation axis, and six microsteps by the deployment axis can be accounted for. Although the deployment axis always loses six microsteps, the elevation axis only loses one. This may be accounted for by the difference in motor sizes, and the difference in static loading on the motors.

None-the-less, the tip deviation for the deployment axis is very small. The deflection due to lost steps in the elevation axis is at least an order of magnitude larger, but this value is for the coarsest step resolution with the boom fully extended. Because of the room geometry, the boom cannot be fully extended in the vertical position. The actual range of tip deviation values is between approximately 0.88 mm and 1.30 mm. After eight positions, if the maximum step loss occurred at each position, the manipulator would have a positioning accuracy of ± 10.4 mm in the elevation direction.

An overall value for positioning accuracy after eight positions can be found by adding the maximum deviations as discussed above for each position. Table 3.3 gives the anticipated tip deviations for the three axes and the overall manipulator accuracy after eight positions, with the anticipated loss of the maximum number of full steps at each position.

| AXIS | MAXIMUM TIP DEVIATION (mm) |
|------------|----------------------------|
| AZIMUTH | ± 11.2 |
| ELEVATION | ± 10.4 |
| DEPLOYMENT | ± 2.1 |
| OVERALL | ± 15.4 |

Table 3.3: Axis and Overall Manipulator Positioning Accuracy After Eight Positions

3.3.3 MANIPULATOR STATIC DEFLECTION

The nature of the manipulator is such that its tip can only reach a given point under a unique set of spherical coordinates. As a result, the static loading conditions on the boom and azimuth turret can result in only one particular static deflection at each point. Within the limits of the positioning accuracy given in the previous section, it is reasonable to assume that the deviation in static deflection at any given point is insignificant.

As a result, the static deflection of the boom tip is not an indication of the performance of the manipulator as much as it is an indication of the validity of the method used to determine the system rigidity. The manipulator rigidity comparison was made by measuring the distance between the tip and the ceiling at the fully retracted and extending positions of the boom at a horizontal elevation angle.

The distance from the top of the boom tip to the ceiling with the boom fully retracted was measured to be 1004 mm. The theoretical value at this position, neglecting any tip deflection, is 1000 mm based on the boom trunnion pin position and a horizontal boom position. This difference could arise from variations in the ceiling surface, but are most likely due to inaccurate positioning of the elevation axis. The apparent elevation angle at the time of the tip deflection measurements is then 0.003 radians. This elevation angle will result in an initial fully extended tip deflection of approximately 15 mm below the horizontal plane.

The distance from the top of the tip to the roof with the boom fully extended was measured to be 1022 mm with no payload and 1028 mm with a 22 N payload. These measurements correspond to net deflections of 7 mm and 13 mm. The theoretical deflection due to the boom geometry were calculated to be approximately 4 mm and 7 mm.

As previously mentioned, the azimuth turret and ball bushing bearings also augment the flexibility of the manipulator. According to the above measurements, the static deflection is approximately double the expected deflection.

3.3.4 OVERALL PERFORMANCE

To this point, the performance of the manipulator has, with one exception, met the design objectives and was found acceptable based on the evaluation criteria. However, certain characteristics of the manipulator operation could somewhat limit its performance. In this section the performance of each of the axes will be discussed.

3.3.4.1 Azimuth Performance

As mentioned previously, the azimuth axis motor is capable of operating at the design speed of 3.4 RPS. This value was arrived at by reasoning that the maximum azimuth rotation that the manipulator must undergo to reach any point in the test volume from any other point was 180°. This is not true with the manipulator as installed.

The position of the end-of-travel switch was chosen to ensure that the manipulator did not move through an azimuth rotation large enough to encounter the supply lines to the motors. As a result, a worst case scenario would require slightly less than one full azimuth revolution. This would double the positioning time to a full minute. However, the worst case scenario need not occur if the test positions are chosen in a logical manner.

Although the axis speed could be increased, this would exceed the value used in the design of the mechanical components, thereby increasing the dynamic loading on the manipulator components. In fact, the axis was not found to perform reliably at rotational speeds above 5 RPS. Since judicious path planning would allow the design objective to be

met for the intended use of the manipulator, this situation is not of major consequence.

Another observation made during the operation of the azimuth axis is that it tends to be rough in situations where the boom is fully retracted. This is probably due to the low load inertia compared with the motor's rotor inertia. The roughness is less noticeable under higher load inertia configurations and during operation of more than one axis within more complex motions. Although the roughness does not appear to be significant, it might be reduced by adding load inertia in the form of a flywheel on the motor tail shaft.

Due to a lack of foresight and planning during the evaluation stage of this project, the manipulator had occasion to encounter one or more of the major room surfaces. Operation of the azimuth axis after these developments was extremely rough, and significant noise was associated with the motion. Although the source of the noise and poor performance is not known, it was discovered that manual rotation of the axis through a small range of motion alleviated the noise and roughness, if not the problem itself. Further investigation into this behaviour was not undertaken, for obvious reasons.

3.3.4.2 Elevation Axis

One noticeable characteristic of the elevation axis operation arises from the possibility that the support bearing journal at the end of the screw may not be true with the screw itself. The run-out causes the motor and trunnion pin assembly to wobble noticeably at the same rate as the screw rotation. The wobble could, and probably does, have an effect on the homing accuracy depending on the loading of the axis.

The source of this run-out is most likely due to the machining of the bearing journal. The ball screw was not supplied with a bearing journal. Rather, the journal was machined on

site. Although competent, experienced machinists were employed for the task, the variation in case hardening depth resulted in the deviation in concentricity or perpendicularity. The screw manufacturer has termed this behaviour "drunkenness" so it might be an expected characteristic.

Another characteristic of the elevation axis is the broad variation in axial loading on the ball screw. The axial load is a maximum at the horizontal position and decreases to a no-load condition at the vertical. When the manipulator is close to the vertical position, the slack in the screw is noticeable not only visually, but audibly. The ball bearings in the ball nut can be heard rattling. Although this might not present a problem in terms of durability, measures are available to correct this. The use of a preloaded ball nut would ensure that the ball bearings are loaded, and might tend to take the slack out of the screw itself. Basically, a preloaded ball nut consists of two ball nuts with a slight offset, which preloads the balls. Normally the use of a preloaded nut does not increase the actuator torque requirement.

A final characteristic of the elevation axis is that the residual torque in the stepper motor, when not energized, is insufficient to retain the elevation position. To compensate for this, an electromagnetic fail-safe brake was used to hold the axis position. The brake must be energized with a 24 VDC potential to allow the unit to turn. The brake was in place during the accuracy trials, and did not contribute to any apparent position loss when the motor was de-energized.

3.3.4.3 Deployment Axis

The major concern with the deployment axis is that the design objective regarding positioning time has not been met. The reliable speed of the axis is approximately 60% of the

design objective. The result is a positioning time of approximately 50 seconds.

The apparent reason for this performance deficiency is that the selected motor is incapable of driving the axis at the design speed. The selection criterion for the motor was that a sufficient torque margin be present at the expected operating speed. The load inertia was altered by a flywheel such that the load inertia was approximately ten times the rotor inertia. A larger torque margin could be supplied by a significantly larger motor, which would also require a larger flywheel.

A more likely reason for the poor axis performance is that stepper motors are not appropriate for high speed, continuous motions. The drive reduction on the deployment axis was chosen on the basis of maximum positioning resolution. As a result, not only was the required motor speed increased to an unrecommended level, but the resolution itself far exceeded the resolution of the other axes. A more appropriate criterion for selecting a drive reduction is that the resulting resolution be on par with that of the other two axes. As selected, the resolution interval is at least an order of magnitude less than the other axes.

Although there are a limited number of reduction ratios available, selection of a 60:1 ratio rather than 160:1 would still give a finer positioning resolution than the other axes, and allow the stepper motor to be run at the more reasonable speed of 20 RPS to exceed the design objective. This change in the drive reduction ratio may affect the positioning accuracy, but the current accuracy value is also at least a third that of the other axes.

The only recommended change in the manipulator is the replacement of the 160:1 Harmonic Drive reduction with a 60:1 reduction unit. This will still give an excellent positioning resolution, as well as allow the motor to operate more reliably at a lower speed.

3.4 OVERALL EXPENSE

The cost of the components required to construct the manipulator are outlined in Table 3.4 below. Included is an estimate of the actual time required to perform the machining of the components of the prototype. An estimate for the required period to construct another manipulator is approximately half that required for the prototype. The overall cost of the prototype constructed and implemented for the small chamber was approximately \$71,000.00.

| ITEM | DESCRIPTION | COST |
|-------------------|-----------------------------------|-------------|
| STRUCTURE | aluminum, bolts, screws, bushings | \$750 |
| MECHANICAL | linear bearings/shafting | \$3800 |
| | drive reductions | \$1500 |
| | lead screw | \$400 |
| | slewing ring | \$500 |
| ELECTRICAL | motors and drivers | \$7500 |
| | indexer card | \$2500 |
| | wiring and I/O devices | \$4000 |
| MACHINING | 1000 hrs @ \$50.00/hr | \$50,000 |

TABLE 3.4: List of Expenses

CONCLUDING REMARKS

4

4.1 SUMMARY

The objective of this project was to implement a manipulator to position a microphone in a sound field generated inside a reverberation chamber at M.E.A.N.U.. Although a number of different systems are in use at similar facilities around the world, a unique approach was undertaken in the form of a spherical coordinate manipulator. This thesis evaluates the preliminary design effort and discusses the final configuration and performance of the manipulator.

The manipulator moves in a spherical coordinate system, and consists of two rotational axes and a translational axis. The two rotational axes provide placement of a telescopic boom in both azimuth and elevation planes. The benefit of this type of manipulator is the assurance that the manipulator will have a small affect in the sound field being measured.

The manipulator is controlled by an integrated controller/indexer installed in an IBM[®] personal computer. The PC also controls other testing procedures at M.E.A.N.U.. This arrangement allows for unsupervised testing to be performed.

The main objective was that the manipulator be capable of moving from its present position to any position in the manipulator's work cell in under thirty seconds. Although the manipulator was designed to structurally withstand the dynamic loading based on the main

design objective, the performance of the manipulator does not meet the expectation.

Under reasonable positioning coordinates, the manipulator, as constructed, is limited to a maximum repositioning time of approximately fifty seconds. "Reasonable" positioning coordinates are those that demonstrate foresight and planning in the selection of testing locations. Absolute motions of the axes ranges can take as long as sixty seconds, in the case of the azimuth rotation.

The main design objective, however, is not satisfied by the performance of the deployment of the telescopic boom. The deployment axis was assigned a drive reduction of 160:1 on the basis of maximizing the positioning resolution while requiring an input speed slightly higher than the maximum recommended for continuous stepper motor operation. The actual reliable operation speed was approximately 60% of that required to meet the design objective.

The manipulator was found to be capable of returning to a preset position with an accuracy of 16 mm in any direction. Although the standards by which the testing procedures are conducted do not stipulate that the testing positions be located with any repeatability, the manipulator's positioning accuracy ensures that obstacles are not physically encountered, and that proper distances between testing positions are maintained.

4.2 RECOMMENDATIONS

Although the performance of the manipulator in the current configuration is acceptable, replacement of the 160:1 drive reduction on the deployment axis might allow the main design objective to be met. The use of a 60:1 Harmonic Drive reduction would require an input speed of 20 RPS, which is in a more reliable range of stepper motor operation. The

motor currently in use would be appropriate for the axis characteristics after this change, and the overall positioning resolution would not significantly increase. The effect on axis operation in terms of positioning accuracy is not known, but an overall decrease is expected.

REFERENCES

1. **I.S.O (International Organization for Standardization) Recommendation R354 (1963)**
Measurement of Absorption Coefficients in a Reverberation Room.
2. **A.S.T.M. (American Society for Testing and Materials) C423 - 90a Standard Test Method for Sound Absorption and Sound Absorption Coefficients by the Reverberation Room Method, Revised 1990.**
3. **A.N.S.I. (American National Standards Institute) standard S12.31 1990 Precision Methods for the Determination of Sound Power Levels of Broad-Band Noise Sources in Reverberation Rooms, American Society of Mechanical Engineers, New York.**
4. **Institute for Research in Construction; National Research Council Canada; Ottawa, Ontario; K1A 0R6**
5. **Bruel & Kjaer; 2850 Naerum; Denmark**
6. **Thomson Industries, Inc. Linear Motion Technology Guide, U.S.A., Form 9910 189-25, 1989.**
7. **Oberg, E., Jones, F.D. and Horton, H.L. Machinery's Handbook, New York, N.Y., Industrial Press Inc., Twenty First Edition, 1980, pp. 477 - 493.**
8. **Juvinall, R.C. Fundamentals of Machine Component Design, New York, John Wiley & Sons, 1983, pp. 273 - 329.**
9. **Warner Electric, Beaver Precision Ball Bearing Screws, U.S.A., Form P-685 2-87, 1987.**

10. **SKF Inc. *RKS Slewing Rings*, Sweden, Elanders, Catalog 3135 E, Reg. 471 81.16000. 1980-04, 1980.**
11. **Harmonic Drive - Quincy Technology Inc. *Power Transmission Products Form SF 12/89 15M*.**
12. **Parker Hannifin Corporation *Compumotor Digiplan - Position Control Systems and Drives*, Catalog 8000, U.S.A., 1991-1992 Catalog , Catalog 8000, 1991.**
13. **Parker Hannifin Corporation *PC23 Indexer User Guide*, p/n 88-007015-03 D, 1992.**
14. **Parker Hannifin Corporation *S Drive User Guide*, p/n 88-011483-01 F, 1992.**
15. **Pacific Scientific *Motion Control Mechanics*, U.S.A., Motion Application Note 100 Form PK 91275.**

ACCELERATION & REACTION COMPONENTS

A

DYNAMIC LOADING

To determine the maximum transverse and radial accelerations at the mass center of each member, the radial position of the mass center of each member is required. Given that the length of the last or fixed (radially) member is 1.22 m (as discussed in Section 2.1.3), and assuming a uniform mass distribution along the member's length, the mass center is located at a radial position of 0.61 m. Each of the subsequent members along the boom extends a distance of three quarters of their overall length from the previous member. Their mass centers will then be located at one quarter of their overall length from the tip of the previous member. This does not hold for the first boom member as it requires sufficient length to accommodate a mounting bracket. Its mass center will then be located half of the pre-extension further than one quarter of its overall length from the tip of the second member. The actual radii of the mass centers for the members, as constructed, are given in Table A.1 below.

| BOOM MEMBER | RADIAL POSITION OF MASS CENTER |
|-------------|--------------------------------|
| 1 | 3.91 m |
| 2 | 3.09 m |
| 3 | 2.29 m |
| 4 | 1.49 m |
| 5 | 0.61 m |

Table A.1: Radial Position of Member Mass Centers

Given the position of the member mass centers, their maximum centroidal transverse accelerations can be determined from (2.16) and (2.17). Given these values and values from Table 2.1, the maximum radial acceleration can also be found from (2.20). The values for these quantities are given in Table A.2.

| BOOM MEMBER | $a_{0max} , (m/s^2)$ | $a_{1max} , (m/s^2)$ | $a_{2max} , (m/s^2)$ |
|-------------|----------------------|----------------------|----------------------|
| 1 | 0.841 | 0.415 | 1.443 |
| 2 | 0.670 | 0.329 | 1.131 |
| 3 | 0.502 | 0.245 | 0.827 |
| 4 | 0.334 | 0.161 | 0.522 |
| 5 | 0.150 | 0.069 | 0.192 |

Table A.2: Individual Member Acceleration Components

The actual mass and inertia of the members as constructed are given in Table A.3.

| BOOM MEMBER | MASS, (kg) | INERTIA, kgm^2 |
|-------------|------------|------------------|
| 1 | 3.14 | 0.323 |
| 2 | 5 | 0.486 |
| 3 | 8.7 | 0.846 |
| 4 | 10.87 | 1.057 |
| 5 | 11.54 | 1.455 |

Table A.3: Individual Member Masses and Inertias as Constructed

The reaction components must be calculated starting with the first (most extended member). Using (2.37) through (2.41) for the first member, and (2.52) through (2.56) for the second, third, and fourth members, the reaction components are given in Table A.4.

| MEMBER | R_{ϕ_1}, N | R_{ϕ_2}, N | R_{ϕ_3}, N | R_{ϕ_4}, N | T, N |
|--------|-----------------|-----------------|-----------------|-----------------|-------|
| 1 | -109.4 | 167.2 | 10 | -14.9 | -8.6 |
| 2 | -333.7 | 442.2 | 28.3 | -36.5 | -14.2 |
| 3 | -747 | 942.9 | 57.8 | -70.4 | -21.4 |
| 4 | -1443.7 | 1748 | 99.7 | -116 | -27.1 |

Table A.4: Dynamic Support Reaction Components

STATIC LOADING

When the boom is not moving, there are no support reactions in the plane of the azimuth rotation. The maximum reactions in the plane of the elevation reaction occur when the boom is in the horizontal position (i.e. $\phi = 0$). These reactions can be determined with equations (2.37) and (2.38) for the first member, and equations (2.52) and (2.53) for the subsequent members, by setting all of the dynamic quantities to zero. In the case of the first member, the static payload reaction is 25 N, as given in the design objectives.

For the first member, equations (2.37) and (2.38) become:

$$R_{\phi_2} = 2m_1g - 4R_{\text{payload}} \quad (\text{A.1})$$

$$R_{\phi_1} = -m_1g + 3R_{\text{payload}} \quad (\text{A.2})$$

Evaluating these for the known values, the static support reactions for the first member are:

$$R_{\phi_2} = (2 \times 3.14 \times 9.81 - 4 \times (-25))N = 161.6N \quad (\text{A.3})$$

$$R_{\phi_1} = (-3.14 \times 9.81 + 3(-25))N = -105.8N \quad (\text{A.4})$$

The static reactions for the subsequent members can be found from:

$$R_{\phi_o}(n) = 2m_n g + 4R_{\phi_o}(n-1) + 3R_{\phi_i}(n-1) \quad (\text{A.5})$$

$$R_{\phi_i}(n) = m_n g + R_{\phi_o}(n-1) + R_{\phi_i}(n-1) - R_{\phi_o}(n) \quad (\text{A.6})$$

A summary of the static support reactions is given in Table A.5.

| MEMBER | OUTBOARD REACTION, R_{ϕ_o} , N | INBOARD REACTION, R_{ϕ_i} , N |
|--------|-------------------------------------|------------------------------------|
| 1 | 161.6 | -105.8 |
| 2 | 427.1 | -322.3 |
| 3 | 912.2 | -722.1 |
| 4 | 1695.8 | -1399.1 |

Table A.5 : Static Support Reaction Components

MEMBER CROSS-SECTION PROPERTIES

B

The second boom member has two different cross sections along its length, as shown in Figure B.1. The cross-section in B.1A is used to house the support bearings, as well as providing rigidity to the bearing shafts and rails at both ends and the mid-span of the member. The cross-section in Figure B.1B shows the regions along the members length that consist only of the bearing shafts and rails.

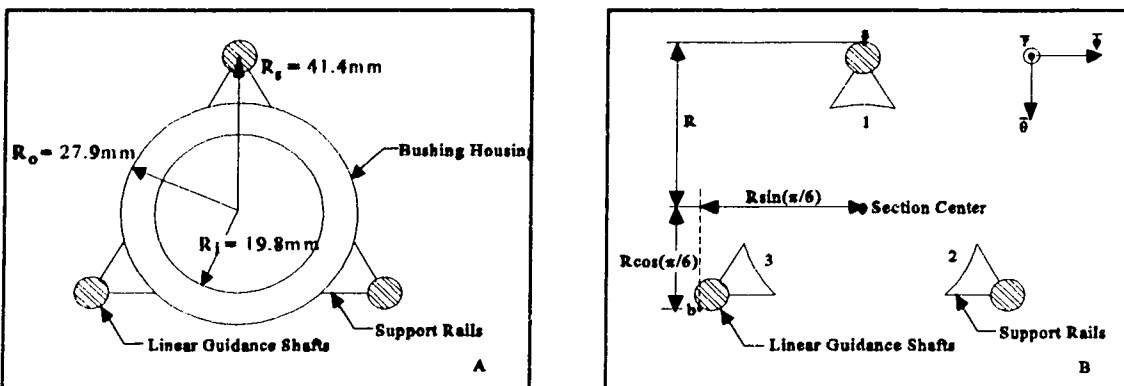


Figure B.1: Second Member Cross-Sections

The shaft support rails used on the second and subsequent members are Thomson low profile shaft support rails, predrilled to match the tapped holes in the bearing shaft. The support rails are manufactured from mild steel. For 1/2" shafts, the part designation is LSR-8-PD, and have weight per unit length of 0.32 lbs/ft (4.71 N/m). Figure B.2A shows the details of the shaft-support rail assembly. Figure B.2B shows the approximation used to model the actual assembly for the purposes of calculating the second moment of area of the cross-section.

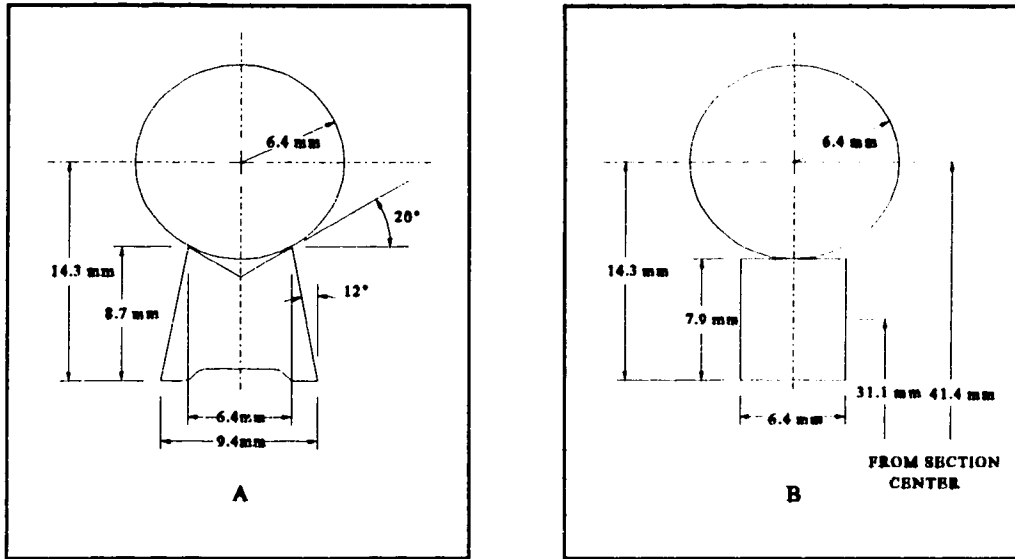


Figure B.2: Bearing Shaft and Support Rail Assembly Geometry and Approximation

The second moments of area for the shaft cross-section for the position 1 as shown in Figure B.1B are:

$$I_{\phi_s} = \frac{\pi R_s^4}{4} + \pi R_s^2 R_{c_s}^2 \quad (\text{B.1})$$

$$I_{\theta_s} = \frac{\pi R_s^4}{4} \quad (\text{B.2})$$

where R_s is the radius of the bearing shaft and R_{c_s} is the radius to the center of the section.

The second moments of area for the approximated support rail are:

$$I_{\phi_r} = \frac{bh^3}{12} + bhR_{c_r}^2 \quad (\text{B.3})$$

$$I_{\theta_r} = \frac{hb^3}{12} \quad (\text{B.4})$$

Combining (B.1) with (B.3) and (B.2) with (B.4) gives the total second moments for the shaft - rail assembly:

$$I_{\phi_1} = \frac{\pi R_r^4}{4} + \frac{bh^3}{12} + \pi R_r^2 R_{e_r}^2 + bhR_{e_r}^2 \quad (\text{B.5})$$

$$I_{\theta_1} = \frac{\pi R_r^4}{4} + \frac{hb^3}{12} \quad (\text{B.6})$$

Substituting in values for the shaft-rail assembly, (B.5) and (B.6) become:

$$I_{\phi_1} = (0.13 R_{e_r}^2 + 0.05 R_{e_r}^2 + 1.58) \times 10^3 \text{ mm}^4 \quad (\text{B.7})$$

$$I_{\theta_1} = 1.49 \times 10^3 \text{ mm}^4 \quad (\text{B.8})$$

It is convenient to leave (B.7) in its current form, since the subsequent boom members have similar geometries with only the distance from the section center varying. For the second member, (B.7) can be evaluated with the information from B.2B to give:

$$I_{\phi_1} = 272.8 \times 10^3 \text{ mm}^4 \quad (\text{B.9})$$

To determine the second moments of area for the shaft-rail assemblies at positions two and three in Figure B.1B, the results of (B.5) and (B.6) can be transformed using:

$$I_{\phi'} = \frac{I_{\theta_1} + I_{\phi_1}}{2} - \frac{I_{\theta_1} - I_{\phi_1}}{2} \cos 2\beta + I_{\alpha\phi_1} \sin 2\beta \quad (\text{B.10})$$

$$I_{\theta'} = \frac{I_{\theta_1} + I_{\phi_1}}{2} + \frac{I_{\theta_1} - I_{\phi_1}}{2} \cos 2\beta - I_{\alpha\phi_1} \sin 2\beta \quad (\text{B.11})$$

where β is the angle of orientation about the section center of area, and $I_{\alpha\phi}$ is the second

product of area. In this case, $I_{\theta\phi}$ is zero for both the shaft and approximated rail cross sections. Relative to position 1, position 2 is oriented at $\beta = -2\pi/3$ rad, and position 3 is at $\beta = 2\pi/3$ rad. Noting that $\cos 2\beta$ at these two locations is $-1/2$, the second moments of area about each axis are identical in positions two and three. This is due to the symmetry about the $\bar{\theta}$ axis. The second moments of area for positions 2 and 3 are:

$$I_{\phi_2} = I_{\phi_3} = \frac{3I_{\theta_1} + I_{\phi_1}}{4} \quad (\text{B.12})$$

$$I_{\theta_2} = I_{\theta_3} = \frac{I_{\theta_1} + 3I_{\phi_1}}{4} \quad (\text{B.13})$$

The total second moments of area for the cross section are the sums of the moments for each axis over the three positions, and are given by:

$$I_{\phi} = \frac{3I_{\theta_1} + 5I_{\phi_1}}{4} \quad (\text{B.14})$$

$$I_{\theta} = \frac{5I_{\theta_1} + 3I_{\phi_1}}{4} \quad (\text{B.15})$$

For the values given in (B.8) and (B.9), the section moments are:

$$I_{\phi} = 342.1 \times 10^3 \text{mm}^3 \quad (\text{B.16})$$

$$I_{\theta} = 206.5 \times 10^3 \text{mm}^4 \quad (\text{B.17})$$

Assuming that this minimum cross section is at the location that the maximum bending moment occurs may not always be valid, due to variations in geometry along the members' length. By determining the maximum stresses in the members assuming that the maximum

bending moment occurs at the minimum cross section, the safety factors may be conservative.

From the bending moment diagram for the second member, located in Appendix C, the maximum bending moments are 7.6 Nm in the horizontal plane and 90.1 Nm in the plane of the elevation rotation. The normal stresses can be determined using (2.61), however there are two locations of interest. These points are distinguished as "a" and "b" in Figure B.1B. At location "a", the normal stress due to bending is:

$$\sigma_a = \frac{M_\phi R}{I_\phi} \quad (\text{B.18})$$

Substituting appropriate values, the normal stress at position "a" is:

$$\sigma_a = \frac{90.1 \text{ kNm} \times (41.4 \text{ mm} + 6.4 \text{ mm})}{3421 \times 10^3 \text{ mm}^4} = 12.6 \text{ MPa} \quad (\text{B.19})$$

Alternatively, the normal stress due to bending at position "b" has two components, which arise from the bending moments with respect to both θ and ϕ axes. These components can be shown to add directly at position "b" whereas at the corresponding location for the shaft-rail assembly at position 3, the components would be of opposite sign. The components are found from:

$$\sigma_{b_\phi} = \frac{M_\phi R \cos(\pi/6)}{I_\phi} \quad (\text{B.20})$$

$$\sigma_{b_\theta} = \frac{M_\theta R \sin(\pi/6)}{I_\theta} \quad (\text{B.21})$$

Substituting appropriate values gives:

$$\sigma_{b_1} = \frac{90.1 \text{ kNm} \times (47.8 \text{ mm} \times 0.5)}{342.1 \times 10^3 \text{ mm}^4} = 6.3 \text{ MPa} \quad (\text{B.22})$$

$$\sigma_{b_2} = \frac{7.6 \text{ kNm} \times (47.8 \text{ mm} \times 0.87)}{206.5 \times 10^3 \text{ mm}^4} = 1.5 \text{ MPa} \quad (\text{B.23})$$

Then, the total normal stress at location "b" is:

$$\sigma_b = \sigma_{b_1} + \sigma_{b_2} = 8.0 \text{ MPa} \quad (\text{B.24})$$

In this case, the normal stress at position "a" is higher than that at position "b". The safety factor for this member is then given by equation (2.63) as:

$$N_2 = 25.2 \quad (\text{B.25})$$

The third and fourth members have the cross-section shown in Figure 2.15. The aluminum member skin has a number of weight reduction holes along its length. As a result, the second moment of area varies along the length. As a minimum approximation, only the bearing shafts and rails will be considered. This will give a conservative estimate, as the material in the skin sections is not accounted for.

The third member, as constructed, has a section-center to shaft-center dimension, $R_{c..}$ of 63.5 mm, and the distance to the rail center, R_{cr} , is 53.2 mm. The corresponding safety factor based on its minimum cross-section can be calculated to be:

$$N_3 = 18.8 \quad (\text{B.26})$$

The fourth member, with $R_{cr} = 101.6 \text{ mm}$ and $R_{cr} = 91.3 \text{ mm}$, has a safety factor of:

$$N_4 = 16.6 \quad (\text{B.27})$$

The fifth member has a construction similar to the third and fourth cross-sections, but does not require the bearing shafts and support rails. As such, its second moment of area must be based on the aluminum skins. Further, the skins are not uniform as there are a number of weight reduction discontinuities along their length. Their minimum cross-section will occur at these locations, and is shown in Figure B.3.

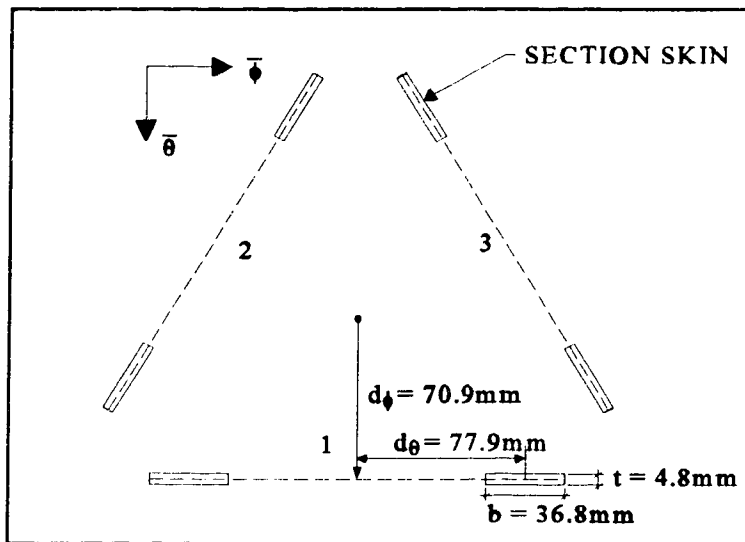


Figure B.3: Schematic of Fifth Member Minimum Cross-Section

At position one, the second moment components are:

$$I_{\phi_1} = \frac{2}{3}bt^3 + 2bt\delta_{\phi}^2 \quad (\text{B.28})$$

$$I_{\theta_1} = \frac{2}{3}b^3t + 2bt\delta_{\theta}^2 \quad (\text{B.29})$$

For the values in Figure B.3, these become:

$$I_{\phi_1} = 1.78 \times 10^6 \text{ mm}^4 \quad (\text{B.30})$$

$$I_{\theta_1} = 2.30 \times 10^6 \text{ mm}^4 \quad (\text{B.31})$$

Using equations (B.14) and (B.15), the total second moments of area for the cross-section are:

$$I_{\phi} = 3.95 \times 10^6 \text{ mm}^4 \quad (\text{B.32})$$

$$I_{\theta} = 4.21 \times 10^6 \text{ mm}^4 \quad (\text{B.33})$$

The stress components are given by:

$$\sigma_{\phi} = \frac{M_{\phi} \delta_{\phi}}{I_{\phi}} \quad (\text{B.34})$$

$$\sigma_{\theta} = \frac{M_{\theta} \delta_{\theta}}{I_{\theta}} \quad (\text{B.35})$$

Substituting appropriate values gives:

$$\sigma_{\phi} = \frac{290.8 \text{ kNm} \times (2 \times 70.9 \text{ mm})}{3.95 \times 10^6 \text{ mm}^4} = 10.4 \text{ MPa} \quad (\text{B.36})$$

$$\sigma_{\theta} = \frac{47.8 \text{ kNm} \times (77.9 \text{ mm})}{4.21 \times 10^6 \text{ mm}^4} = 0.9 \text{ MPa} \quad (\text{B.37})$$

The safety factor is then:

$$N_s = 24.3 \quad (\text{B.38})$$

SHEAR FORCES & BENDING MOMENTS

C

DYNAMIC LOADING

Figures C.1 through C.5 are the shear force and bending moment diagrams for the dynamic loading. The radii to the area centers of the bearing shafts and support rails for the members are given in Table C.1. The section moments can be determined using equations (B.14) and (B.15). The safety factor, N , can be determined using equation (2.63).

| MEMBER | R_{cs} , mm | R_{cr} , mm | $I_{\phi}, \times 10^3 \text{mm}^4$ | $I_{\theta}, \times 10^3 \text{mm}^4$ | N |
|--------|---------------|---------------|-------------------------------------|---------------------------------------|------|
| 1 | N/A | N/A | 17.8 | 17.8 | 15.9 |
| 2 | 41.4 | 31.1 | 342.1 | 206.4 | 25.2 |
| 3 | 63.5 | 53.2 | 835.2 | 502.3 | 18.8 |
| 4 | 101.6 | 91.3 | 2201.5 | 1322.1 | 16.6 |
| 5 | N/A | N/A | 3950 | 4210 | 24.3 |

Table C.1: Summary of Dynamic Loading on Individual Members

STATIC LOADING

Table C.2 contains the flexural rigidity, and linear weights for the members.

| MEMBER | FLEXURAL RIGIDITY (EI, $\times 10^3$ Nm ²) | LINEAR WEIGHT (ω , N/m) |
|--------|---|------------------------------------|
| 1 | 3.56 | 27.8 |
| 2 | 68.4 | 45.4 |
| 3 | 167 | 79 |
| 4 | 440.3 | 98.7 |
| 5 | 284.4 | 92.8 |

Table C.2 : Member Section Properties

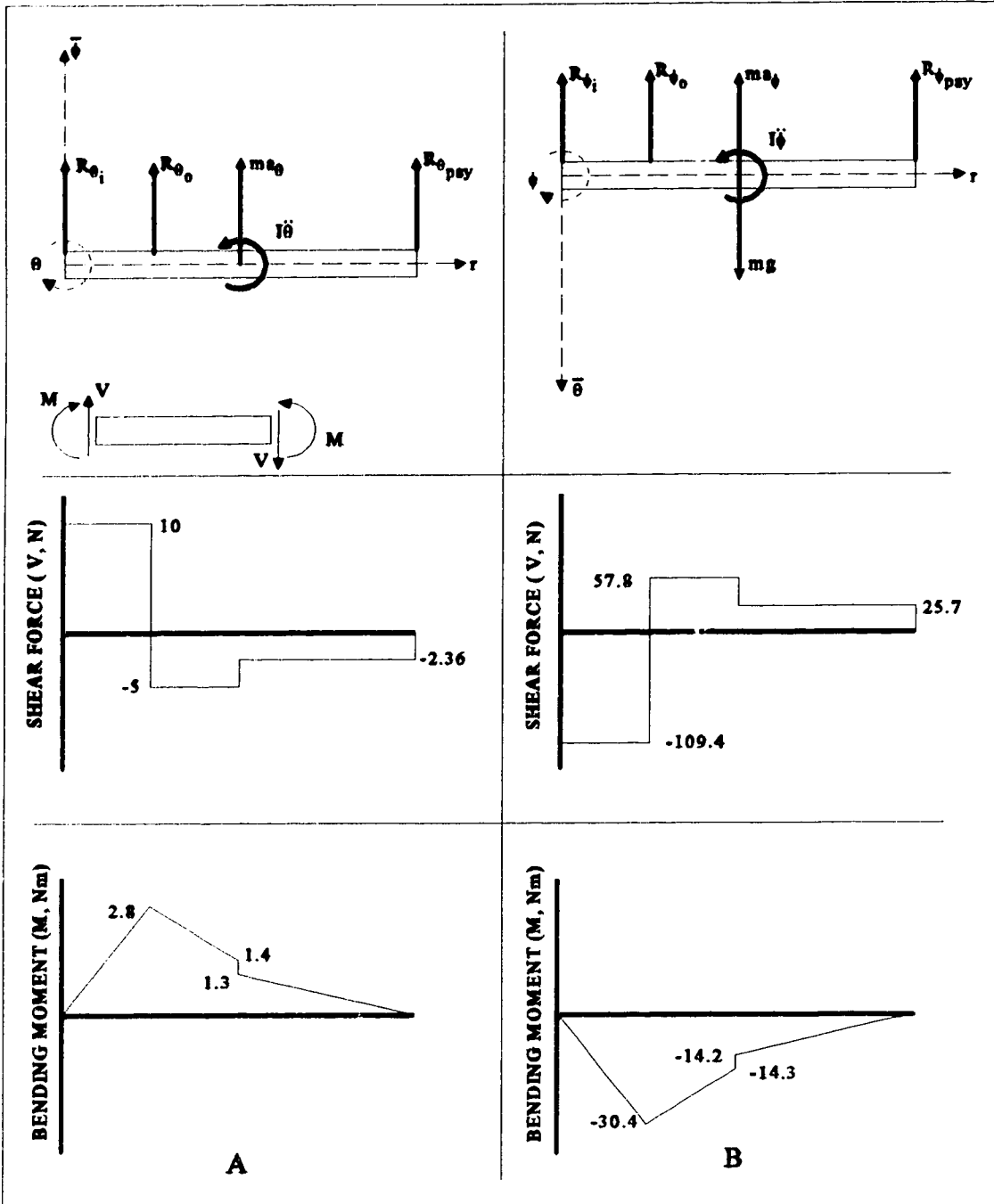


Figure C.1 : Shear Force and Bending Moment Diagrams for Transverse Dynamic Loading of First Member

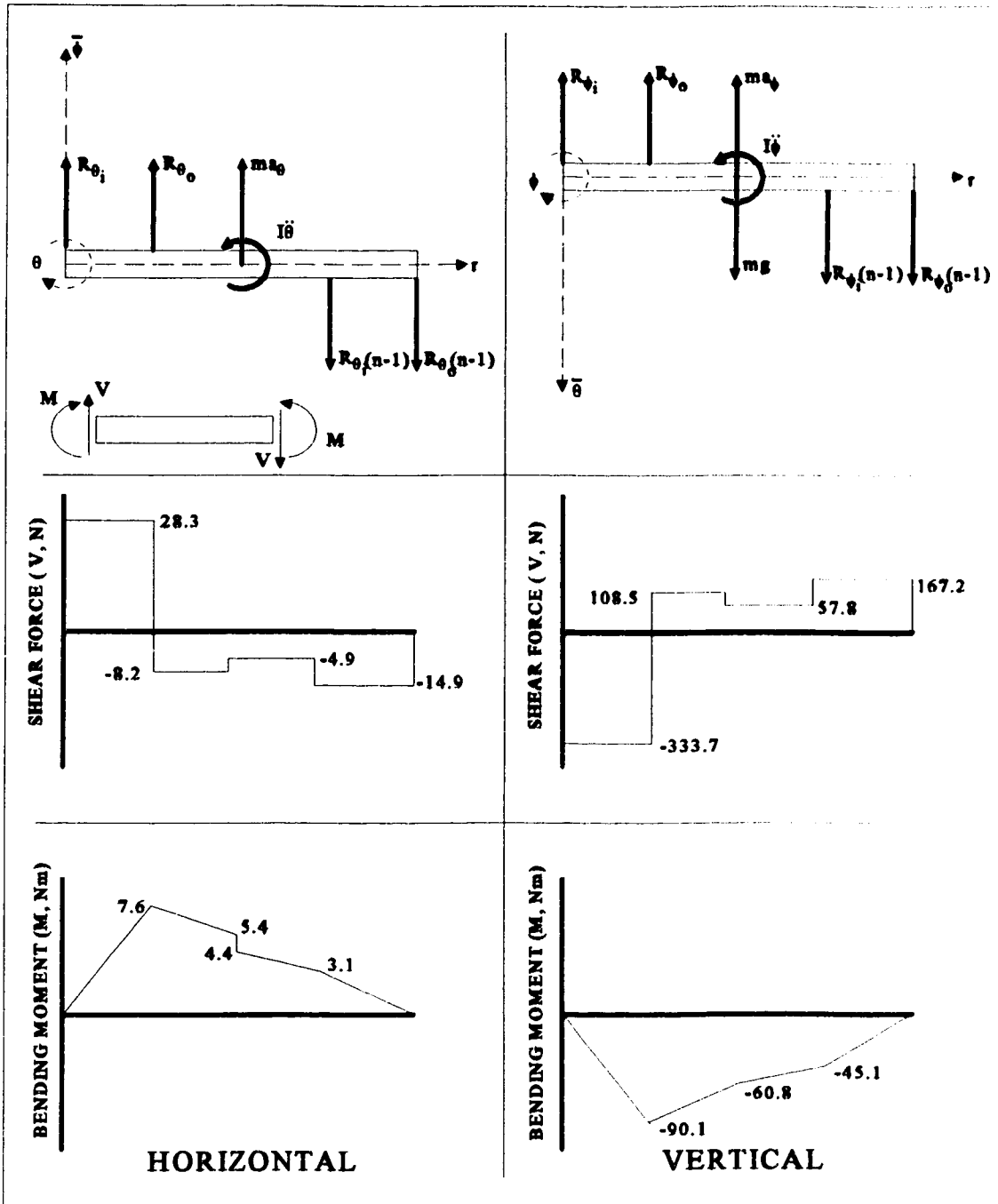


Figure C.2 : Shear Force and Bending Moment Diagrams for Transverse Dynamic Loading of Second Member

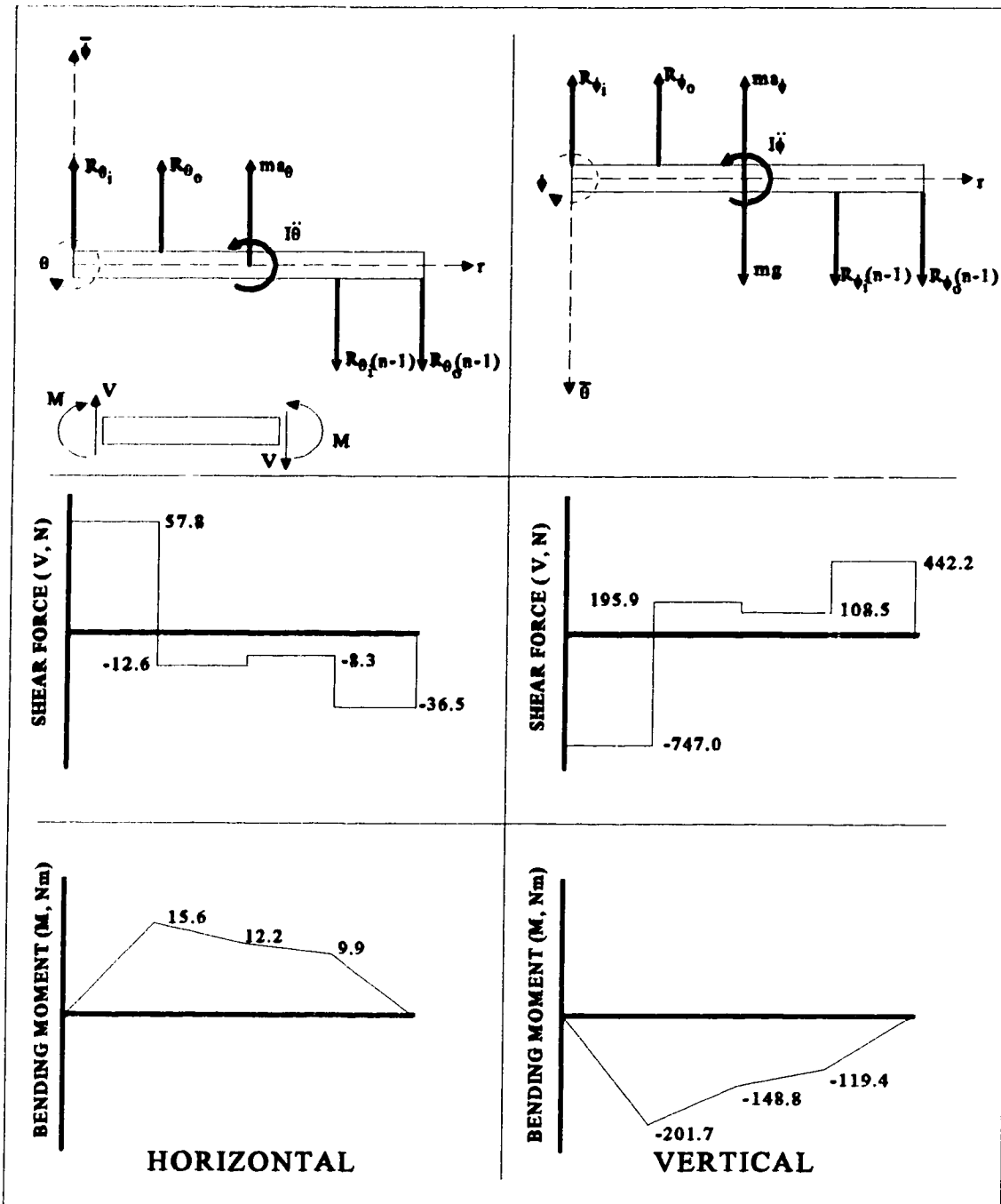


Figure C.3: Shear Force and Bending Moment Diagrams for Transverse Dynamic Loading of Third Member

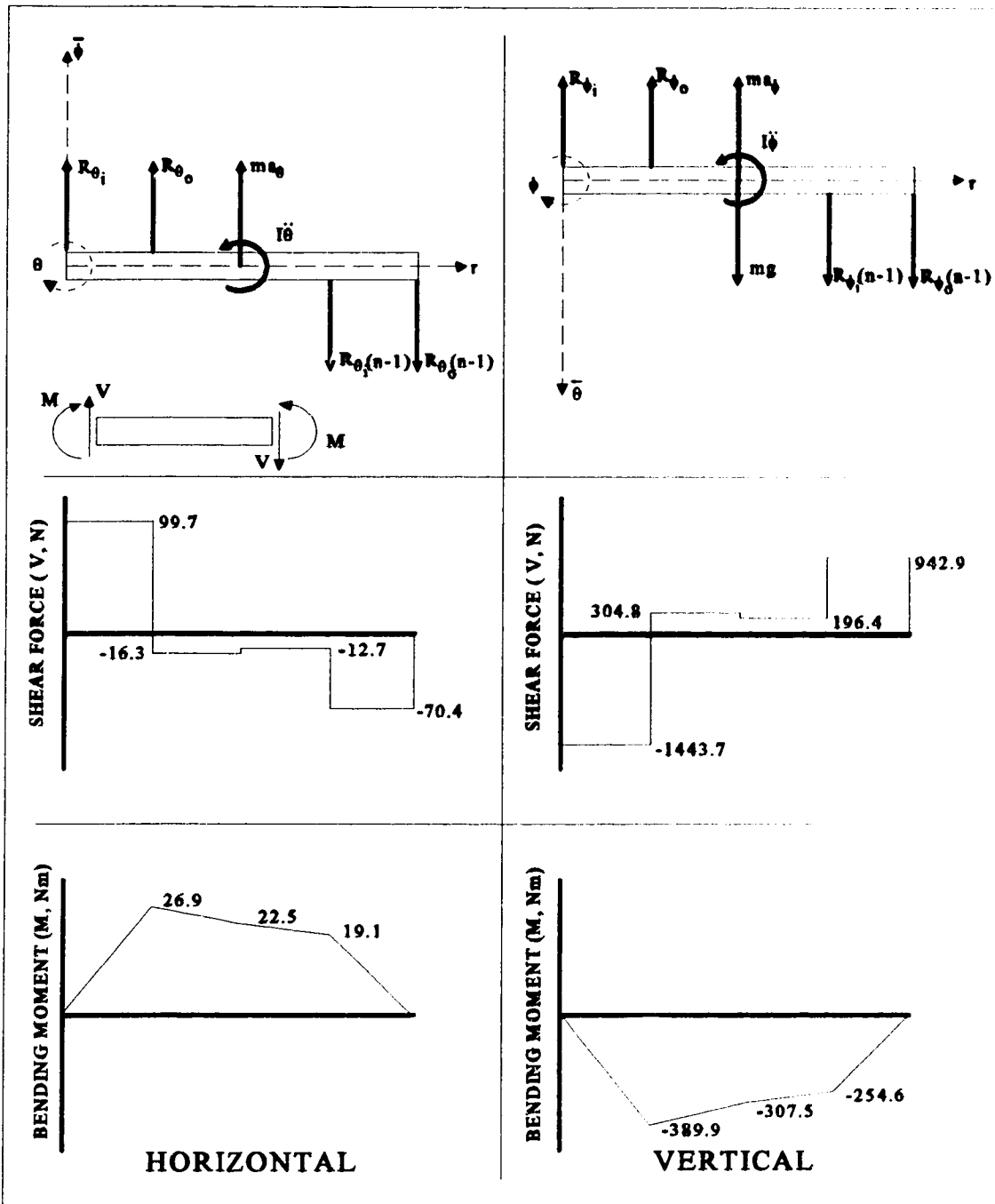


Figure C.4: Shear Force and Bending Moment Diagrams for Transverse Dynamic Loading of Fourth Member

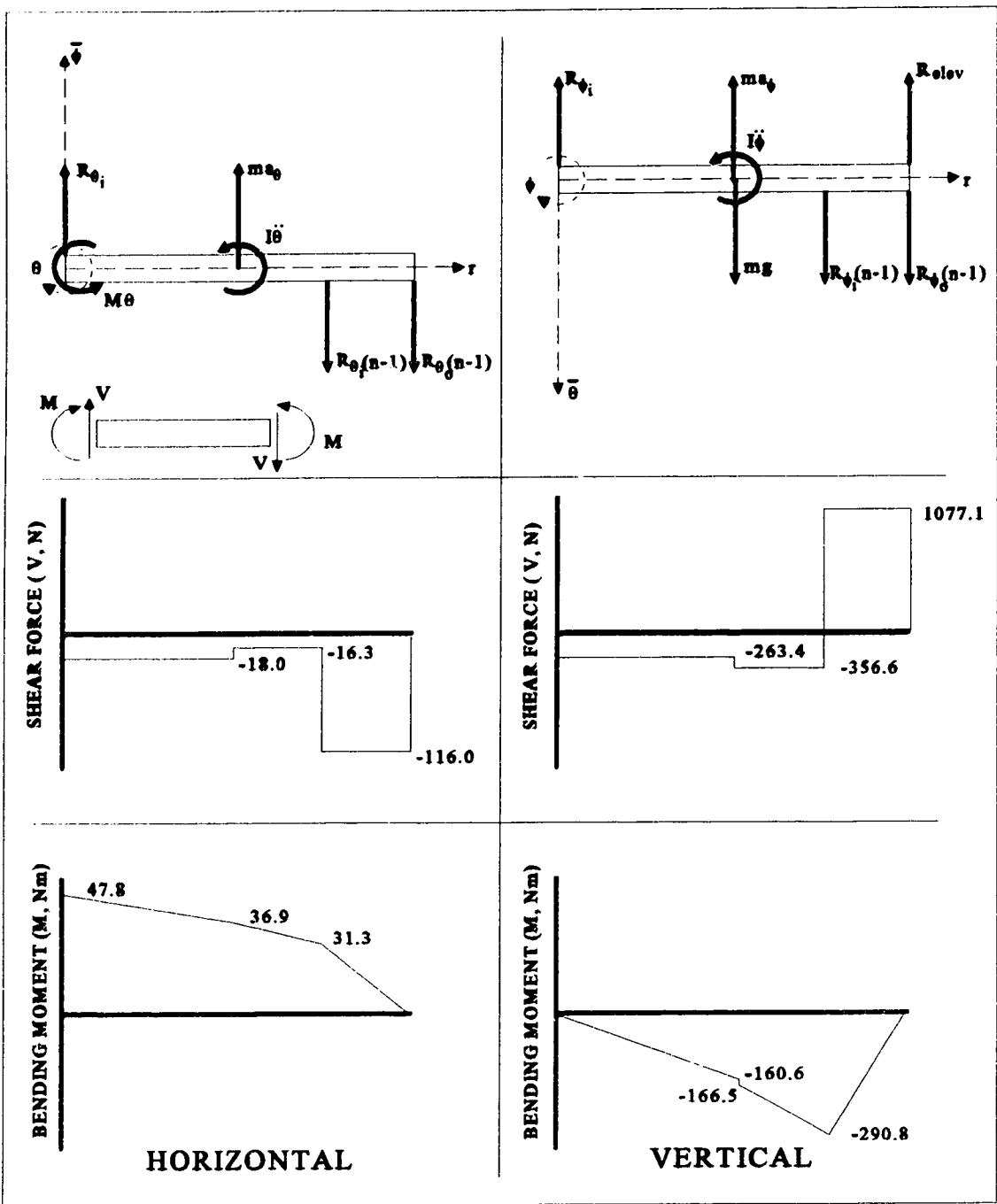


Figure C.5: Shear Force and Bending Moment Diagrams for Transverse Dynamic Loading of Fifth Member

PC-23 DRIVER ROUTINE

D

The following is a listing of a QuickBASIC routine that currently controls the M.E.A.N.U. manipulator system.

```
*****
***** PC23 DRIVER ROUTINE *** Aug 12/94 *****
***** MECHANICAL ENGINEERING ACOUSTICS*****
***** AND NOISE UNIT (M.E.A.N.U.)*****
*****
***** PC-23 SUBROUTINES BY VINCENT PISIO*****
***** MAIN MODULE BY VINCENT PISIO AND GERALD KISS*****
***** OTHER SUBROUTINES BY GERALD KISS*****
*****
'
'
***** MAIN MODULE *****
'
DECLARE SUB CaseSelect (Menu%, Menu$(), Row%, Column%, Choice%)
DECLARE SUB Delay (DelayTime!)
DECLARE SUB execute (address%, pc23command$(), numcommand!, idbready!,
cmdready!)
DECLARE SUB getcommand (cmdfile$, pc23command$(), numcommand!)
DECLARE SUB indexerreset (address%, halt!, fail!, restart!, mask!, ready!, control!, intrclr!)
DECLARE SUB readresponse ()
DECLARE SUB writecommand (address%, pc23command$, numcommand!, idbready!,
cmdready!, control!)

*****
*** NOTE : THIS ROUTINE ASSUMES DECIMAL ADDRESS OF PC-23 IS "788" ***
***** => This can be changed in "PROGRAM PARAMETERS" section below *****
*****
'
'
***** PROGRAM PARAMETERS *****
'
'
***
*** address% - This is the board address of the PC-23 indexer.
```

```

address% = 788
****
****   control - This is the normal state of the Control Byte
****           (only bits 5 and 6 are set).
control = &H60   ' = binary 01100000
****
****   halt - This parameter is for setting Control Bit 2 (to
****           signal the "WATCHDOG TIMER" to time-out (active high)).
halt = &H64   ' = binary 01100100
****
****   cmdready - This parameter is for setting Control Bit 4 (to
****           signal that a command byte is ready in the "Input
****           Data Buffer" (active high)).
cmdready = &H70   ' = binary 01110000
****
****   restart - This parameter is for clearing Control Bit 5 (to
****           signal "RESTART WATCHDOG TIMER" (active low)).
restart = &H40   ' = binary 01000000
****
****   intrclr - This parameter is for clearing Control Bit 6 (to
****           signal "RESET INTERRUPT OUTPUT" (active low)).
intrclr = &H20   ' = binary 00100000
****
****   recieved - This parameter is for setting Control Bit 7 (to
****           signal that the message has been recieved from
****           the "Output Data Buffer" (active high)).
recieved = &HE0   ' = binary 11100000
****
****   ready - This is the normal state of the Status Byte
****           (bits 0, 1, 2, and 4 are set).
ready = &H17   ' = binary 00010111
****
****   mask - This parameter is a mask for testing the Status Byte
****           (to insure that the PC-23 has recovered from reset).
mask = &H7F   ' = binary 01111111
****
****   stopped2 - This parameter is a mask for testing Status Bit 0 (to
****           indicate that AXIS 2 motor has stopped (active high)).
stopped2 = 1   ' = binary 00000001
****
****   stopped1 - This parameter is a mask for testing Status Bit 1 (to
****           indicate that AXIS 1 motor has stopped (active high)).
stopped1 = 2   ' = binary 00000010

```

```

****   stopped3 - This parameter is a mask for testing Status Bit 2 (to
****   indicate that AXIS 3 motor has stopped (active high)).
stopped3 = 4   ' = binary 00000100
****
****   odbready - This parameter is a mask for testing Status Bit 3 (to
****   indicate that a response is waiting in the "Output
****   Data Buffer" (active high)).
odbready = 8   ' = binary 00001000
****
****   idbready - This parameter is a mask for testing Status Bit 4 (to
****   indicate that the "Input Data Buffer" is ready for
****   a command byte (active high)).
idbready = &H10   ' = binary 00010000
****
****   fail - This parameter is a mask for testing Status Bit 5 (to
****   indicate processing failure in the PC-23(active high)).
fail = &H20   ' = binary 00100000
****
*****
*****
*****

*****
***** PROGRAM VARIABLES *****
*****
****
****   byte - This variable contains the input for the Control
****   byte or the output from the Status Byte.
****
****   timeout - This variable contains the time-out duration.
****
****   character$ - This variable passes a command or response
****   character between this host program and the
****   PC-23 indexer.
****
****   pc23command$() - This array variable contains the command strings
****   to be sent to the PC-23 indexer.
****
****   numcommand - This variable contains the number of commands
****   to be sent to the PC-23 indexer.
****
****   answer$ - This variable contains the response from the
****   PC-23 indexer.

```



```

****
****   cmdfile$ - This variable indicates the file containing the
****   command instruction strings.
****
*****
*****
*****

```

****** SYSTEM INITIALIZATION**

```

'Make all arrays dynamic
'$DYNAMIC

```

```

DIM pc23command$(1)

```

```

PA = 784   'temperature port
PB = 785   'relative humidity port
PC = 786   'mic selector/noise generator/stepper drive/ port
PIO = 787  'control port

```

```

Mic = 0    'default to use of Mic A/B
Noise = 0  'default to both noise generator channels off
Drive = 0  'turns off power bar to drives and power supply

```

```

PCData = Mic + Noise + Drive
PIOData = 146 'control port setup
           'PA and PB as input; PC as output; all in mode 0

```

```

OUT PIO, PIOData
OUT PC, PCData

```

```

CLS
LOCATE 10, 30
PRINT "ROBOT DEMO PROGRAM"
PRINT
PRINT TAB(28); "Hit any key to continue"
Continue$ = INPUT$(1)

```

```

CLS
PRINT "Check that solenoid switch on power supply is in AUTO position"
PRINT
PRINT "Turn the power supply power switch on"
PRINT "Turn the relay box power switch on"
PRINT "Currently, the relay box is being unplugged so that when the indexer"

```

```

PRINT "is reset, the drives status will remain OK"
PRINT
PRINT "Ensure all stepper drives are plugged into the power bar"
PRINT
PRINT "Power to all units should still be off"

LOCATE 20, 1
PRINT "Hit any key to remotely apply power to the above units"
Continue$ = INPUT$(1)

Drive = 128   'turns on power bar to drives and power supply

PCData = Mic + Noise + Drive
OUT PC, PCData

'let drives and steppers energize
CLS
CALL Delay(2)

***** RESET THE PC-23 INDEXER *****

'Call "reset" subroutine to reset the indexer
CALL indexerreset(address%, halt, fail, restart, mask, ready, control, intrclr)

CLS
PRINT "Check that power has been supplied to:"
PRINT "the power supply"
PRINT "the relay box"
PRINT "the stepper drives"
PRINT

PRINT "Check that the status lights on each drive is showing 'POWER' (green light)"
PRINT "and no other status light should be lit"

LOCATE 20, 1
PRINT "Hit any key to continue"
Continue$ = INPUT$(1)

DO

  CLS

  LOCATE 1, 25

```

```
COLOR 0, 7
PRINT "ROBOT ARM DEMO PROGRAM"
COLOR 7, 0
PRINT
```

```
Menu$(0) = "Full Motion demo"
Menu$(1) = "NRC mic positions"
Menu$(2) = "STC mic positions"
Menu$(3) = "Home azimuth"
Menu$(4) = "Home elevation"
Menu$(5) = "Home extension"
Menu$(6) = "Shell to Terminal Emulator Program"
Menu$(7) = "Shell to SEE Text editor"
Menu% = 7
Row% = 7
Column% = 25
```

```
CALL CaseSelect(Menu%, Menu$(), Row%, Column%, TestType%)
```

```
SELECT CASE TestType%
CASE 0
  cmdfile$ = "c:\bc7\source\fullmge.txt"
CASE 1
  cmdfile$ = "c:\bc7\source\nrcpoint.txt"
CASE 2
  cmdfile$ = "c:\bc7\source\stcpoint.txt"
CASE 3
  cmdfile$ = "c:\bc7\source\homeazim.txt"
CASE 4
  cmdfile$ = "c:\bc7\source\homeelev.txt"
CASE 5
  cmdfile$ = "c:\bc7\source\homeextn.txt"
CASE 6
  CLS
  LOCATE 10, 20
  PRINT "Use 788 IO address for emulator program"
  PRINT
  PRINT TAB(25); "Reset indexer board at prompt"
  PRINT TAB(20); "The brake relay will click during reset"
  PRINT
  PRINT TAB(25); "Hit any key to continue"
  Continue$ = INPUT$(1)
  SHELL "c:\pc23\pc23term"
```

CASE 7

Menu\$(0) = "Edit Full Motion demo"
Menu\$(1) = "Edit NRC mic positions"
Menu\$(2) = "Edit STC mic positions"
Menu\$(3) = "Home azimuth"
Menu\$(4) = "Home elevation"
Menu\$(5) = "Home extension"
Menu\$(6) = "Edit another file"
Menu% = 6
Row% = 7
Column% = 25
EditType% = 0
CLS

CALL CaseSelect(Menu%, Menu\$(), Row%, Column%, EditType%)

SELECT CASE EditType%

CASE 0

SHELL "e:\util\see c:\bc7\source\fullmge.txt"

CASE 1

SHELL "e:\util\see c:\bc7\source\nrcpoint.txt"

CASE 2

SHELL "e:\util\see c:\bc7\source\stcpoint.txt"

CASE 3

SHELL "e:\util\see c:\bc7\source\homeazim.txt"

CASE 4

SHELL "e:\util\see c:\bc7\source\homeelev.txt"

CASE 5

SHELL "e:\util\see c:\bc7\source\homeextn.txt"

CASE 6

SHELL "e:\util\see"

CASE 4

END SELECT

END SELECT

IF TestType% < 6 THEN

***** RESET THE PC-23 INDEXER *****

'Call "reset" subroutine to reset the indexer

CALL indexerreset(address%, halt, fail, restart, mask, ready, control, intrclr)

*******:***** RETRIEVE PC-23 COMMAND STRINGS *******

'Acquire command string data and details
CALL getcommand(cmdfile\$, pc23command\$(), numcommand)

******* EXECUTE PC-23 COMMAND STRINGS *******

'Call "execute" subroutine to execute the PC-23 command strings
CALL execute(address%, pc23command\$(), numcommand, idbready, cmdready)

END IF

LOOP WHILE TestType% < 8

CLS

OUT PC, 0 'turns power off
LOCATE 12, 20
COLOR 12, 0
PRINT "Do you wish to exit to DOS? Press y/N"
COLOR 7, 0

DO
 IS = ""
 WHILE IS = "": IS = UCASE\$(INKEY\$): WEND
 IF IS = "N" OR IS = CHR\$(13) THEN END
 IF IS = "Y" THEN CLS : SYSTEM
LOOP

END

REM \$STATIC
SUB CaseSelect (Menu%, Menu\$(), Row%, Column%, Choice%)
'=====

Flag% = 0 'implies that the ESC key is active

IF Menu% < 0 THEN 'deactivate ESC key
 Menu% = -Menu%
 Flag% = 1
END IF

'LOCATE 1, 1

```
'PRINT "Fre-1: DOS memory"; FRE(-1); "bytes"  
'PRINT "Fre-2: stack space"; FRE(-2); "bytes"  
'PRINT "Fre-3: Exp memory"; FRE(-3); "Kbytes"
```

```
LOCATE Row%, Column%  
PRINT "Choose one of the following :"
```

```
FOR I% = 0 TO Menu%  
  LOCATE Row% + 2 + I%, Column%  
  PRINT Menu$(I%)  
NEXT I%
```

```
IF Row% = 3 THEN  
  LOCATE Row% + 2, 1  
  PRINT "Use the cursor"  
  PRINT "keys to select"  
  PRINT  
  PRINT "Press ENTER"  
  PRINT "when ready"
```

```
IF Flag% = 0 THEN  
  PRINT  
  PRINT "Press <ESC> to"  
  PRINT "exit menu"  
END IF
```

```
ELSE  
  PRINT  
  PRINT TAB(Column%); "Use the cursor keys to select"  
  PRINT TAB(Column%); "Press the ENTER KEY when ready"
```

```
IF Flag% = 0 THEN  
  PRINT TAB(Column%); "Press <ESC> to exit"  
END IF  
END IF
```

```
DO
```

```
  COLOR 0, 7          'set inverse color  
  LOCATE Row% + 2 + Choice%, Column%    'locate cursor  
  PRINT Menu$(Choice%)  
  COLOR 7, 0         'set normal color
```

```

IS = ""                'clear IS for While loop
WHILE IS = "": IS = INKEYS: WEND    'get 1 or 2 characters

IF IS = CHR$(13) THEN EXIT SUB      'enter key
IF IS = CHR$(27) AND Flag% = 0 THEN
    Choice% = Menu% + 1: EXIT SUB    '<ESC> key
END IF

LOCATE Row% + 2 + Choice%, Column%  'restore old item
PRINT Menu$(Choice%)

IF IS = CHR$(0) + "H" THEN          'up arrow
    Choice% = Choice% - 1
    IF Choice% < 0 THEN Choice% = Menu%
END IF

IF IS = CHR$(32) OR IS = CHR$(0) + "P" THEN 'down arrow or spacebar
    Choice% = Choice% + 1
    IF Choice% > Menu% THEN Choice% = 0
END IF

IF IS = CHR$(0) + "G" THEN Choice% = 0  'home key
IF IS = CHR$(0) + "O" THEN Choice% = Menu% 'end key

LOOP

END SUB

SUB Delay (DelayTime)
=====
Finish = TIMER + DelayTime
WHILE TIMER < Finish
WEND

END SUB

SUB execute (address%, pc23command$, numcommand, idbready, cmdready)

*****
***** EXECUTE PC-23 COMMANDS SUBROUTINE *****
*****

```

```

'This subroutine executes the PC-23 commands contained in the "pc23command$"
'array one command at a time. This subroutine waits for each command to be
'executed and writes the command and post-command status into the response
'file "pc23response.txt"

'Open output file
'OPEN "c:\pc23response.txt" FOR OUTPUT AS #1

'Perform each command in "pc23command$"

FOR command = 1 TO numcommand
  pc23command$ = pc23command$(command)

  'Check for a "PAUSE" command
  IF UCASE$(pc23command$) = "PAUSE" THEN
    PRINT "PAUSED - PRESS A KEY TO EXECUTE NEXT COMMAND"
    WHILE INKEY$ = "": WEND

  'Check for a "DELAY" command
  ELSEIF UCASE$(MID$(pc23command$, 1, 5)) = "DELAY" THEN

    'parse delay time, stripping chr$(13) from end
    ndelay = VAL(MID$(pc23command$, 7, LEN(pc23command$)))

    PRINT "COMMAND EXECUTION DELAYED FOR"; ndelay; "SECONDS"
    CALL Delay(ndelay)

  ELSEIF UCASE$(MID$(pc23command$, 1, 3)) = "REM" THEN
    PRINT MID$(pc23command$, 5, LEN(pc23command$))

  ELSE

    ***** WRITE COMMANDS TO THE PC-23 *****
    CALL writecommand(address%, pc23command$, numcommand, idbready, cmdready,
control)

    ***** READ RESPONSE FROM THE PC-23 *****

  ' CALL readresponse

  END IF
NEXT command
END SUB

```


SUB getcommand (cmdfile\$, pc23command\$(), numcommand)

***** **PC-23 COMMAND RETRIEVAL** *****

'This subroutine opens "cmdfile\$" and reads the command string data into
'"pc23command\$()". The subroutine reads a command and stores it into the next
'available array location. The subroutine returns the command string array
'and the number of commands. Each command may be up to 32,767 characters
'long but must be followed with a "carriage return"

'Open command string file
OPEN cmdfile\$ FOR INPUT AS #1

'See how many command lines are in the file
numcommand = 0
DO WHILE NOT EOF(1)
 LINE INPUT #1, Dummy\$
 numcommand = numcommand + 1
LOOP
CLOSE

'Reopen command string file
OPEN cmdfile\$ FOR INPUT AS #1

'Redimension command string array
REDIM pc23command\$(numcommand)
CLS
PRINT numcommand; " command lines read"

'Retrieve command strings
FOR I% = 1 TO numcommand
 LINE INPUT #1, pc23command\$(I%)
NEXT I%

'Close command string file
CLOSE #1

'Command strings have been retrieved
END SUB

SUB indexerreset (address%, halt, fail, restart, mask, ready, control, intrclr)

```
*****  
***** PC-23 RESET SUBROUTINE *****  
*****
```

'This subroutine allows the "Watchdog Timer" to time-out and reset the PC-23
'indexer. The timer is restarted after the time-out. This subroutine was
'devised following the PC-23 Indexer User Guide, page 60. This routine does
'not follow the method contained in "SIMPLEX.BAS".

'Initialize and set time-out duration limit

byte = 0

timeout = 10000

'Stop "Watchdog Timer" by setting Control Bit 2

OUT address% + 1, (halt)

'Test for desired "Fail" during timeout limit

WHILE (byte AND fail) = 0 AND timeout > 0

 byte = INP(address% + 1)

 timeout = timeout - 1

WEND

'Check that reset occurred during time-out limit

IF (byte AND fail) > 0 THEN 'reset has occurred

'Restart "Watchdog Timer" with Control Bit 5

OUT address% + 1, (restart)

'Restore Control Bit to it normal state

OUT address% + 1, (control)

'Monitor Status Byte for recovery from Fail state

byte = 0

timeout = 10000

WHILE (byte AND mask) <> ready AND timeout > 0

 byte = INP(address% + 1)

 timeout = timeout - 1

WEND

'Check that Status Byte was restored

```

IF (byte AND mask) = ready THEN      'Status Byte has been restored

    'Acknowledge Interrupt condition with Control Bit 3
    OUT address% + 1, (8)

    'Reset Interrupt Output condition with Control Bit 6
    OUT address% + 1, (intrclr)

    'Restore Control Bit to normal state
    OUT address% + 1, (control)

ELSE                                  'Status Byte has not been recovered
    PRINT " TIMEOUT DURING RECOVERY !!!"
    END
END IF

ELSE                                  'PC-23 has not been reset
    PRINT " TIMEOUT DURING RESET !!!"
    END
END IF

'PC-23 indexer has been reset
END SUB

```

SUB readresponse

```

*****
***** PC-23 RESPONSE GATE *****
*****

```

'This subroutine reads response strings to be read from the PC-23 to the
'PC BUS. This data is sent from the PC-23 one character at a time.

```

'Initialize the answer string to null
answer$ = ""

```

```

'Initialize "byte" and set timeout duration
byte = 0
timeout = 10000

```

```

'Test that PC-23 has a message waiting during time-out limit
WHILE (byte AND odbready) = 0 AND timeout > 0
    byte = INP(address% + 1)      'Read Status Byte

```

```
    timeout = timeout - 1
WEND
```

```
'Check that PC-23 had message ready during time-out limit
IF (byte AND odbready) > 0 THEN    'Message is waiting
```

```
    'Read response while characters are still being sent
    WHILE Char$ <> CHR$(29)
```

```
        'Read "character$" from PC-23 ODB
        character$ = CHR$(INP(address%))
        'Signal that character was recieved with Control bit 7
        OUT address% + 1, (recieved)
```

```
        'Test for PC-23 busy or time out
        byte = 255
        timeout = 10000
        WHILE (byte AND odbready) > 0 AND timeout > 0
            byte = INP(address% + 1) 'Read Status Byte
            timeout = timeout - 1
```

```
        WEND
```

```
    WEND
```

```
END IF
```

```
END SUB
```

```
SUB writecommand (address%, comm$, numcommand, idbready, cmdready, control)
```

```
*****
***** PC-23 OUTPUT DRIVER *****
*****
```

```
'This subroutine allows command string to be transferred from the PC BUS to
'the PC-23 Indexer. The subroutine sends the data contained in the array
'variable "pc23command$" to the PC-23 one character at a time. A carriage
'return signals the end of a command string. The maximum length of a command
'string is 32,767 characters.
```

```
'Add "carriage return" to end of command string
pc23command$ = comm$ + CHR$(13)
```

```
'Send command characters to the PC-23 one at a time
```

```

FOR character = 1 TO LEN(pc23command$)
  character$ = MID$(pc23command$, character, 1)

  'Initialize "byte" and set timeout duration
  byte = 0
  timeout = 10000

  'Test that PC-23 Indexer ready to receive command during time-out limit
  WHILE (byte AND idbready) = 0 AND timeout > 0
    byte = INP(address% + 1)      'Read Status Byte
    timeout = timeout - 1
  WEND

  'Check that PC-23 was ready for next "character$" during time-out limit
  IF (byte AND idbready) > 0 THEN    'IDB is ready

    'Write "character$" to PC-23 IDB
    OUT address%, ASC(character$)

    'Signal that character is waiting with Control Bit 4
    OUT address% + 1, (cmdready)

    'Monitor PC-23 for acceptance of character
    byte = 255                      ' = binary 11111111
    timeout = 10000
    WHILE (byte AND idbready) > 0 AND timeout > 0
      byte = INP(address% + 1)      'Read Status Byte
      timeout = timeout - 1
      PRINT "timeout="; timeout
    WEND

    'Check that the character was accepted
    IF (byte AND idbready) = 0 THEN  'Character has been written PC-23

      'Restore Control Bit to normal state
      OUT address% + 1, (control)

    ELSE
      'Status Byte has not recovered
      PRINT "TIMEOUT AFTER WRITE !!!"
      END
    END IF

  ELSE
    'Status Byte is not responding

```

```
PRINT "TIMEOUT DURING WRITE !!!"  
END  
END IF
```

```
NEXT character  
PRINT " [ "; comm$; " ] command executed"  
'Command string has been written to the PC-23  
END SUB
```

SAMPLE COMMAND FILE

E

The following is a listing of a command file which provides motion information to the PC-23 indexer. The "rem" statements as well as "pause" and "delay #" are intrinsic to the PC-23 Driver program in Appendix D. The remaining commands are the Compumotor X-code commands that are written directly to the indexer one character at a time. A command prefix between "1" and "3" is related to the axis that the command is intended for.

```
rem this is a full motion demo of the arm
rem the arm may or may not be at home
rem indexer initialization
pause
1mr22
2mr22
3mr21
1a50
2a50
3a50
1d0
2d0
3d0
1mn
2mn
3mn
1a3.333
2a10
3a15
1v3.333
2v10
3v30
o00100
rem home the arm extension
pause
3d-4000000
```

```

3g
rem home elevation and azimuth
pause
2d-15000000
2g
1d-10000000
1g
rem move azimuth through full range
pause
1pz
2pz
3pz
1mr
1d10000000
1i
1g
delay .5
1s
1ld0
1g
rem move azimuth to point to chamber door
delay 62
1d-3000000
1ld3
1g
1ld0
delay 20
rem lower arm completely
2mc
2h
2g
delay 31
rem bring arm up to point at door
2mn
2d-9000000
2g
delay 19
rem extend arm fully
3mc
3h
3g
rem insert some complex moves here
rem leave arm out fully and swing towards home a bit

```


delay 53
pause
1mn
1d-1000000
1g
rem retract halfway
delay 7
3mn
3d-30000000
3g
rem fully drop arm
delay 10
2mc
2h
2g
rem turn azimuth towards home corner and fully raise arm
delay 19
1mn
1d-4550000
1g
2mc
2h
2g
rem extend arm partially over top of diffuser in corner
delay 31
3mn
3h
3d15000000
3g
rem HOME the arm, retract first
pause
1mn
2mn
3mn
3d-40000000
3g
rem home elevation and azimuth
delay 33
2d-15000000
2g
1d-11000000
1ld0
1g

rem de-energize brake
pause
o000000

POSITIONING ACCURACY DATA

F

The results of the positioning accuracy trials are contained in the following two tables.

Table F.1 contains the results for the motion of the manipulator only. Table F.2 contains the overall lost steps when the motors were de-energized at two resting positions in the motion.

| RUN # | AXIS 1 | AXIS 2 | AXIS 3 |
|-------|--------|--------|--------|
| 1 | -184 | -1001 | -1506 |
| 2 | -256 | -1 | -3006 |
| 3 | 51 | 999 | 1494 |
| 4 | -174 | -1 | 1494 |
| 5 | -256 | 999 | 1494 |
| 6 | -50 | -2001 | -6 |
| 7 | 146 | 999 | -6 |
| 8 | 38 | 999 | -1506 |
| 9 | -228 | -3001 | -1506 |
| 10 | 163 | -1 | -6 |
| 11 | 144 | 2999 | 1494 |
| 12 | -216 | -1001 | -3006 |
| 13 | 247 | 999 | 2994 |
| 14 | -166 | -1 | -1506 |
| 15 | -256 | -1001 | -6 |

Table F.1: Apparent Homing Error in Microsteps for the First Trial

| RUN # | AXIS 1 | AXIS 2 | AXIS 3 |
|--------------|---------------|---------------|---------------|
| 1 | 282 | 1999 | 2994 |
| 2 | 336 | -1001 | -1506 |
| 3 | 256 | 1999 | 1494 |
| 4 | 256 | -1001 | -6 |
| 5 | 437 | 999 | -1506 |
| 6 | 318 | -2001 | -1506 |
| 7 | 598 | 999 | -6 |
| 8 | 273 | -2001 | 1494 |
| 9 | 256 | 999 | 1494 |
| 10 | 341 | -1001 | -3006 |
| 11 | 455 | 1999 | 1494 |
| 12 | 256 | -1001 | -1506 |
| 13 | 301 | 999 | -6 |
| 14 | 288 | -1001 | -6 |
| 15 | 413 | 999 | 1494 |

Table F.2: Apparent Homing Error in Microsteps for the Second Trial